Quantum mechanical study of perfect and defective solids

Roberto Nada

Department of Geological Sciences,
University College, London

The Royal Institution of Great Britain
Davy Faraday Laboratory

Submitted for the degree of Doctor of Philosophy,
University of London

October, 1991

ProQuest LLC.
789 East Eisenhower Parkway
P.O. Box 1346
Ann Arbor, MI 48106 – 1346

ABSTRACT

In this thesis we study the ground state properties of perfect and defective materials using quantum mechanical techniques. A number of different approximations are used to investigate the electronic structure of the systems studied.

We adopt the Hartree-Fock Hamiltonian for the description of the problem, which we solve ab-initio, i.e. with only knowledge of the atomic number and the geometrical arrangement of the nuclei. The Hartree-Fock equations, that have been applied with great success for many years to the study of molecules, can be reformulated in order to satisfy the periodic boundary conditions that apply in a perfect, translationally invariant lattice. A review of Hartree-Fock theory is given in Chapter 2. In Chapter 3 we discuss the state-of-the-art of Hartree Fock computational schemes in quantum chemistry and we describe the structure of the program CRYSTAL, that adopts the ab-initio periodic Hartree-Fock approach. This program was used to study the electronic properties of silicates (SiO_2 α-quartz and stishovite polymorphs, and of the ilmenite-structured $MgSiO_3$. Results of this study are presented in Chapter 5.

The availability of an accurate description of the perfect lattice makes possible the development of techniques to study point defects that locally perturb the host crystal. In Chapter 4 first we review some standard techniques for the study of point defects. Next we discuss an embedding method, where an isolated cluster of atoms, containing the defect, is embedded into the host by means of Green function techniques. We developed a computer program, EMBED, that was thoroughly tested during the work reported in the thesis. The major shortcoming of this approach is the inadequate treatment of long-range polarization effects and of charged defects. We present a technique to interface the quantum mechanical

method with a classical description of the polarization potential produced in the relaxed host lattice.

We have applied this latter technique to the study of defects in LiF: the bound Schottky pair and the Na substitutional impurity have been considered. Results are presented in Chapter 6, and are compared with classical simulations, where the system is described as a set of point charges interacting via interatomic potentials.

ACKNOWLEDGEMENTS

Firstly I would like to thank my supervisor, Professor C.R.A. Catlow, who supported this topic for study and gave me advice and help throughout my research work. His patience and confidence were always of great support, especially when I was faced with the many difficulties that often accompany a research work.

I am also indebted to Dr. G.D. Price, my UCL supervisor, for the many hours of discussion and his valuable suggestions; his help allowed me to understand better the challenging problems of geochemistry that the quantum theory may contribute to solve.

I would particularly like to thank the people of the Institute of Theoretical Chemistry at the University of Torino, Italy. Firstly I would like to thank Prof C. Pisani, who originally suggested this research project. Since the time when he supervised my thesis work in Torino, and throughout the years of my Ph.D. research, his help and support have never failed. I am indebted to him for the many discussions and suggestions concerning my research activities and my Ph.D. thesis, and for his careful proof-reading - his opinions, if expressed while climbing and hill-walking in the Alps, or in the more relaxing Cheshire's countryside, always had a great impact on my work. Prof. R. Dovesi and Prof. C. Roetti not only gave me valuable support with the use of CRYSTAL, but , on many occasions, patiently helped me when I was faced by awkward questions. I also thank Dr. R. Orlando, who was involved from the beginning in the development of the program EMBED, for his friendly and kind help. Dr. M. Causa's help made possible the production of many of the electron charge density maps presented in this thesis.

I am very grateful to Dr. V.R. Saunders and Dr. M. Leslie, for their help and advice. The several, stimulating, discussions we had in Daresbury, cast light on the problem of charge defects. I hope to be able to continue to collaborate with them in the years to come. Dr. Saunders's also provided invaluable support with the use of CRYSTAL.

I would like to thank Dr. N. Ross and J. Stuart, from UCL, for their helpful suggestions on the interpretation of my results on silicates.

The calculations were performed using the facilities provided by the SERC Rutherford Laboratory: both the CRAY-XMP and the IBM3090 supercomputers were intensively used. The User Support Group always patiently dealt with my many questions and doubts.

My Ph.D. was sponsored by a research contract awarded by the Commission of the European Community, that is gratefully acknowledged.

As important as the technical and scientific support, was the support and help that I received from my parents, from my brother, Enrico, and from my friends. Thanks to all of you.

In particular I would like to thank Nona; her friendship and affection never failed me since I started my research work three years ago. Every page of this thesis reminds me of her !

"Atomics is a very intricate theorem and can be worked out with algebra but you would want to take it by degrees because you might spend the whole night proving a bit of it with rulers and cosines and similar other instruments and then at the wind-up not believe what you had proven at all"

(" The Third Policeman ", Flann O' Brien)

CONTENTS

LIST OF TABLES

Chapter 5.
Ab-initio periodic Hartree-Fock calculations on silicates and magnesium silicates

Chapter 6.
Ab-initio Hartree-Fock Perturbed Cluster embedding study of neutral defects in LiF

6.1 Basis set adopted for Li and F in the perfect bulk and defect calculations.

6.2 Basis set adopted for Na in the defect calculations.

6.3 Cluster size vs. cost: we report the number of atomic orbitals in C (N_C), the number of atomic orbitals in the D^* region (N_{D*}), the number of integrals (in millions) (N_I), the CPU time to evaluate them (t_1, in seconds) and the CPU time necessary for each SCF cycle.

6.4 Atomic Mulliken net charges for the different clusters considered in the self-substitution case compared to the LiF bulk calculated by CRYSTAL.

6.5 Optimized interatomic displacements (Δd, in a.u.), formation energies (ΔE, in eV) and Mulliken net charges on the defect and nearest neighbours) for the Na substitutional and the BSP.

LIST OF FIGURES

Chapter 5.
Ab-initio periodic Hartree-Fock calculations on silicates and magnesium silicates

5.13 Electron charge deformation map (crystal - isoalted atoms) corresponding to a plane cutting the O-Si-O plane.

5.14 Electron charge deformation map (crystal - isoalted atoms) corresponding to a plane cutting the O-Mg-O plane.

Chapter 6.
An ab-initio Hartree-Fock Perturbed-Cluster embedding study of neutral defects in LiF

6.1. (a) Clusters used to study the Na substitutional in LiF and (b) the Bound Schottky Pair in LiF.

6.2. Total electron charge density for cluster II in the autoembedding case. The map is drawn in the (100) plane.

6.3. Formation energies (in hartree) in the autoembedding clusters I,II and IV, as a function of the F-Li distance (d, in a.u.).

6.4. Effect of the relaxation of the nearest neighbouring F^- ions on the defect energies in cluster CI and CII (Na substitutional) and C IV (BSP), respectively.

6.5 Difference electron density maps of the relaxed cluster I (Na+6F+6Li). The map is drawn in the (100) plane.

6.6 Difference electron density maps of the relaxed cluster II (Na+6F+12Li). The map is drawn in the (100) plane.

6.7 Difference electron density maps of the relaxed cluster III (Na+6F+12Li+8F+6Li).

6.8 Total electron charge density maps of the relaxed cluster II (Na+6F+12Li), corresponding to the contributions to the density matrix as calculated in equations 4.4.36, 4.4.37.

6.9 Difference electron density maps of the relaxed cluster IV (BSP + 5 Li). The map is drawn in the (100) plane.

6.10 Difference electron density maps of the *unrelaxed* cluster IV (BSP + 5 Li).

6.11 Difference electron density maps of the relaxed cluster V (BSP + 5 Li + 5 F).

6.12 Difference electron density maps corresponding to a cluster containing a Li ion surrounded by six O, and embedded in MgO.

6.13 Position of the 2p HF levels of F^- as calculated for the ion in the "auto-embedded" cluster CI, CII and CIII and for F^- in the defective clusters (containing the substitutional Na) CI, CII and CIII respectively.

Chapter 1.
Introduction

This thesis is concerned with the study of the *electronic properties of crystalline materials.*

As we are interested in electronic properties, i.e. those properties that depend on the behaviour of the electrons in the system, we must use quantum theoretical methods. According to quantum mechanics, the physical properties of a system are described by its wavefunction.We are first interested in calculating the total energy, and how it varies as a function of the atomic positions, to predict the equilibrium configuration of the atoms in crystals. This information also yields vibrational frequencies, reaction paths and reaction barriers, and the relative stabilities of different crystalline phases. By applying appropriate operators to the wave-function we obtain the values for the other physical observables: in particular we are interested in the electron charge distribution, that provides us with an insight into the properties of the bonding.

The Schroedinger equation of the many-electron system must be solved by introducing approximations, even in the case of small molecules. For example we can neglect some interactions in order to simplify the expression of the Hamiltonian. In this thesis work we adopt the Hartree-Fock approximation, that is discussed in Chapter 2. We use an ab-initio approach, that is, we evaluate the ground-state properties, corresponding to the chosen Hamiltonian, from the knowledge only of the atomic numbers and of the geometrical positions of the nuclei.

We are concerned with crystals, i.e. extended objects containing a very large number of atoms (and therefore an even larger number of electrons). Indeed the systems are, effectively, infinite. The complexity of the problem is therefore clearly understandable; the quantum equations that describe the interactions

between electrons, even if simplified by approximations, surely cannot be solved for a system containing millions of interacting particles!

To simplify the problem, we can restrict our attention to a small number of atoms, i.e. a finite region of the crystal, whose electronic properties are accurately calculated. The rest of the system can be described in a more approximated way; for example by assuming that the interactions between the two sub-systems are governed by classical forces, and that the finite region we are interested in, 'sees' the rest of the system as a dielectric continuum. This approach is in essence that adopted by cluster calculations, where the quantum theory is used to calculate the wave-function of the electrons associated with a cluster of atoms. The underlying assumption is that we are only interested in the properties of a finite region of the crystal (for example an active site in a catalytic substrate or the neighbouring atoms of a point defect). We return to this method below.

Alternatively, we can redefine the problem taking into consideration the geometrical properties of the system under study. If the crystal is perfect, i.e. it can be generated by applying translational operators to a generating unit cell, then it can be shown that, by exploiting the translational invariance of the system, the problem can be greatly simplified. All the unit cells of the crystal are equivalent by definition; therefore we can focus on the atoms contained in only one cell, knowing that all the other atoms of the crystal are exactly equivalent (so that they will have the same charge, electron charge distribution etc.). The periodic symmetry of the crystal makes it possible for the interactions between unit cells to be calculated by means of rapidly converging numerical series; these procedures are discussed in Chapter 3.

The accuracy of this technique, that is rapidly becoming a standard method in quantum chemistry, has been assessed in this study. We studied the properties of minerals containing silicon (two SiO_2 polymorphs and the ilmenite-structured $MgSiO_3$); the investigation focused on the differences in bonding between the three systems due to the different coordination number of silicon. Silicates were

chosen for this study because they provide an interesting example of partially ionic bonding. It is also important to gain a better understanding of the properties of the Si-O bond in different minerals, since silicates play a vital role in both geochemistry of the Earth and in modern technology.

The study of a perfect, translationally invariant, crystal, yields valuable information about microscopic and macroscopic properties; on the other hand, many interesting processes, and properties of the matter, are connected with the presence of defects and impurities. The theoretical study of the properties of defect centres is intrinsically more complicated. In this work we focused on point defects, where one atom of the perfect lattice is removed to create a vacancy, or is substituted by an impurity, or an interstitial species is added. Ideally, the theoretical method should accurately describe the local properties of the defect centre, taking into account the perturbation generated in the host (that causes the host atoms surrounding the defects to be displaced and to polarize) and including all the interactions between the defect, the perturbed atoms and the rest of the crystal. The 'Cluster Approach' has been very popular in quantum chemistry; as noted above, this approach uses a molecular fragment, which contains the defect and reproduces the local environment of the host crystal, to study the properties of the defect and of its neighbours. Although widespread, the method suffers from the obvious implicit shortcomings of the model: the crystal field is not correctly reproduced and the periodic nature of the host lattice is not included in the model; surface states associated with dangling bonds introduce unphysical features that can be only partially corrected by terminating the cluster with, for exmple, hydrogen atoms.

We have therefore developed and tested an embedding technique, the first requirement of which is the availability of an accurate description of the perfect, unperturbed lattice and also of an isolated cluster of atoms, locally reproducing the symmetry of the host and containing the defect. Next the wave-function of the

isolated cluster is corrected, by means of a Green functions technique, in order to account for the surrounding lattice. A computer program, EMBED, was developed and thoroughly tested during the work reported in the thesis; we provide, as a supplement to this thesis, a copy of the EMBED user manual. EMBED was used to study the properties of neutral defects in LiF. We have focused our attention on this class of defects to avoid the problems associated with charged states, that will be discussed in section 4.4.3. Moreover, the case of neutral defects is an important test for the validity of our method, as they induce a local perturbation that causes a relaxation of the neighbouring atoms. We have also increased the sophistication of our embedding approach by including, in a self-consistent way, the effects of the polarization of the more distant regions of the crystal surrounding the defect. The development and implementation of this new method, that is discussed in section 4.5, is presently being pursued in collaboration with M. Leslie and V.R. Saunders at the Daresbury Laboratory.

We have chosen to print references, tables, and figures at the end of each chapter. We feel that this format makes the thesis more readable.

Chapter 2.
Hartree-Fock Theory

2.1 THE HARTREE-FOCK HAMILTONIAN

In this section we shall review Hartree-Fock theory and derive the Hartree-Fock equations referred to in the rest of work. An extensive discussion of the theoretical basis of quantum mechanics, and of the properties of the Schroedinger equation, can be easily found in several books. An introduction to the subject is for example, given in 'Quantum Chemistry' by Levine (1974), while an elegant and more extensive discussion of the formalism can be found in von Neumann (1955).

The Schroedinger equation for a system of N nuclei and n electrons can be written as:

$$H\ (1,2,...,N;\ 1,2,...,n)\ \Psi(1,2,..,N;1,2,..,n) = E\ \Psi(1,2,..,N;1,2,..,n) \qquad (2.1)$$

where H is the Hamiltonian for the whole system, E is the total energy and Ψ is the corresponding wave-function.

H can be approximated by assuming that the nuclei are fixed, and that only the motion of the electrons in the average nuclear field is considered (i.e. the Born-Oppenheimer approximation). We also choose to neglect interactions due to magnetic fields or to relativistic terms.

This assumption yields to the following Hamiltonian:

$$H = \sum_{i}^{n}\left[-\frac{1}{2}\nabla_i^2 + \sum_{k}^{N}\left(-\frac{Z_k}{r_{ik}}\right) + \sum_{j(j>i)}^{n}\frac{1}{r_{ij}}\right] + \frac{1}{2}\sum_{k,k'}^{N'}\frac{Z_k Z_{k'}}{r_{kk'}} \qquad (2.2)$$

where r is the distance between the pairs of species; Z_k is the charge of the k-th nucleus. n is the total number of electrons in the system and N is the number of nuclei. The first term is the kinetic energy of the electrons; the second is their potential energy in the field of the nuclei and the third represents the electrostatic interactions between pairs of electrons.

In the Hartree-Fock method the ground-state electronic wave function is approximated by a determinant of orthonormal one-electron functions, denoted as $\psi_q(i)$. These functions are two components spinors, e.g. the product of a spatial and spin functions (q stands for all the quantum numbers required to specificy the one electron functions).

The determinental wave function has the form:

$$\Psi(1....n) = \frac{1}{\sqrt{n!}} \begin{vmatrix} \psi_1(1) & .... & \psi_n(1) \\ .... & \psi_q(i) & .... \\ \psi_1(n) & .... & \psi_n(n) \end{vmatrix} \qquad (2.3)$$

This wave function satisfies the antisymmetry requirements, since the interchange of two particles corresponds to the interchange of two rows of the determinant, that changes the sign of the determinant. It also causes the introduction of some form of correlation effects, since the motion of two electrons with parallel spins will be correlated.

The best determinantal wave function Ψ that can be constructed is the one which minimizes the expectation value of the energy. The variational principle can then be used to determine the best spin orbitals, that will be those which minimize the electronic energy (for electrons in the same state of spin):

$$E^{HF} = \Sigma_i \varepsilon_i^{core} + 1/2 \, (\Sigma_{i,j} J_{ij} - \Sigma_{i,j} K_{ij}) \qquad (2.4)$$

where:

i) ε_i^{core} is the energy of the i-th electron in the field of bare nuclei.

ii) J_{ij} represents the Coulomb interaction of the i-th electron with the j-th electron in the system, that is:

$$J_{ij} = \langle \psi_i \psi_j | \frac{e^2}{r_{ij}} | \psi_i \psi_j \rangle \qquad (2.5)$$

iii) The exchange term K_{ij} is in the form:

$$K_{ij} = \langle \psi_i \psi_j | \frac{e^2}{r_{ij}} | \psi_j \psi_i \rangle \qquad (2.6)$$

The variational principle requires that for small changes in the wavefunction Ψ the expectation value of the Hamiltonian is stationary, that is:

$$\delta E = \delta \int \Psi^* H \Psi \, d\tau = 0 \qquad (2.7)$$

If this is true, then Ψ is a solution of the Schoedinger equation that describes a stationary state. Applying this condition to the espression of the energy, the corresponding Hartree-Fock one-electron equation can be derived:

$$F_i \psi_i = \varepsilon_i \psi_i \qquad (2.8)$$

where:

F_i is the one-electron operator, defined as:

$$F_i = [H_i^{core} + \sum_{j \neq i,\ (\chi_j \neq \chi_i)} J_j + \sum_{j \neq i,\ (\chi_j = \chi_i)} (J_j - K_j)] \qquad (2.9)$$

where χ indicates the spin, J_j is the interaction of the j-th electron with all the other elctrons of opposite spin (Coulomb repulsion averaged over the distribution defined by the orbitals ψ_j ; (J_j-K_j) is the interaction of the i-th electron with all the other electrons of the same spin (Coulomb repulsion reduced by the spin correlation); H_i^{core} corresponds to the kinetic energy of the i-th electron plus the Coulomb interaction of this electron with the nuclei and can be written as:

$$H_i^{core} = -1/2\ \nabla^2_i - \sum_A \frac{Z_A e^2}{r_{iA}} \qquad (2.10)$$

where Z_A is the charge of the A-th nucleus and the sum is over all the nuclei in the system.

The additivity of the Hamiltonian, expressed as a sum of one-electron terms, depends on the initial form of the Coulomb and exchange operators; they introduce the correlation between electrons in the form of the correlation of each electron with the average distribution of all the other electrons. That is, they underestimate correlation effects.

The corresponding expression for the total energy (sum of one-electron energies) is:

$$E = 1/2\ \sum_i \langle \psi_i | H_i^{core} | \psi_i \rangle + 1/2\ \sum_i \langle \psi_i | F_i | \psi_i \rangle =$$
$$= 1/2 \sum_i (E_i^{core} + \varepsilon_i) \qquad (2.11)$$

The energy $-\varepsilon_i$ represents the so called Koopman's potential, that is the energy required to remove the i-th electron leaving the other electrons

unperturbed. Clearly this quantity does not coincide with the experimental ionization energy.

The average value of the energy can also be written as:

$$E = 1/2 \sum_i \langle \psi_i | H_i^{core} + F_i \quad | \psi_i \rangle = \langle \Psi | 1/2 \sum_i (H_i^{core} + F_i \quad) | \Psi \rangle \tag{2.12}$$

We can consequently define an effective Hartree- Fock Hamiltonian as:

$$H^{HF} = 1/2 \sum_i (H_i^{core} + F_i) \tag{2.13}$$

The Hartree-Fock equations can be solved by using a method of successive approximations. An initial approximation for the one-electron orbitals can be used to calculate the Coulomb and exchange interactions, and then the F operator. Then the one-electron orbitals can be recalculated. The process continues until convergence, that is, until the changes in the total energy are below a given threshold.

The use of a self-consistent field (SCF) method makes a distinction between two subsets of orbitals: the occupied and the virtual ones. Only the occupied orbitals are used to define the Hamiltonian. If ψ_i is an occupied orbital the terms corresponding the electronic interaction in the Hamiltonian, describe the interaction of the electron i with the (n-1) electrons that occupy the spin/orbitals different from i. If ψ_i is a virtual state, then the electronic interaction terms describe the interaction of an electron in i with the n electrons of the occupied many-fold. The addition of the ψ_i orbital, in a sense, describes a possible solution for a system with (n+1) electrons. On the other hand it does not represent an H-F solution for such a system, since we do not take into account the distribution of charge associated to the (n+1)-th electron in the definition of the Hamiltonian !

2.2 PERIODIC BOUNDARY CONDITIONS

It is important to see how the above equations can be generalized in order to describe electrons in a periodic potential. A detailed treatment of the lattice symmetry and its influence on the form of the Schroedinger equation can be found, for example, in Madelung (1981). Here we will only comment on the most important aspects and results of such a treatment.

The fundamental assumption is that the whole Hamiltonian satisfies periodic boundary conditions, that is:

$$H(T_{\mathbf{R}}\,\mathbf{r}) = H(\mathbf{r}) \tag{2.14}$$

with $T_{\mathbf{R}}$ is an operator that replace the space vector **r** by **(r+R)**, **R** being a primitive translation. Applying this operator to the (2.8) yields:

$$T_{\mathbf{R}}(F_i\,\psi_i) = T_{\mathbf{R}}(\varepsilon_i\,\psi_i) \tag{2.15}$$

and using the (2.14):

$$F_i\,(T_{\mathbf{R}}\psi_i) = \varepsilon_i\,(T_{\mathbf{R}}\psi_i) \tag{2.16}$$

All $(T_{\mathbf{R}}\psi_i)$ are, simultaneously with ψ_i, eigenfunctions to the same eigenvalue ε_i.

To impose periodic boundary conditions, the wave-function must satisfy the Bloch's theorem, which states that the non-degenerate solutions of the Schroedinger equation and suitably chosen linear combinations of the degenerate solutions are at the same time eigenfunctions $\psi_i(\mathbf{k},\mathbf{r})$ of the translational operator

T_R with the eigenvalues exp (ik·R), where **k** is a wave-vector in the first Brillouin zone; that is:

$$T_R \psi_i (\mathbf{k}, \mathbf{r}) = \exp (i\mathbf{k}\cdot\mathbf{R})\, \psi_i (\mathbf{k},\mathbf{r}) \qquad (2.17)$$

It follows that:

$$\psi_i (\mathbf{k}, \mathbf{r}+\mathbf{R}) = \exp (i\mathbf{k}\cdot\mathbf{R})\, \psi_i (\mathbf{k},\mathbf{r}) \qquad (2.18)$$

The equation (2.17) expresses the condition that the i-th electron wave-function must obey in order to satisfy the periodical boundary conditions; in particular, we note that by applying a primitive translation to the function ψ_i (**k**,**r**), we obtain the same function except for a 'phase factor' exp (i**k**·**R**).

REFERENCES

d'Espagnat B (1976), Conceptual foundations of quantum mechanics, WA Benjamin inc., London

Levine I N (1974), Quantum Chemistry, Allyn and Bacon Inc., Boston

Madelung O (1981), Introduction to solid-state theory, Springer-Verlag, Berlin

von Neumann J (1955), Mathematical Foundation of Quantum Mechanics, Princeton University Press, Princeton, NJ

Chapter 3.
Hartree-Fock methods: from molecules to crystals

3.1 INTRODUCTION

The goal of this section is to discuss the state of the art of Hartree-Fock (HF) computational schemes for the study of molecules and perfect crystals. The methods we shall discuss are *ab-initio* in the sense that we wish to evaluate the ground-state properties, and to predict what happens when the system is perturbed, from *the knowledge only of the atomic number and the geometrical arrangement of the nuclei.*

It required considerable effort to implement computationally the HF equations discussed in the previous chapter. However, this has provided physicists and chemists with powerful and reliable tools for investigating the properties of the matter. New computer architectures make it possible to implement increasingly more sophisticated and efficient programs.

In section 3.2 we will first outline how molecular HF programs have become a standard tool in quantum chemistry. The development of techniques for the study of periodic, infinite crystals is then discussed and the different approaches are compared. In section 3.3 we examine the main characteristics of the code used in this work and discuss the physical properties that can be investigated. Finally, in section 3.4 we consider possible improvements that can be included in periodic HF calculations, in order to overcome some of its well-known limitations.

3.2 HF SCHEMES IN QUANTUM CHEMISTRY

The first attempt made by quantum chemists to solve ab-initio the Schoedinger equation for a many-electron system referred to simple, small molecules. As a result of many years work, very reliable and general-purpose codes are now available to the scientific community for the study of finite systems. GAUSSIAN-82 (Binkley et al., 1981) is an example of this family of codes (a list of similar codes is given in Appendix A), with an user-friendly input and a self-explanatory output; it is able to evaluate one-electron properties, optimize the geometry of the system with respect to the energy, to calculate force constants and vibrational properties and it includes sophisticated procedures to include the correlation energy (Wilson, 1984). Most of the computational schemes adopt the same basic ingredients: the linearized HF-Roothaan equations are solved by using a basis set of a small number of atomic orbitals (AO); the molecular orbitals are obtained through a self-consistent field (SCF) procedure; correlation corrections are then applied to the ground state wave-function. As discussed above, this approach provides the single-determinantal wavefunction with the lowest expectation value for the energy, within the functional space spanned by the adopted basis set; the one-electron Hamiltonian contains terms that depend on the ground state one-electron density matrix, so that the problem must be solved by a self-consistent, iterative procedure. The method proves reliable and accurate in characterizing the electronic properties of many systems; many chemical and physical properties can be accurately predicted. Not only can experimental results be reproduced, but the *predictive* capability of the method allows the study of systems that have not yet been synthesized or not well experimentally characterized. These types of program have therefore become very popular and widely used: they can be easily implemented on different machines; they are highly optimized with respect to

CPU time and there are compilations of ready-to-use basis sets that can suit many problems. Indeed these powerful numerical techniques have become a probe whose proper use does not require a high level of expertise in quantum chemistry: they are, in effect, a "black box" - an additional tool to probe the chemistry of molecules.

The success of these methods has not only allowed them to survive and succesfully multiply, it also produced a new fertile offspring, able to describe infinite systems.

The description of the electronic properties of an infinite, periodic crystal is a much more demanding task; but decades of successes in molecular quantum chemistry generated a strong stimulus in this direction, as a natural development of previous techniques. Of course, existing molecular programs, can be used to simulate the properties of a crystal, by representing it as a finite object. These calculations consider a cluster of atoms, whose geometry reproduces locally the crystal geometry (Colbourn, 1989) : the presence of the rest of the system is ignored, or simulated by saturating dangling bonds with hydrogen atoms and by creating the correct long-range Madelung field by means of point charges surrounding the cluster. Only a small number of atoms can typically be included in the cluster (10-20 atoms); although in recent studies, the availability of supercomputers has allowed larger clusters, containing 50 or more atoms, to be included (Mainwood at al., 1978). There are however intrinsic limitations in this sort of calculation, for example the incorrect description of the long-range interactions and of the periodicity; therefore these methods are of limited value.

By taking advantage of the translational symmetry, as shown in the previous section, the HF equations can be usefully re-formulated in order to get, formally, the correct solution for a periodic system. In comparison with molecular codes, a much greater variety of techniques are currently employed, resulting in much less standardization.

The solution of the HF equations for perfect crystals can be derived by following different routes. If a minimal basis set of AO is used (i.e. the number of spin/orbitals that can be constructed is equal to the number of electrons in the system), then no variational freedom is left to the problem and the one-electron density matrix is simply the inverse of the overlap matrix, and the problem is reduced to a trivial one. This approach has been used to study ionic system; in principle the method is exact for insulators if the generating AOs closely resemble the crystal's Wannier functions (Callaway 1974, pp.375-382).

Unfortunately, in general, this procedure can not be followed and a more flexible basis set must be used, in order to allow a larger variational freedom; a self-consistent field (SCF) procedure must be followed to obtain the best variationally optimized wave-function. The sequence of steps to be undertaken is as follows:

(a) Definition of the geometry, atoms and basis set
(b) Evaluation and storage of the integrals
(c) Define a trial density matrix P_0 to start the SCF procedure
[begin loop over a selected set of $\mathbf{k}_i$ points in the first Brillouin zone]
(d) Calculate the Fock matrix F ($\mathbf{k}_i$) in the Bloch's function representation
(e) Diagonalize F in each $\mathbf{k}_i$ point, finding eigenvalues E ($\mathbf{k}_i$) and eigenvectors A($\mathbf{k}_i$)
[end loop]
(f) Calculate a new P_n matrix from the knowledge of E and A
(g) Check for convergency (by comparing P_n and P_{n-1}), if not reached repeat (d)..(f)

The evaluation of the Fock matrix (step (d)) can be performed either in a 'Configuration Space' (CS) or in a 'Momentum Space' (MS).

In the CS all the integrals are performed in direct space and the Fock matrix evaluated, then F is Fourier transformed to reciprocal space just before the diagonalization (Del Re et al.,1967) (Andre' et al.,1967). The Coulomb and exchange series are expressed as triple sums over all the crystal cells, and efficient

truncation criteria are necessary in order to reduce the number of terms to be calculated and stored.

In the MS approach, the Fock matrix is evaluated analytically in reciprocal space after expressing both BFs and Coulomb and exchange operators as a combination of plane waves (Harris and Monkhorst, 1970) (Stoll and Preuss, 1975), (Brener and Fry, 1978), (Delhalle and Harris, 1985). This approach allows a reduction in the number of integrals. On the other hand, use of the CS approach makes it easier to exploit the powerful numerical techniques developed in molecular quantum chemistry; the storage requirements, if the problem is treated adequately, are quite manageable.

The other choice regards the analytical expression of the basis functions used to simulate the crystalline orbitals (CO); the CO must satisfy Bloch's theorem, because of the translational symmetry of the crystal. Each CO can therefore be expressed as:

$$\Psi(\mathbf{k};\mathbf{r}+\mathbf{g}) = \Psi(\mathbf{k};\mathbf{r})\exp(i\mathbf{k}\cdot\mathbf{g}) \qquad (3.2.1)$$

where **k** is the wavevector and **g** is a direct lattice vector of the crystal.

The CO can be expressed in terms of plane waves (PW):

$$\Psi(\mathbf{k};\mathbf{r}) = \sum_{\mathbf{K}} a(\mathbf{k};\mathbf{K})\ \exp[i(\mathbf{k}+\mathbf{K})\cdot\mathbf{r}] \qquad (3.2.2)$$

being **K** the reciprocal lattice vectors.

PWs form an orthonormal set, with the correct asymptotic behaviour. Although PWs are an attractive choice , it is necessary to use a high number of PWs to describe sharp local features of the wavefunction, especially in the core region. Instead of PWs, Bloch's function (BF) $\varphi_\mu(\mathbf{k})$ can be used. In this case each function will have the form:

$$\varphi_\mu(\mathbf{k};\mathbf{r}) = \sum_{\mathbf{g}} \chi_\mu(\mathbf{r}-\mathbf{g}) \exp(i\mathbf{k}\cdot\mathbf{g}) \qquad (3.2.3)$$

where χ_μ are normalized local functions, usually centered at the nuclei positions. Their angular dependence is that of the corresponding atomic orbitals, so that they are usually called AOs. The AOs are usually expressed in terms of linear combination of Gaussian Type Orbitals (GTOs). Each Bloch's function can be considered a contracted set of an infinite number of plane waves; BFs therefore allow a dramatic reduction in the number of basis function needed to construct a given crystalline orbital. This is especially true for COs corresponding to core states. Another advantage of COs is that the algorithms developed for molecular problems can be exploited in the case of periodic systems. On the other hand, BFs do not form an universal set and they are not orthogonal, so that overlap terms are not zero. Furthermore, Bloch's functions generated by diffuse valence AOs often are almost linearly dependent, giving rise to numerical problems.

To overcome the problems associated with PWs and BFs two routes seem particularly interesting: first of all, core states can be described by pseudo-potentials.This would restrict the calculation to valence electrons, that can accurately be described by a limited number of plane waves. Pseudo-potentials techniques will be discussed again, in section 3.3. Secondly, mixed basis sets can be employed, which use BFs for the deep core levels and PWs for the delocalized valence bands and conduction states. This choice is becoming increasingly popular (Kerker, 1981; Baroni et al., 1985).

In the next section we shall discuss in more details the problems associated with Bloch's functions, that are used to represent crystalline orbitals in the approach followed in the present research.

A general purpose HF program for perfect crystals should show a number of desirable features:

(a) It should resemble molecular programs regarding the basic algorithms

(b) Treatment of systems with one-, two- and three-dimensional periodicity should be possible

(c) Good performance and high efficiency are necessary: powerful numerical techniques and algorithms must be used to reduce costs and thereby increase the number of systems that can be studied.

The practical implementation of periodic HF schemes was rapid and successful in the case of ideal polymers (one-dimensional periodic systems) (Kertesz, 1983). In 3-D, the problem is intrinsically more complicated: the truncation criteria cannot be based only on the distance between the centres of the AOs as the number of integrals increases very rapidly with the truncation radius, while their magnitude decreases with the inverse radius; the exploitation of symmetry is more difficult, if one wants to preserve generality; and the reconstruction of the Fock matrix at each k point requires sophisticated numerical techniques.

It was in the early 1970's that, for the first time, a research group at the Aerospace Research Laboratories, Dayton, Ohio, succesfully implemented a HF-Roothan scheme, using a CS approach, for three-dimensional systems . They used a set of contracted lobe Gaussian functions as the basis set, and employed sophisticated techniques in order to exploit the crystal symmetry and reduce to a minimum the number of integrals to be computed. The first calculations studied diamond (Euwema et al., 1973) (Surratt et al., 1973), cubic boron nitride (Euwema et al., 1974 a) and lithium fluoride (Euwema et al., 1974 b).

In more recent years similar attempts have been undertaken by many other research groups; a useful review of them is given in Pisani et al. (1988) (pp.14-15).

The scheme used for the present research was developed at the Institute of Theoretical Chemistry of the University of Torino (Italy) in collaboration with V. Saunders, at the SERC Daresbury Laboratory (Pisani et al, 1988; Dovesi et al., 1988), and has been systematically improved over ten years. The CS approach used is similar to the original one adopted by Euwema et al. . The resulting computer program, CRYSTAL, has been succesfully applied to a very large variety of one, two- and three-dimensional systems, including insulators, semiconductors and metals; although, for a long while, limited computational resources have restricted the calculations to systems with a small unit cell described by relatively small basis sets (see for example Pisani et al, 1988). The quality of these results shows the accuracy of the approach and the reliability of the code.

In the following section we give an account of the methodology, and discuss some of the general characteristic and capabilities of CRYSTAL.

3.3 THE "CRYSTAL" CODE

In this section we shall discuss in more detail a specific HF-CS approach for the calculation of the electronic structure of crystalline systems, as implemented in the program CRYSTAL.

The general steps of the program are: first the geometry and the basis sets for each atomic species is given by input, and the computational conditions are defined. The program performs a symmetry analysis of the structure and classifies and calculates the integrals accordingly, storing them on disk. Then the self-consistent procedure is started: the Fock matrix is calculated in direct space, Fourier transformed into reciprocal space and diagonalized. The knowledge of the eigenvalues and the eigenvectors allows the density matrix P to be evaluated. The P matrix will be used to start the following cycle. The process continues until convergence of the total energy is reached.

A detailed description of the code and of the algorithms can be found in the literature (for example Pisani et al., 1988 and Dovesi et al., 1988). We give here only a brief account of the general structure of the code, with special reference to those notations and formalisms that will be used in Chapter 4, for the discussion of the embedding techniques. Therefore we shall first introduce some conventions to describe in a concise form the basic functions and the charge distributions, used when the Coulomb interactions are evaluated. Then we shall focus on the terms of the Fock matrix, discussing their structure and the technique adopted for their evaluation in CRYSTAL.

3.3.1 Basis functions and charge distribution

3.3.1.1 AOs

A finite number (p) of AOs belongs to the reference zero cell. All the other AOs in the crystal can then be generated by applying appropriate translations.

The ω-th AO in the cell g will be denoted as

$$[\omega g] = \chi_{\omega}^{\ g}(r) = \chi_{\Omega}(\mathbf{r}-g-s_{\omega}) \qquad (3.3.1)$$

where s_{ω} is the fractional vector that specifies the atom to which it belongs and the set of quantum numbers Ω=(n,l,m) characterizes the individual AO.

Each AO is expressed as a linear combination of a certain number t_{nl} of individually normalized real spherical Gaussian functions (GTO) with fixed coefficients d_j and exponents α_j:

$$\chi_{(nlm)}(\mathbf{r}-\mathbf{s}_{\omega}) = \Sigma_j d_{nl,j} G_l^m(\alpha_{nl,j}; \mathbf{r}-\mathbf{s}_{\omega}) \qquad (3.3.2)$$

$$G_l^m(\alpha, \mathbf{r}) = N_l^m(\alpha) X_l^m(\mathbf{r}) \exp(-\alpha \mathbf{r}^2) \qquad (3.3.3)$$

$$N_l^m(\alpha) = ([\alpha^{l+3/2} 2^{2l+3/2} (2-\delta_{mo}) (2l+1) (l-|ml)!] / [\pi^{3/2} (l+|ml)! (2l+1)!!])^{1/2} \qquad (3.3.4)$$

3.3.1.2 Shells

AOs belonging to the same atom can be grouped into 'shells'. Each shell contains all AOs characterized by the same n and l quantum numbers (for instance: 2p,3d,3s shells) or even all AOs with the same principal number n if the number of GTOs and the corresponding exponents are the same (Hehre et al, 1969).

The use of shells is an effective means of reducing the number of functions that need to be calculated in the evaluation of the integrals. The total charge distribution can be decomposed into a sum of 'shell charge distributions', indexed by λ.

3.3.1.3 Adjoined Gaussians

A single normalized s-type GTO G_λ is associated with each shell. Its exponent is such as to reproduce approximately the absolute value of the corresponding AO's at intermediate and long range. The adjoined Gaussians are used quickly and effectively to estimate the overlap between two shells, in order to classify them in terms of 'importance' for the selection of the integrals.

3.3.1.4 Compact expressions for charge distributions

As will be discussed in the following sections, the essential problem in HF studies of periodic systems is how to deal with infinite sums of Coulomb integrals, necessary to calculate the electrostatic interaction between an infinite number of charge distributions. To do so, it is useful to introduce some formalisms for the expressions of the charge distributions and their Coulomb interactions in the crystal, that was originally used by the authors of CRYSTAL.

$$\rho(r) = \{\text{type; location}\} \qquad (3.3.5)$$

indicates a generic charge distribution, where "type" indicates the set of indices that describe the characteristics of the charge distribution with respect to the crystal cell(s) specified by "location".

$$(\{ty1;loc1\} \mid \{ty2;loc2\}) = \int dr_1\, dr_2\, \rho_1(r_1)\, \rho_2(r_2)\, |r_1 - r_2|^{-1} \qquad (3.3.6)$$

indicates the interaction between two distributions ρ_1 and ρ_2.

In particular, the following notations will be used:

i) AO overlap distributions, that are the product of two AO's, are written as:

$$\{12g\,;\,\mathbf{0}\} \equiv \{12g\} \equiv \chi_1^{o}(\mathbf{r})\ \chi_2^{g}(\mathbf{r}) \qquad (3.3.7)$$

$$\{12g\,;\,\mathbf{h}\} \equiv \{12g\} \equiv \chi_1^{h}(\mathbf{r})\ \chi_2^{h+g}(\mathbf{r}) \qquad (3.3.8)$$

The interaction between two AO overlap distributions can be written as:

$$(10\ 2g|\ 3\mathbf{h}\ 4n+\mathbf{h}) \equiv (\{12g\}|\ \{34n;\mathbf{h}\}) \equiv$$

$$\equiv \int dr\, dr'\, \chi_1^{o}(r)\ \chi_2^{g}(\mathbf{r})\, |r-r'|^{-1}\, \chi_3^{h}(\mathbf{r})\ \chi_4^{h+n}(\mathbf{r}) \qquad (3.3.9)$$

ii) A capital letter B used for "location" corresponds to a sub-set of lattice cells over which the local distribution {type;**h**} is summed. For example, if we consider a sub-set B of lattice cells where all the two-electron integrals are evaluated exactly , we can write:

$$\{12g\,;\,B\} \equiv \Sigma_{\mathbf{h}\,\varepsilon\,B}\,\{12g;\mathbf{h}\} \qquad (3.3.10)$$

If the sum is extended to all lattice cells, a translationally invariant distribution is obtained, whose location will be denoted by the letter T.

$$\{12g\,;\,T\} \equiv \Sigma_{h}\ \{12g;h\} \qquad (3.3.11)$$

iii) A Greek letter identifies the charge distribution of 'shells', that is , the electronic charge attributed to shell λ according to a Mulliken analysis:

$$\{\lambda;h\} = \Sigma_{1\,\varepsilon\,\lambda}\,\Sigma_{2}\,\Sigma_{n}\,P_{12}^{\,n}\,\{12n;\,h\} \qquad (3.3.12)$$

where P is the density matrix element referring to the AOs χ_1 and χ_2 in the zero and n-th cell.

iv) Unit nuclear charge distributions are defined as:

$$\{Z;h\} = \delta\,(r\text{-}h\text{-}s_z) \qquad (3.3.13)$$

The nuclear charge Z can formally be split into integer nuclear shell charges Z_λ, each one approximately compensating the electron charge attributed to a given shell. Nuclear attraction integrals are expressed as:

$$(\{12g\}|\{Z;h\}) \equiv \int dr\ \chi_1^{o}(r)\ \ \chi_2^{g}(r) / |r\text{-}h\text{-}s_z| \qquad (3.3.14)$$

3.3.2 Basic equations

In this section we first sketch the equations and the general procedures. A more detailed discussion then follows, in which we analyze the form of the HF Hamiltonian and the computational parameters involved. We also comment on the procedure adopted for the integration in reciprocal space. More details of CRYSTAL can be found in the literature cited above . We shall emphasize those computational features that will be used in the embedding method discussed in Chapter 4.

A periodical HF Hamiltonian can be defined:

$$F_{12}^{\mathbf{g}} = H_{12}^{\mathbf{g}} + B_{12}^{\mathbf{g}} \qquad (3.3.15)$$

where $H^{\mathbf{g}}_{12}$ and $B^{\mathbf{g}}_{12}$ are respectively the one- and two-electron contributions in the basis set of the AO $\chi_i^{\mathbf{g}}$, $\mathbf{g}$ being a direct lattice vector ($\chi_i^{\mathbf{g}} = \chi_i(\mathbf{r} - \mathbf{s}_i - \mathbf{g})$) and $\mathbf{s}_i$ the position in the reference cell of the atom to which χ_i belongs.

The Fock matrix and the overlap matrix $S^{\mathbf{g}}$ are then Fourier transformed into the reciprocal space, in the Bloch function (BF) basis; eigenvalues (E) and eigenvectors (A) are obtained after solving for each $\mathbf{k}$ vector, in the first Brillouin zone (BZ), the matrix equation:

$$F(\mathbf{k})\, A(\mathbf{k}) = S(\mathbf{k})\, A(\mathbf{k})\, E(\mathbf{k}) \qquad (3.3.16)$$

Once the eigenvalues are known, the new density matrix, in the AO basis, is calculated, by integration over the BZ volume:

$$P_{12}^{g} = 2 \sum_{n} \int_{BZ} dk \exp(i\, k .g)\, a^{*}_{1n}(k)\, a_{2n}(k)\, \theta[\varepsilon_F - \varepsilon_n(k)] \qquad (3.3.17)$$

where the $a_{jn}(k)$ element of $A(k)$ is the coefficient of the j-th BF in the n-th crystalline orbital at point k; $\varepsilon_n(k)$ is the corresponding eigenvalue and ε_F is the Fermi level (note that here, and in the following, only closed shell systems are considered).

The knowledge of P allows the Fock matrix, in direct space, to be re-evaluated. The process continues, iteratively, until convergence in the total energy is reached.

The implementation of these equations requires the calculation of infinite summations over direct lattice vectors (Coulomb and exchange series) and a technique for integration in reciprocal space. The scheme adopted in CRYSTAL will be discussed with particular reference to these problems.

3.3.2.1 Coulomb terms

In eq. 3.3.15, the 'one-electronic' term H_{12}^{g} includes the kinetic contribution (T_{12}^{g})

$$T_{12}^{g} = \langle 10 | - \nabla^2 / 2 | 2g \rangle \qquad (3.3.18)$$

and the nuclear attraction term (Z_{12}^{g}), that corresponds to the Coulomb interaction between the AO overlap distribution $\{12\ g\}$ with the nuclear charges in the crystal:

$$Z_{12}^{g} = -\sum_{\lambda} \{ Z_{\lambda} (\{12\ g\} | \{Z_{\lambda}\ ; T\}) =$$

$$= -\sum_{\lambda} \sum_{h} (12g \mid Z_{\lambda}\, h) \qquad (3.3.19)$$

B_{12}^{g} is the sum of the Coulomb and exchange terms:

$$C_{12}^{g} = \sum_{34n} P_{34n} [\, \Sigma_{h} (10\ 2g \mid 3h\ 4n+h)\,] =$$

$$= \sum_{\lambda} (\{\, 12\ g\} \mid \{\lambda;\, T\}) \qquad (3.3.20)$$

$$X_{12}^{g} = -1/2 \sum_{34n} P_{34n} [\, \Sigma_{h} (10\ 3h \mid 2g\ 4n+h)\,] \qquad (3.3.21)$$

where P is the density matrix; and the n and h summations are in principle extended to all direct lattice vectors. Because of translational invariance the first vector can always be centred in the origin cell, identified by the null vector **0**.

We first rearrange the Z and C contributions:

$$C_{12}^{g} + Z_{12}^{g} = \sum_{\lambda} \sum_{h} \int dr\, dr'\, \chi^{0}{}_{1}(r)\ \chi^{g}{}_{2}(r) \mid r-r' \mid^{-1} \rho_{\lambda}(r'-h) =$$

$$= \sum_{h} [\, \sum_{34n} P_{34n}\ (10\ 2g \mid 3h\ 4n+h) - \sum_{\lambda} (12g \mid Z_{\lambda}\, h)] \qquad (3.3.22)$$

defining Mulliken shell net charge distributions :

$$\rho_{\lambda}(r'-h) = \{\lambda;h\} - Z_{\lambda}\, \{Z_{\lambda};h\} \qquad (3.3.23)$$

In this last expression we have two infinite summations, over **h** and **n** vectors.

We first note that, due to the localized nature of the basis set, the total amount of charge q_1 and q_2 associated with the two overlap distributions $\{G_1 G_2\ \mathbf{g}\}$ and $\{G_3 G_4\ \mathbf{n};\mathbf{h}\}$ (where G_1 is the adjoined Gaussian of the shell to which the AO χ_1 belongs) decays exponentially to zero with increasing |g| and |n|. A Coulomb overlap threshold S_c (or $s_c = -\log_{10} S_c$) can be defined, such that when either q_1 and q_2 are smaller than S_c the two-electron integral is disregarded.

The problem of the **h** summation is more delicate. Each shell λ can be classified in two different sets:

i) a long-range set of **h** vectors that includes the interactions between the charge distribution $\chi^0{}_1(r)\ \chi^g{}_2(r)$ and the λ-th shell distributions $\rho_\lambda{}^h$ within the cell h, when their penetration is smaller than a threshold S_M (or $s_M=-\log_{10}S_M$). These interactions are evaluated by an Ewald type technique, after a multipole expansion of ρ_λ.

ii) a short-range set (B) of h vectors, complementary to the long-range one, whose integrals are evaluated exactly.

3.3.2.2 Exchange terms

According to eq. 3.3.21 we have:

$$X_{12}^{\mathbf{g}} = -1/2 \sum_{34\mathbf{n}} P_{34\mathbf{n}} [\, \Sigma_{\mathbf{h}} (10\ 3\mathbf{h} \mid 2\mathbf{g}\ 4\mathbf{n}+\mathbf{h})] \qquad (3.3.24)$$

The h summation can be truncated after a few terms, because the $\{1\ 3\mathbf{h}\}$ AO overlap distribution decays exponentially with h. A threshold S_X (or $s_x=-\log_{10} S_X$) can be defined for this purpose. The **g** and **n** series are again more delicate, as the convergency rate of the series largely depends on the asymptotic behaviour of the density matrix. Consider, for instance, the exchange constribution to the energy, due to the long-distance leading terms, corresponding to h=0, n=g and $\lambda=\mu,\rho=\nu$:

$$e^{g}_{\mu\nu} = -1/4\ (P^{g}_{\mu\nu})^{2}\ (\mu 0\ \mu 0 \mid \nu g\ \nu g) \approx -\ (P^{g}_{\mu\nu})^{2} / (4\ |g|) \qquad (3.3.25)$$

Since the number of terms of this kind per unit distance increases as $|g|^{d-1}$, where d is the dimensionality of the system, it is clear that the convergence of the series depends critically on the long range behaviour of the bond order matrix.

A 'pseudo-overlap' criterion is adopted, consisting in truncating the g and n summations when the overlaps between the distributions {1 2**g**} and {3 4**n**} are smaller than a given threshold P_X (or $p_x = -\log_{10} P_X$). Actually, two thresholds are defined, one for the **n** and one for the **g** summation, in order to take in account their different role in the SC procedure; this problem is discussed in details by Pisani (Pisani et al., 1988, section II.5)

3.3.2.3 Integration in reciprocal space

This problem is not present in molecular quantum problems, where eigenvalues and eigenvectors form a finite manifold and it is possible to sum over all of them.

Eigenvalues and eigenvectors are evaluated at a given set $\{\mathbf{k}_i\}$ of 'sampling' points, inequivalent by symmetry. In a 3-D lattice the sampling points belong to a net, with basis vectors $\mathbf{b}_1/s_1$, $\mathbf{b}_2/s_2$, $\mathbf{b}_3/s_3$, where $\mathbf{b}_i$ are the reciprocal lattice vectors and s_i are the sampling points of a regular net.

In the case of insulators the integrand function that appears in (3.3.17) is regular and all the bands are either fully occupied or empty. The integral is performed as a weighted sum, limited to the occupied bands, of the integrand function over the set $\mathbf{k}_i$ with weights w_i. In the case of conductors there are one or more bands partially occupied and the density of sampling points in k space must be much higher (because of the problem of determining the Fermi surface).

3.3.3 Basis set selection

The choice of the basis set used to describe the atomic species in the crystal is a very important preliminary step in a calculation. The experience gained in molecular quantum chemistry can be largely exploited: in particular the atomic core can usually be described by the standard atomic solutions (Clementi and Roetti, 1974). As regards valence shells molecular basis sets can be used as a convenient starting point. They usually perform well in the case of covalent crystals, while in the case of metallic or ionic compounds the valence must be completely redefined. Semi-ionic compounds, like most of the silicates, require particular care, and the problem will be discussed in details in Chapter 5.

In all cases diffuse Gaussian orbitals (with exponent coefficients of less than 0.15 a.u.) have a critical effect on periodic HF calculations: they cause a dramatic increase in the number of integrals that are evaluated and they increase the risk of pseudo-linear dependence. In periodic calculations, however, very diffuse AO's do not play the same important role as in molecular calculations. In the latter case they are used to describe the tails of the electronic distribution in the vacuum, which of course does not apply for infinite systems.

Many calculations have been performed using relatively poor basis sets, such as the STO-3G sets proposed by Pople and co-workers (Hehre et al., 1969, 1970; Pietro et al. 1980,1981). Split valence basis sets, such as the 6-21 G set (Binkley et al, 1981; Gordon et al, 1982) often provide accurate results, especially when the variational freedom is increased by adding polarization function in the form of d-orbitals (Hariharan and Pople, 1973; Pietro et al., 1982).

3.3.4 Calculation of observable quantities in the HF approximation

In this section we consider the ground state energy and the electronic properties that can be evaluated by CRYSTAL.

3.3.4.1 Ground State Energy

The ground state energy E_0 of a system is one of the most interesting and important parameters that can be extracted from an electronic structure calculation. Equilibrium geometries, relative stabilities of different phases, reaction paths, formation energies can be derived in terms of the variation of E_0 as a function of the internal coordinates of the system.

The total energy per cell can be expressed as a sum of kinetic (E_k), exchange (E_x) and Coulomb interaction (E_c) terms.

They can be synthetically expressed as:

$$E_k = \Sigma_{12g} P_{12}^{g} T_{12}^{g} \quad , \tag{3.3.26}$$

$$E_x = {}^1/_2 \Sigma_{12g} P_{12}^{g} X_{12}^{g} \tag{3.3.27}$$

$$E_c = E_c^{ee} + E_c^{en} + E_c^{ne} + E_c^{nn} \tag{3.3.28}$$

(where the superscripts ee, en, ne and nn refers to electron-electron, electron-nuclear, nuclear-electron and nuclear-nuclear interactions, respectively), and where T and X have been defined in equation (3.3.18, 3.3.21) and the terms in the expression of E_c correspond to the interaction between the charge distributions (nuclear and electronic) in the zero cell and the overall charge distribution throughout the crystal.

Comparison of E_0 with experimental energies requires some care. First of all the HF total energies are affected by the absence of correlation terms, as will be discussed in the next section. Furthermore we must consider the effects of incomplete basis sets, numerical approximations and, for heavy atoms,the absence of relativistic corrections. In any case, the total HF energies must be extrapolated to room temperature (or the temperature at which the experiment was carried out), the nuclear zero-point energy subtracted and the isolated atoms energies added, in order to obtain a quantity that may be compared with experimental measurements. We note that this procedure implicitly assumes the validity of the Born-Oppenheimer approximation, i.e. the separation of nuclear and electronic motion.

Problems relating to the basis set may arise when evaluating the HF binding energy. The isolated atomic energies should be evaluated to the same degree of accuracy as the total HF crystal energy. However, using the same AOs for the isolated atoms as for the crystalline species, leads to an overestimation of the binding energy, since the variational freedom is larger in the crystal, where valence orbitals are shared by a large number of neighbouring atoms. This is a well known problem in quantum chemistry, often referred to as "basis set superposition error" (BSSE). In order to correct it, the counterpoise method (Boys and Bernardi, 1970) may be used: the reference atomic energy is obtained using all AOs of that atom supplemented by the valence AOs of the surrounding atoms.

Notwithstanding these difficulties, it is often possible to compare energies of 'similar' systems, or of different geometries of the same crystal: within these limits, the errors tend, to a large extent, to cancel. It is however clear that particular care and caution are necessary when properties directly related to the energy are studied and discussed.

3.3.4.2 Physical observables: electronic properties

It is useful to recall some general and interesting results produced by the density matrix formalism applied to the problem of determining the mean value of an observable. This formalism is discussed at length in many reference books, for example in Landau and Lifshitz (1965).

The mean value of any observable that corresponds to a one-electron operator $\langle f_1 \rangle$, can be expressed in terms of the density matrix of first order:

$$\langle f_1 \rangle = \int [\, f_1(1)\, \rho_1(x_1,x_1') \,]_{x'_1 \to x_1} \, dx_1 \qquad (3.3.29)$$

where $\rho_1(x_1,x_1') = \int dx_2..dx_n \, \Psi(x_1, x_2..x_n)\, \Psi^*(x_1, x_2..x_n)$.

The mean value of any observable that corresponds to a two-electron operator f_2 can always be expressed in terms of the density matrix of second order:

$$\langle f_2 \rangle = {}^1/_2 \iint [\, f_2(1,2)\, \rho_2(x_1,x_2; x_1',x_2') \,]_{x'_1 \to x_1,\ x'_2 \to x_2} \, dx_1\, dx_2 \qquad (3.3.30)$$

Since the study of the observables of many-electron systems always refers to one- and two-electron operators, and considering that the first order density matrix can be expressed in terms of the second-order density matrix, we can conclude that the mean value of any observable can be expressed in terms of the second order density matrix of the many-electron system under study. It is interesting to note that, as a result, the amount of information contained in the multi-electronic (let say n-electron) wave-function (that, in principle, allow n-th order density matrices to be evaluated) is more than that needed to determine the

mean value of the observables in that system. This result is explained if we take into account the 'statistical' nature (mean value) of the information that is provided.

A number of properties can be evaluated using CRYSTAL. We will briefly comment on those that are used in Chapter 5 to characterize the electronic structure of silicates.

3.3.4.2.1 Band structure and Density of States (DOS)

The eigenvalues of the one-electron Fock Hamiltonian are only an approximation for the electronic spectrum of the real crystal; in particular, states that belong to the conduction band are very poorly described; band gaps and band widths are systematically overestimated. A further unsatisfactory feature is the sharp fall to zero of the density of states at the Fermi energy (Monkhorst, 1979; Delhalle and Calais 1986, 1987).

In spite of these limitations, useful information can be obtained from band structures and DOSs; projected DOSs into sets of orbitals characterize the crystalline orbitals associated with a particular band, and allow, for example, contributions to the bonds and hybridation processes to be analyzed. Projected density of states can also be compared to experimental X-ray and UV emission spectra.

The total density of states is defined as:

$$\rho(\varepsilon) = \sum_{j=1}^{p} \rho^{(j)}(\varepsilon) \qquad (3.3.31)$$

with the summation j extended over all the AOs.

By integrating the individual contributions $\rho^{(j)}(\varepsilon)$ one can obtain Mulliken band populations or total Mulliken populations (if the integration is performed up to the Fermi level).

It is well known that Mulliken populations can sometimes be misleading, being strongly dependent on the basis set and on the partition scheme adopted. However, they provide useful preliminary information about the nature of the bonding, as will be shown and discussed throughout this thesis.

3.3.4.2.2 Electron Charge Density (ECHD) and related quantities

The ground-state electron charge density $\rho(r)$ is an important observable (Coppens and Stevens, 1977) usually well described by the HF approximation. It is not greatly affected by the correlation error (that usually causes only a small expansion of anion size in highly ionic systems).

The charge density can be expressed as follows:

$$\rho(r) = \Sigma_{g,l} \Sigma_{\mu,\upsilon} [P_{\mu,\upsilon}{}^{g-l}] \chi_{\mu}{}^{g}(r) \chi_{\upsilon}{}^{l}(r) \qquad (3.3.32)$$

Charge density maps can be obtained by plotting $\rho(r)$ along a plane cutting the crystal, usually along the chemical bonds. In fact, difference maps are usually plotted where the density of a superposition of isolated ions or atoms is subtracted from the total $\rho(r)$. This procedure allows us to analyze how the charge density varies when the atoms interact and the chemical bonds are formed.

The Fourier transform of the ground state charge density provides the electronic static structure factors of the crystal, F_{hkl}. These factors can be determined by experiment, using X-ray diffraction techniques (after taking in account a number of corrective terms, like the thermal and zero-point motion of the nuclei (Dawson, 1969)). It is therefore possible to perform interesting and valuable comparisons with experiment, after Fourier transforming the calculated

ECHD. Alternatively, calculated density maps may be compared with experiment after the latter have been obtained by Fourier transforming the measured structure factors.

3.4 LIMITS OF ALL-ELECTRON HF AND HOW TO OVERCOME THEM

Two problems will be considered in this section. The first concerns the explicit inclusion of both valence and core electrons in the HF scheme, which limits the feasible calculations to systems which do not contain atoms heavier than those in the 3rd row of the periodic table; thus heavy atoms cannot be included in the unit cell. Secondly, single determinant wavefunctions do not describe the correlation between the motion of single electrons (the only form of correlation included into the HF equations corresponds to the interaction of one electron with the average distribution of the density of probability of the other electrons).

3.4.1 Pseudo-potential techniques

The absence of core electrons impairs, in principle, the quality of the calculation. Furthermore, there are cases in which the HF method is used to study core properties, like core relaxation due to the crystal field (Dovesi et al, 1982), shifts in the core levels and properties of high-pressure phases (Causa' et al, 1986). On the other hand there are indeed situations in which core electrons do not play an important role, for instance if the bonding properties of systems containing heavy atoms are under investigation. The use of core pseudo-potentials, that describe the core electrons by using an effective potential one-electon operator, appears to be a promising technique.

Particularly suitable to use in CRYSTAL are pseudo-potentials specially designed for HF calculations, such as the 'non-empirical' pseudo-potentials developed by the Toulouse group (Durand and Barthelat, 1975; Barthelat et al., 1977), or the HF 'effective core potentials', recently tabulated by Hay and Wadt

(1985). The saving factor in terms of CPU time is not very favourable as regards the evaluation of the integrals (it is $[N^4_v + N_c N_v^3]$ rather than $[(N_c+N_v)^4]$, N_c and N_v being the number of core and valence AOs, respectively). The advantage is more considerable in the SCF stage, where the order of the matrices that are manipulated reduces from (N_c+N_v) to (N_v). Pseudo potentials in CRYSTAL have been used to study, for example, spinel compounds (Mg_2SiO_4, Mg_2GeO_4, Al_2MgO_4, Ga_2MgO_4) (D'Arco et al., 1991) that would have been untreatable at the all-electron levels.

We have not employed pseudo-potentials in the calculations that are presented in this thesis though, as will be discussed in the later chapters, we believe that future works may greatly benefit from this technique.

3.4.2 Correlation corrections

The absence of a proper treatment of the electronic correlation is often considered the principal shortcomings of the HF method (Catlow and Price, 1990). A number of techniques have been developed in order to include these effects. Configuration interaction techniques, used for molecules, are not easily transferable to periodic systems; the expression of the correlation energy is not asymptotically proportional to the number of electron in the system. For all those problems where the interest is in obtaining a corrected ground state energy, the more straighforward solution is to carry out a normal HF calculation, obtaining the HF one-electron density matrix. Correlation functionals, developed in the framework of Density Functional (DF) theories, can be employed to correct the HF densities. Two schemes are at present being investigated with a view to then incorporating them into CRYSTAL. One refers to the correlation functional proposed by Perdew and Yue (Perdew and Yue, 1986; Perdew, 1986). The other

implements the non-local DF formulated by Colle and Salvetti (1975, 1979, 1983), as discussed by Causa' (Causa' et al., 1987).

REFERENCES

Andre' JM, Gouverneur L and Leroy G (1967), Int J Quantum Chem, 1, 451

Baroni S, Pastori Parravicini G, Pezzica G (1985), Phys Rev B, 32, 4077

Barthelat JC, Durand PK, Serafini A (1977), Mol Phys, 33, 159

Binkley JS, Pople JA, Hehre WJ (1980), J Am Chem Soc, 102,939

Binkley JS, Whiteside RA, Krishnan R, Seeger R, De Frees IJ, Schleger HB, Topiol S, Kahn LR and Pople JA (1981), QCPE 1981, 13,406

Boys SF, Bernardi F (1970), Mol Phys, 19,553

Brener N and Fry JL (1978), Phys Rev B, 17, 506

Callaway J (1974), Quantum Theory of Solid State part A and B, Academic Press:NY,

Catlow CRA and Price GD (1990), Nature, 6290, 243

Causa' M, Dovesi R, Pisani C, Colle R, Fortunelli A (1987), Phys Rev B, 36, 891

Causa' M, Dovesi R, Pisani C, Roetti C (1986), Phys Rev B, 33, 1308

Clementi E and Roetti C (1974), Atomic Data Nucl. Data Tables, 14,177

Colbourn EA (1989), Adv Solid State Chemistry (Ed CRA Catlow), 1,1

Colle R, Salvetti O (1975), Theor Chim Acta, 37, 329

Colle R, Salvetti O (1979), Theor Chim Acta, 53, 55

Colle R, Salvetti O (1983), JChem Phys, 79, 1404

Coppens P, Stevens ED (1977), in Lodwin OD (ed) Adv in Quantum Chem, Ac Press, NY, 1-35

D'Arco Ph, Silvi B, Roetti C, Orlando R (1991), to be printed

Dawson B (1969), Acta Cryst A, 25, 12

Del Re G, Ladik J and Biczo G (1967), Phys Rev, 155, 997

Delhalle , Calais JL (1986), J Chem Phys, 85, 5286

Delhalle , Calais JL (1987), Phys Rev B, 35,9460

Delhalle J, Harris FE (1985, Phys Rev B, 31, 6755

Dovesi R, Pisani C, Roetti R, Causa' M and Saunders VR (1988), CRYSTAL88, Program n577, Quantum Chemistry Program Exchange, Indiana

Dovesi R, Angonoa G et Causa M (1982), Phil Mag 45, 601

Durand PH, Barthelat JC (1975), Theor Chim Acta, 38, 283

Euwema RN, Surratt GT, Wilhite DL, Wepfer GG (1974a), Philos Mag, 29, 1033

Euwema RN, Wepfer GG, Surratt GT, Wilhite DL (1974b), Phys Rev B, 9, 5249

Euwema RN, Whilite DL and Surratt GT (1973), Phys Rev B, 7, 818

Gordon MS, Binkley JS, Pople JA, Pietro WJ, Hehre WJ (1982), J Am Chem Soc,104,2797

Hariharan PC, Pople JA (1973), Theor Chem Acta,28,213

Harris FE and Monkhorst HJ (1970), Phys Rev B, 2, 4400

Hay PJ, Wadt WR (1985), J Chem Phys, 82,270

Hehre WJ, Ditcgfield R, Stewart RF and Pople JA (1970), J Chem Phys,52,2769

Hehre WJ, Stewart RF and Pople JA (1969) J Chem Phys, 51, 2657

Kerker G (1981), Phys Rev B, 23, 6312

Kertesz M (1983), Electronic Structures of Polymers, Advances in Quantum Chemistry Vol 5 (NY:AcPress), pp161-214

Landau LD and Lifshitz EM (1965), Quantum Mechanics, Pergamon Press

Mainwood A, Larkins FP and Stoneham AM (1978), Solid State Electron 21, 1431

Monkhorst HJ, Pack JD, Freeman DL (1979), Solid State Comm, 29, 735

Paakkari T, Halonen V, Aikala O (1976), Phys Rev B, 13, 4602

Perdew JP (1986), Phys Rev B, 33, 8822

Perdew JP, Yue W (1986),Phys Rev ,116, 287

Pietro WJ, Levi BA, Hehre WJ, Stewart RF (1980), Inorg Chem,19,2225

Pietro WJ, Blurock ES, Hout RF, Hehre WJ, DeFrees WJ and Stewart RF (1981), Inorg Chem, 20,3650

Pisani C, Dovesi R, Roetti C (1988), Lecture Notes in Chemistry 48, Springer Verlag: Heidelberg

Stoll H and Preuss H (1975), Int J Quantum Chem, 9, 775

Surratt GT, Euwema RN and Wilhite DK (1973), Phys Rev B, 8, 4019

Wilson S (1984), Electronic correlation in molecules, Clarendon Press:Oxford

Chapter 4.
Simulation techniques and quantum chemistry methods for the study of point defects in solids

4.1 INTRODUCTION

In this chapter we shall be concerned with the computer simulation of point defects and their influence on the properties of solids. The defective system (crystal + point defect) can be considered, from a fundamental viewpoint, as a set of interacting particles (electrons and nuclei). However, depending on the nature of the solid and on the problems we want to investigate, we can develop techniques to simulate the system by semi-classical models based on interatomic potentials, as is done in many fields of computational chemistry and physics. These simulation methods are well established in the study of ionic and semi-ionic materials and can be translated into computer codes that are straightforward to use. Moreover interatomic potentials for many different systems have been optimized and listed (Catlow and Mackrodt, 1982; Lewis and Catlow, 1985) and simulation techniques have been employed to study topics ranging from classical solid state problems, such as bulk defect properties of alkali halides to those in biological sciences, e.g. protein conformation. However, although this approach is adequate for solving a large number of problems, there are several obvious shortcomings implicit in its basic assumptions: in particular, to describe the behaviour of the electrons we need a more sophisticated model, that explicitly takes into account the electronic wave-function; that is, quantum mechanical techniques are needed.

In the following section we shall first describe and compare some of the "standard" techniques available for the study of point defects in solids. We will refer to the CASCADE code (Leslie, 1981) as an example of a successful implementation of semi-classical modelling techniques and we will review possibilities and shortcomings of "standard" techniques available in quantum chemistry, that is the cluster and the super-cell methods. Then, in section 4.2, we discuss the embedding approach, the study of which is a major component of this thesis, and its possible formulations, i.e. the perturbed host system and the perturbed cluster approach. The general assumption of all these methods, is that the presence of the defect perturbs only a finite region of the host crystal, where all the effects of the defect (geometrical relaxation, charge transfer and polarization effects) are confined.

In section 4.3 we will present the perturbed-cluster embedding technique developed and used in this study ; the theory, and its implementation in the form of a computer code (EMBED) will be reviewed and discussed. The development of EMBED has been an important part of this research work, pursued in collaboration with Prof. C. Pisani at the University of Turin, Italy.

This method yields unsatisfactory results when charged defects are considered: the problem of defining the defect charge states is discussed. The treatment of the long-range polarization effects induced by charged defects is considered in section 4.5. A new technique, that allows the polarizability of the medium to be described within a classical framework in EMBED , is presented, together with a number of suggestions to deal with the "charge problem". The structure of a new code (EMBRYON) that implements these techniques is finally described.

4.2 COMPUTATIONAL TECHNIQUES FOR THE STUDY OF POINT DEFECTS

We will consider first the case of ionic crystals, in which we create vacancy, interstitial or substitutional defects. We are interested in the properties of the ground state, and specifically in the energy as a function of the atomic coordinates, which is needed to predict the equilibrium configuration of the atoms surrounding the defect and its formation energy. This information also yields the vibrational frequencies of the local modes associated with the defect, reaction paths and reaction barriers and the relative stabilities of different configurations. We also wish to study the charge distribution in the defect region, that may clarify the nature of the bonding and the nature and degree of localisation of the defect states.

4.2.1 Simulation Methods

These techniques consider the system to be composed of point ions interacting via two- and three-body potential energy functions.They have enjoyed considerable success in both qualitative and quantitative studies of defect processes by providing a reliable and accurate estimate of relaxation effects and formation energies in the case of ionic and semi-ionic crystals (Catlow and Mackrodt, 1982). The approach is largely limited to ionic and semi-ionic materials, and cannot be used to study defects in a covalent material, where chemical bonds can be broken (although the methods could be used to study for example closed shell interstitials in covalent solids), and of course no information is provided about the electronic distribution. A successful example of the

implementation of these techniques is provided by the program CASCADE (Leslie, 1981).

According to the scheme adopted by CASCADE the defective crystal is described by surrounding the defect with an inner region, that contains a finite number of ions that are allowed to move until the forces on them are zero, i.e. until they reach a minimum energy configuration, which is treated atomistically; and an outer region that extends to infinity, containining ions whose positions are calculated using the Mott-Littleton approximation (1938).

The total energy of the system is the sum of three contributions:

$$E = E_1(\underline{x}) + E_2(\underline{x},\underline{z}) + E_3(\underline{z}) \qquad (4.2.2)$$

where E_1 is the energy of region I, E_3 is the energy of region II and E_2 is the interaction energy between the two regions. $\underline{x}$ are the coordinates of the ions in region I and $\underline{z}$ are the vectors of the displacements of the ion in region II.

$E_3(\underline{z})$ is assumed to be a quadratic function of $\underline{z}$; thus:

$$E_3(\underline{z}) = 1/2\ \underline{z}^T \cdot \mathbf{A} \cdot \underline{z} \qquad (4.2.3)$$

where A is the force constant matrix, and the superscript T indicates the transpose.

Using the equilibrium condition:

$$\partial E/\partial \underline{z} = \partial E_2(\underline{x},\underline{z}) / \partial \underline{z} \Big|_{z=z'} + \mathbf{A}\cdot\underline{z} = 0 \qquad (4.2.4)$$

where $\underline{z}'$ are the equilibrium values for the $\underline{z}$, we can rearrange E as:

$$E = E_1(\underline{x}) + E_2(\underline{x},\underline{z}) - 1/2\ \partial E_2 / \partial \underline{z}\Big|_{z=z'} \cdot \underline{z}' \qquad (4.2.5)$$

With this expression an important formal result has been achieved, i.e. we have expressed the total energy without including the explicit expression for E_3, which formally extends to infinity. Equation (4.2.5) is expressed only in terms of interactions between pairs of ions in region I and terms involving the potential interaction of region I and II. The simplest approach is to assume the potential to be central (three body interactions can be included by the addition of angular dependent terms) and the ions to be unpolarized (techniques can then be introduced to describe dipolar distortions (Dick and Overhauser, 1958) so that the electrons are modelled by a massless shell coupled to the core, which is given the mass of the total ion. The interaction is assumed to be harmonic. The 'shell model' is thoroughly reviewed in J. Chem.Soc. Faraday Trans. II, 1989, ed. Catlow CRA, Stoneham AM, page 85).

Short range interactions are described by means of interatomic potentials, that include electron-electron repulsion and electron exchange correlation, whose expressions and properties have been discussed at length, for example in Catlow and Mackrodt (1982).

Here we are more interested in discussing the treatment of the Coulomb potential, that is relevant for the discussion of charged defects in section 4.5. In order to evaluate the contribution to the energy due to the interactions between the outer and the inner region we separate off the interactions between explicit ions in a finite region of the crystal and describe the remaining long range part by means of a Madelung potential; the latter terms are handled analytically using an Ewald's summation (see Appendix E). Therefore region II is actually subdivided into two

sub-regions, IIa and IIb. In region IIa the terms arising from interactions of the ions with those in region I are calculated explicity. Region IIb (that extends to infinity) is treated as a dielectric continuum interacting with the effective charge of the defect (assumed to be a point charge positioned at the centre of the cluster), so that there is no interaction with displacement dipoles in region I.

This method is valid only when the sizes of region I and IIa are large enough to justify the approximations; in other words, when any increase of the region sizes has a negligible effect on the defect energy.

4.2.2 Quantum Mechanical Methods

To take explicit account of the electronic distribution, and the ways in which it is modified by the defect, one must solve the Schroendiger equation for the defective crystal. The "standard" ab-initio HF techniques available in quantum chemistry for the study of molecules and periodic crystals (i.e. the molecular HF and the periodic HF) can be applied to the simulation of lattice defects. We will focus on these techniques in the following discussion.

In the 'Cluster Approach' an isolated molecule is used, containing the defect and reproducing the local environment of the host crystal (Simonetta, 1986; Colbourn and Mackrodt, 1984; Shangda et. al., 1989).

Although widespread, the method suffers from the obvious implicit shortcomings of the model: the crystal field is not correctly reproduced and the periodic nature of the host lattice is not included in the model; surface states associated with dangling bonds introduce unphysical features that can be only partially corrected by terminating the cluster with hydrogen atoms (Surratt and Goddard, 1978; Kenton and Ribarsky, 1981). The convergence with cluster size is usually very slow, and depends not only on the size but also on the shape of the cluster adopted.

In ionic crystals the problems associated with dangling bonds are less important, and the electrostatic field generated by the rest of the crystal can be simulated by surrounding the cluster with a lattice of point ions that generate the correct Madelung field (Almlof and Wahlgren, 1973). A similar method has been applied, for example, to the study of defects in MgO (Grimes at al., 1989). A different approach is adopted by Barandiaran and Seijo (1988). Their formulation considers the solution for a cluster taking into account its interactions with a "frozen" crystalline environment within the lattice model potential approximation (Bonifacic and Huzinaga, 1974), so that the multi-electron wavefunction of the whole system can be factorized in the product of the cluster wave-function multiplied by the wave-functions of the external closed-shell ions.

A further improvement of the cluster method is the inclusion of the polarizability of the outer medium, by interfacing the QM cluster with the Mott-Littleton methodology. A successful example of this approach is the ICECAP code (Vail et al., 1984; Harding et al. 1985), where the HF equations are solved for a molecular cluster embedded in a crystalline lattice of point ions, whose positions are allowed to relax around the defect. The response of the lattice outside the cluster is calculated using the Mott-Littleton theory, including ion polarization effects described by the shell model. A self-consistent process guarantees that the matching of the quantum cluster with the outer region is correctly performed. The localizing potential developed by Kunz and Klein (1987) is adopted in order to avoid the spreading of the N-electron cluster wave-function into the outer lattice (Vail, 1990). Such spreading is undesirable, since there are no electrons in the sites outside the cluster, that are not treated quantum mechanically. ICECAP has been used to characterize electronic defects and impurities in alkali halides and MgO (Vail, 1990), (Shluger et al., 1991).

As an alternative to the cluster approach, periodic boundary conditions can be imposed, to create a "superlattice": each unit cell contains the defect, and it is large

enough to minimize the interaction between neighbouring defects. This technique is very effective when the perturbation generated by the defect is small and localized as, for instance, in the case of chemisorbed molecules on a surface. A recent study of impurities in silicon (Nichols et al, 1989) has shown that even more complicated defects can be accurately treated. This method is less adequate for treating defects that induce long range relaxation processes and charged defects that generate long-range Coulombic fields; it has been suggested that a compensating field corresponding to a uniform charge distribution can be superimposed in order to make charged states treatable by the supercell approach (Bar-Yam and Joannopoulos, 1984).

An alternative is to employ again a partitioned scheme, by dividing the crystal in two regions, both described quantum-mechanically. The problem is then reduced to two simpler ones: the solution for the periodic, defect-free, infinite host lattice and the description of the finite region surrounding and containing the defect. The aim of these 'embedding' techniques is to obtain the correct solution for the cluster region, including all the interactions with the host lattice (short range exchange and Coulomb interactions, Madelung field, polarization effects etc.).

A first route to the solution of this problem is the Koster-Slater technique (Koster and Slater, 1954; Baraff and Schluter, 1984), that may be classified as a "perturbed host system" (PHS) embedding scheme; the Green function in the defect region is evaluated in the framework of the perturbation theory, taking as a reference the host crystal Green function, after assuming that the Hamiltonian matrix remains unchanged outside a localized defect region. As an alternative, a "perturbed cluster" (PC) scheme can be used: in this case the starting point is the solution for a molecular cluster, to which corrections are applied in order to remove boundary and limited size effects and ensuring the correct matching with the surrounding perfect crystal.

An essential prerequisite for the application of both the PHS and PC techniques, is the availability of the solution for the perfect host crystal, obtained with the same Hamiltonian and the same computational techniques (basis set, numerical accuracy etc.) as employed for the defect region.

The following discussion will first show and discuss the PHS and the PC embedding equations. We also comment on an alternative scheme proposed by Inglesfield. In section 4.4, we shall concentrate on the latest formulation of the PC equations, that will be employed in this work; the solution for the perfect host crystal will be provided by CRYSTAL, as discussed in Chapter 3.

4.3 METHODS OF EMBEDDING

4.3.1 Notation

We wish to introduce a formalism that can be used in the rest of the discussion. Such a formalism must employ a synthetic notation, general enough to be used to discuss different theoretical methods. The problem of adopting a general and yet unambiguous language is indeed not trivial and has been considered, for example, by Ballantine and Kolar (1986) who proposed a very elegant notation that should enable the matrix relations to be written in an unambiguous way. Here we will use, for consistency, the conventions that have been adopted in a number of recent papers (for example Pisani et. al., 1990). Special care is necessary when one refers to semi-classical simulation techniques (i.e. CASCADE), where the similar sub-division in"zones" corresponds, in fact, to different concepts and assumptions; for example, semi-classical methods define a "region" in terms of the number of atoms within a sphere of a given radius, centred on a chosen origin. A quantum mechanical method will rather use the concept of probability functions that decay more or less rapidly with the distance from the origin; the actual extension of the "cluster", e.g. the spatial region where an electron associated with an atom included in the "perturbed" region can be found, will go beyond the actual position of the border atoms in the inner region.

The defective system is described by a non-orthogonal set $\{\chi\}$ of real, local functions that are expressed as a linear combination of GTOs centred at the nuclear positions. Three different and complementary sub-sets can be defined, so that $\{\chi\} \equiv \{\alpha\} \cup \{\beta\} \cup \{\delta\}$.

$\{\alpha\}$ is the subset that describes the proper defective region A, e.g. impurity atoms that are introduced or perfect crystal atoms that are displaced from their original position;

$\{\beta\}$ is the subset used to describe a finite "border" region B, that surrounds A, including perfect crystal atoms that are not displaced but that are assumed to be perturbed by the defect;

$\{\delta\}$ describes all the other atoms of the host, perfect and infinite lattice (region D).

The subset $\{\gamma\} = \{\alpha\} \cup \{\beta\}$ defines a cluster region C; this corresponds to the hypothesis that the effects of the perturbation are essentially confined in the cluster region. As we will see below, some methods allow us to take in account, at least in part, perturbation effects in the outer region D.

We can also analogously define, for the perfect lattice, a set

$$\{\chi\}' \equiv \{\alpha'\} \cup \{\beta\} \cup \{\delta\}$$

where $\{\alpha'\}$ is the subset that describes the perfect crystal atoms that are removed to be substituted (in the case of an impurity or of a lattice vacancy) or displaced from their original positions (in the case of lattice relaxation). A subset $\{\gamma'\} \equiv \{\alpha'\} \cup \{\beta\}$ defines the cluster region C', that contains only unperturbed atoms.

This notation allows a partitioned matrix formalism to be used. For example T_{CD} is the CD block of the matrix T, and comprises elements $\gamma\delta$ with γ in C and δ in D.

A superscript "f" (free) will identify a matrix that refers to the host unperturbed crystal; for instance H_{DD}^{f} and H_{DD} are the DD blocks of the

Hamiltonian matrix before and after the defect is created, respectively. S will indicate the overlap matrix ($S_{\sigma\rho} = \langle\sigma|\rho\rangle$) and G(z) the Green matrix, defined as the inverse of Q(z) = (zS - H), where z is an energy point that lies in the complex plane with nonzero imaginary part, and therefore not coinciding with any of the energy eigenvalues either of the perfect or of the defective crystal.

4.3.2 Expressions for the embedding equations

4.3.2.1 Perturbed Host Crystal (PHS)

For simplicity we adopt the same basis set for C and C', as the equations become considerably more complicated in the general case, as discussed by Pisani et al. (1983)

The Hamiltonian matrix for the defective system can be written as:

$$H = H^f + V \qquad (4.3.1)$$

where V is a matrix that contains the information relative to the perturbing field generated in C by the defect, that we assume to be zero outside C:

$$V = H - H^f = Q^f - Q \qquad (4.3.2)$$

and, in a partitioned form:

$$V = \begin{bmatrix} V_{CC} & O_{CD} \\ O_{DC} & O_{DD} \end{bmatrix} \qquad (4.3.3)$$

Due to the structure of V, the Dyson's equation becomes:

$$G_{CC} = G^{f}_{CC} + G^{f}_{CC}\, V_{CC}\, G_{CC} \qquad (4.3.4)$$

$$\text{so that } G^{f}_{CC} = [\, I_{CC} - G^{f}_{CC} V_{CC} \,]\; G_{CC} \qquad (4.3.5)$$

After having introduced a *multiplicative corrective operator*

$$J_C(z) = [\, I_{CC} - V_{CC}\, G^{f}_{CC}(z) \,]^{-1}$$

we have:

$$G_{CC} = J_{CC}\; G_{CC}{}^{f} \qquad (4.3.6)$$

In this form of the Koster and Slater (1954) equation, J_{CC} is an operator that restores the correct Green function when it is applied to the solution for the host crystal projected onto the cluster region G^{f}_{C}.

4.3.2.2 Perturbed Cluster (PC)

The H matrix can be written in a form that makes explicit the partition between the cluster region and the correction introduced in order to couple C to the indented lattice :

$$H = \begin{bmatrix} H_{CC} & 0_{CD} \\ 0_{DC} & 0_{DD} \end{bmatrix} + \begin{bmatrix} 0_{CC} & H_{CD} \\ H_{DC} & H_{DD} \end{bmatrix} \qquad (4.3.7)$$

where $H_{CD} = \tilde{H}_{DC}$

Note that we are not assuming here that $H_{DC}=H_{DC}^{f}$

In this case we describe the perturbation in terms of the interaction between the isolated cluster containing the defect, described by H_{CC}, and the indented system.

From the identity $Q(z)\,G(z) = G(z)\,Q(z) = I$, we have:

$$G_{DC}\,Q_{CC} = -\,G_{DD}Q_{DC} \qquad (4.3.8)$$

$$Q_{CC}\,G_{CC} = I_{CC} - Q_{CD}G_{DC} \qquad (4.3.9)$$

We can also define, for a general complex z value, the finite cluster Green matrix:

$$\underline{G}_{CC} = [\,Q_{CC}(z)\,]^{-1} \qquad (4.3.10)$$

that is calculated after solving the molecular problem for the cluster

$$\underline{F}_{CC}\,\underline{V}_{CC} = \underline{S}_{CC}\,\underline{V}_{CC}\,\underline{E}_{CC} \qquad (4.3.11)$$

where $\underline{F}_{CC}$ is the submatrix of the Fock matrix corresponding to the defective crystal (so that it includes already the correct crystalline field acting on the cluster).

Multiplying (4.3.8) and (4.3.9) by $\underline{G}_{CC}$ we obtain:

$$G_{DC} = -\,G_{DD}\,Q_{DC}\,\underline{G}_{CC} \qquad (4.3.12)$$

$$G_{CC} = \underline{G}_{CC} - G_{CC}Q_{CD}G_{DC} = \underline{G}_{CC} - \underline{G}_{CC}\,Q_{CD}\,G_{DD}\,G_{DC}\,\underline{G}_{CC} =$$
$$\underline{G}_{CC}\,(1 - Q_{CD}G_{DD}Q_{DC}\,G_{CC}) = \underline{G}_{CC}\,J_{CC}' \qquad (4.3.13)$$

where $J_{CC'} = (1 - Q_{CD} G_{DD} Q_{DC} \underline{G}_{CC})$ (4.3.14)

4.3.2.3 The Inglesfield method

An alternative approach was proposed by Inglesfield (1981), who proposed a method of performing embedding calculations in real space. The inner region (I), where the Schroendiger equation is solved, is separated from the outer region (II) by a surface S. If G_{OE} is a Green function satisfying:

$$[-1/2 \nabla_r^2 + V(\mathbf{r}) - E] G_{OE} (\mathbf{r},\mathbf{r}') = \delta^3 (\mathbf{r}-\mathbf{r}') \quad (4.3.15)$$

with **r** and **r'** in II.

It is possible to define an embedding potential Σ_E by:

$$\Sigma_E (\mathbf{r}-\mathbf{r}') = G_{OE}^{-1} + 1/2 \int_S d^2 \mathbf{r}_s \, G_{OE}^{-1} (\mathbf{r}-\mathbf{r}_s) (\partial/\partial n_s) G_{OE} (\mathbf{r}_s,\mathbf{r}') \quad (4.3.16)$$

where G_{OE}^{-1} is the inverse of G_{OE} calculated over the surface S:

$$\int_S d^2 \mathbf{r}_s \, G_{OE}^{-1} (\mathbf{r}-\mathbf{r}_s) G_{OE} (\mathbf{r}_s,\mathbf{r}') = \delta^2 (\mathbf{r}-\mathbf{r}') \quad (4.3.17)$$

with **r** and **r'** on S; $(\partial/\partial n_s)$ represents the normal derivative at S in the direction outwards from region I into region II. Σ_E does not depend explicitly on the Hamiltonian thoughout region I, but only on the properties of G_{OE} at the surface.

This embedding potential has the properties that the normal derivative at the surface S of any function ψ satisfying the Schroendiger equation in region II with eigenvalue E, is given in terms of the values of ψ on S by the integral:

$$\partial\psi/\partial n_s(\mathbf{r}_s) = 2\int_S d^2\mathbf{r}_s'\, \Sigma_E(\mathbf{r}_s,\mathbf{r}_s')\,\psi(\mathbf{r}_s') \qquad (4.3.18)$$

with $\mathbf{r}_s$ on S.

This may also be regarded as a boundary condition to be satisfied on S by solutions of the Schroendiger equation in the full space I+II, to ensure that the values and normal derivatives of the wavefunction are continuous at the surface. Such constraints can be incorporated automatically by including the embedding potential and a normal derivative term in the Schroendiger equation for region I alone, which becomes:

$$[-1/2\nabla_r^2 + 1/2\delta(n-n_s)\partial/\partial n_s + V(\mathbf{r})]\,\psi(\mathbf{r}) - \delta(n-n_s)\int_S d^2\mathbf{r}_s\,\Sigma_E(\mathbf{r},\mathbf{r}_s)\,\psi(\mathbf{r}_s) =$$

$$= E\,\psi(\mathbf{r}_s) \qquad (4.3.19)$$

with $\mathbf{r}$ in I or on S .

The advantage of this method is that the inverse of the Green function is required only on the surface S and not throughout region I.

4.4 THE PC APPROACH AND THE "EMBED" PROGRAM

In the following sub-sections we will discuss an ab-initio HF PC embedding scheme and its practical implementation in the form of a FORTRAN computer code.

4.4.1 Derivation of the PC equations used in "EMBED"

The PC equations obtained in the previous section are:

$$G_{DC} = - G_{DD} Q_{DC} \underline{G}_{CC} \qquad (4.4.20)$$

$$G_{CC} = \underline{G}_{CC} - G_{CC}Q_{CD}G_{DC} = \underline{G}_{CC} - \underline{G}_{CC} Q_{CD} G_{DD} G_{DC} \underline{G}_{CC} =$$

$$\underline{G}_{CC} (1 - Q_{CD}G_{DD}Q_{DC} G_{CC}) = \underline{G}_{CC} J_{CC}' \qquad (4.4.21)$$

Using the explicit expression for the general element $\underline{G}_{\mu\nu}$ of $\underline{G}_{CC}$:

$$\underline{G}_{\mu\nu}(z) = \sum_j \underline{v}_{\mu j} \underline{v}_{\mu j}^{*} / (z-\underline{e}_j) \qquad (4.4.22)$$

(where $\underline{e}_j$ are the cluster pseudo-eigenvalues, and $\underline{v}_{\mu j}$ the corresponding eigenvectors, obtained by diagonalizing the F_{CC} block of the Fock matrix) and the identity:

$$Q(z) \equiv zS - F = Q(e) + (z-e) S \qquad (4.4.23)$$

we can make explicit the dependence of G_{CC} and G_{CD} on z:

$$G_{CD}(z) = -\Sigma_j A^j G_{DD}(z) / (z-\underline{e}_j) - BG_{DD}(z) \qquad (4.4.24)$$

$$G_{CC}(z) = \Sigma_j \{ R_{CC}{}^j + [A^j G_{DD}(z) \tilde{A}^j] / (z-\underline{e}_j) + \\ + A^j G_{DD}(z) \tilde{T}^j + T^j G_{DD}(z) \tilde{A}^j \} / (z-\underline{e}_j) + B^j G_{DD}(z) \tilde{B}^j \qquad (4.4.25)$$

Where some auxiliary matrices have been defined:

$$B = (S_{CC})^{-1} S_{CD} \qquad (4.4.26)$$

$$A^j = | v_j >< v_j | (\underline{e}_j S_{CD} - F_{CD}) \qquad (4.4.27)$$

$$T^j = \Sigma_{m \neq j} A^j / (\underline{e}_j - \underline{e}_m) + B \qquad (4.4.28)$$

Equations (4.4.24) and (4.4.25) are defined only in terms of the perfect crystal Green matrix G_{DD} and of the auxiliary matrices defined above.

For a given real energy value E, not coinciding with any of the isolated impurity levels of the defective crystal, these equations allow us to calculate the corresponding integrated density of states (IDOS) $N_{CD}(E)$ and $N_{CC}(E)$. The general relationship can be used:

$$N(E) = -1/(i\pi) \int_{\gamma(E)} dz\, G(z) \qquad (4.4.29)$$

where γ is a path in the complex plane that encloses all poles and analytical cuts of G(z) with energy $e < E$. The integral is solved as discussed in Appendix B. If E coincides with the Fermi level (E_F), the equation (4.4.29) yields the density matrix:

$$P_{CD} = -\Sigma_j A^j M_{DD}(\underline{e}_j) - BP_{DD} \qquad (4.4.30)$$

$$P_{CC} = \Sigma_j [\Theta(e-E_F) R_{CC}{}^j + A^j M_{DD}(\underline{e}_j) \tilde{A}^j + A^j M'_{DD}(\underline{e}_j) \tilde{T}^j + \\ T^j M_{DD}(\underline{e}_j) \tilde{A}^j] + B^j M_{DD}(\underline{e}_j) \tilde{B}^j \qquad (4.4.31)$$

Where M and M' are energy dependent complex matrices for which both indices belong to the outer region D that depend on the density of states in the outer region D (see equation B4 and B5):

$$M_{DD}(e) = \Theta(e-E_F)\int_{-\infty}^{E_F} d\varepsilon\, \rho_{DD}(\varepsilon) / (\varepsilon-e) - \Theta(E_F-e)\int_{E_F}^{\infty} d\varepsilon\, \rho_{DD}(\varepsilon) / (\varepsilon-e) \qquad (4.4.32)$$

$$M'_{DD}(e) = \partial M(e) / \partial e \qquad (4.4.33)$$

The integral that appears in (4.4.32) is discussed in Appendix C.

Equations (4.4.30) and (4.4.31) are exact. They include all the interactions between the defective region and the indented system, including polarization of the medium, charge transfer between C and D and long range Coulomb effects.

Their solution requires some approximation to be introduced, in order to reduce the problem to one of finite dimensions (at present no assumption has been made on the block DD of the density matrix, density of states etc.). For this purpose, we shall take advantage of the fact that the projected DOSs in the D region (indented crystal) are likely to be only marginally affected by the presence of the defect: this assumption is asymptotically exact in the limit of an increasingly large cluster C and satisfies our initial intention of studying defects whose perturbation is localized.

Thus the key assumption of our method is that we can substitute in equations (4.4.32), (4.4.33) $\rho_{DD}(\varepsilon)$ *with the corresponding quantity for the unperturbed host crystal* $\rho^{f}_{DD}(\varepsilon)$.

The latter is calculated by CRYSTAL. Thus:

$$P_{DD} = P^{f}_{DD} \tag{4.4.34}$$

$$M_{DD}(e) = M^{f}_{DD}(e) \tag{4.4.35}$$

These are the only approximations that are adopted in the present scheme. Their substitution in equations (4.4.30) and (4.4.31) gives the P_{CD} and P_{CC} blocks of the density matrix:

$$P_{CD} = -\Sigma_j A^j M^f(\underline{e}_j) - BP^f = P^{COUP}_{CD} + P^{CONST}_{CD} \tag{4.4.36}$$

$$P_{CC} = \Sigma_j [\Theta(e-E_F) R_{CC}{}^j + A^j M^f(\underline{e}_j) \tilde{A}^j + A^j M'^f(\underline{e}_j) \tilde{T}^j +$$

$$= T^j M^f(\underline{e}_j) \tilde{A}^j] + B^j M^f(\underline{e}_j) \tilde{B}^j = P^{CLUST}_{CC} + P^{COUP}_{CC} + P^{CONST}_{CC} \tag{4.4.37}$$

In equation (4.4.37) we note first the term P^{CLUST}_{CC}, that corresponds to filling all cluster eigenvalues up to the Fermi energy. This term must be corrected to include the interactions with the indented crystal (i.e. to "embed" the cluster). The term P^{CONST}_{CC} gives account of the effects of the non-orthogonality between AOs belonging to the C and D set, and is zero in the case of orthogonal sets; it is not redefined during the SCF procedure. The other corrective term, P^{COUP}_{CC}, depends on the position of the cluster eigenvalues with respect to the manifold of the host crystal one-electron eigenvalues, and realizes the "chemical" coupling between C and D. In this form, the "perturbed cluster" character of the scheme is fully evident.

Since the P matrix of the defective crystal is now completely defined by equations (4.4.36), (4.4.37), we can calculate the Fock matrix blocks F_{CC} and F_{CD}, hence obtain $\underline{e}_j$, R_{CC}, A^j, T^j and, then, the new P_{CC} and P_{CD} matrices

and repeat the calculation up to self-consistency. The procedure is discussed in the following subsection.

4.4.2 Implementation of the PC equations used in "EMBED"

The important issues in implementing our approach are as follows:

4.4.2.1 The general structure of the matrices

Three types of matrices appear in the embedding equations: first, matrices that contain information about the perfect host lattice (i.e. M and M'). The generic element of this matrices will have both the indexes in the D region, so that we will refer to them as (D.D) matrices. They show the full translational symmetry of the periodic lattice. Accordingly, a generic atomic orbital is identified by its position in the primitive cell and by the translational **g** vector associated with the cell to which it belongs. For simplicity let us consider an ideal lattice with only one atomic orbital per unit cell. The generic matrix element $M_{\mu\nu}$, with the AO μ belonging to a cell identified by a translational vector **s** and ν to a cell identified by a vector **t** will be the same, for all pairs of cells identified by the same **(t-s)**. This consideration reduces the range of these matrices, although they remain, in principle, infinite: if the first index is an atomic orbital ν in the primitive cell (**g**=0), then an infinite number of elements $M_{\nu\mu}$ is defined , where μ are all the other AOs in the crystal.

Truncation criteria must then be adopted, following the criteria discussed in section 3.2.2. If the overlap between the two adjoined Gaussians (see 3.2.1) corresponding to μ and ν , is below a given threshold, then the matrix element $M_{\mu\nu}$ is neglected. In this way the matrices (D.D) are reduced to a finite number of elements.

Next we consider matrices containing purely "cluster" information, e.g. the cluster Fock matrix F_{CC}. Their dimensions are $N_C * N_C$, where N_C is the number of atomic orbitals in the C region. Therefore these matrices have finite dimensions as, by definition, C is a finite, well localized region and there are no problems with their manipulation.

Thirdly, we have the matrices that contain information about the interaction between the cluster and the indented host crystal. For example the density matrix has elements $P_{\mu\nu}$ with μ in C and ν in D.These matrices are, in principle, infinite, since the number of atomic orbitals in D is infinite. Therefore we must define a sub-ensemble of D that defines a finite set of AOs in the outer region that interact with at least one of the AOs in C. This can be done by adopting a criteria based on the overlap of adjoined Gaussians (as was discussed in Chapter 3), to define which AOs in D interact with the inner region. An "active" region D^* containing N_{D*} AOs is so defined, and the total, finite dimension of the density matrix is $(N_C * (N_C+N_{D*}))$. We will sometimes refer to the complementary, non-active, region as to D^-, so that $[D^- \bigcup D^* \equiv D]$.

We note the different levels of approximation that have been introduced: first formally exact expressions have been derived, using a concise mathematical formalism (equations 4.4.30 and 4.4.31). Then the (4.4.34) and (4.4.35) have been assumed to be correct, in the limit of a localized perturbation. This approximation corresponds to using a simplified physical model to reduce the complexity of the problem. It is qualitatively similar to the assumption that the electrons move in the average field generated by the nuclei, or that relativistic effects can be neglected. It expresses the necessity of an interpretative formal model (by necessity approximate) to describe the underlying "reality".

The further approximations introduced in this subsection are of a different nature: they are not directly due to the physical model we have adopted, but rather to the way we have chosen to test (or, according to Popper, to invalidate) the model itself. The implementation of the theory into a computer code requires the

theory itself to be re-formulated in a different language, whose structures (or rather their rigidity) can and will reduce the generality of the formulation.

4.4.2.2 The Fock matrix of the defective crystal

In calculating the Fock matrix blocks F_{CC} and F_{CD} that enter directly or indirectly into equations (4.4.30) and (4.4.31), one must be sure that the approximations adopted, e.g. the truncation criteria, are as similar as possible to those used in the solution of the perfect host crystal problem. This is an essential prerequisite for the PC equations to provide the correct result $P_{CD} = P^{f}_{CD}$, $P_{CC} = P^{f}_{CC}$, in the limiting case where the defective crystal coincides in fact with the perfect crystal (self-substitution case: see below). The expression of the Fock matrix adopted in CRYSTAL was discussed in section 3.2.2. In this section we will adopt the same notation, with the difference that matrix elements will be identified by Greek letters (e.g. $F_{\gamma\mu}$ rather than by the notation used in Chapter 3 (F_{12})) in order to note the fact that, in the matrices that refer to the defective solid, the translational symmetry is lost; reference will usually be made to the "region" an AO belongs to, and not to the translational **g** vector associated with it.

Because of the truncation conditions listed above, terms $S_{\gamma\mu}$ or $F_{\gamma\mu}$ are different from zero only for μ belonging to C or to the finite subset D^* of the indented crystal. We can distinguish a constant part of the F matrix, F^{const}, that remains unchanged during the self-consistency cycle, and a variable part, F^{var}, that does not. F^{const} comprises not only kinetic and nuclear attraction terms, but also those P-dependent (exchange or Coulomb) terms, where the P terms have indices that refer both to the D set.

We may write:

$$F = F^{const} + F^{var} \qquad (4.4.38)$$

where:

$$F^{const}_{\gamma\mu} = T_{\gamma\mu} + Z^{sr}_{\gamma\mu} + \Sigma^{sr}_{\sigma,\tau\notin C} P^{f}_{\sigma\tau} [(\gamma\mu|\sigma\tau)] +$$

$$+ V^{Mad}_{\gamma\mu} - \Sigma^{sr}_{\sigma,\tau\notin C} P^{f}_{\sigma\tau} [1/2 (\gamma\sigma|\mu\tau)] \qquad (4.4.39)$$

$$F^{var}_{\gamma\mu} = \Sigma^{sr}_{\sigma,\tau\ (\sigma\text{ or }\tau\in C)} P^{f}_{\sigma\tau} [(\gamma\mu|\delta\tau) - 1/2 (\gamma\sigma|\mu\tau)] \qquad (4.4.40)$$

In (4.4.39) $V^{Mad}_{\gamma\mu}$ is the term that corresponds to the long range Coulomb interactions, described by a Madelung potential and the sums Σ^{sr} are limited to terms belonging to "short-range" nuclear or electronic distributions, selected in a way analogous to that discussed in 3.3.2 with reference to the treatment of the Coulomb terms in CRYSTAL.

4.4.2.3 Defect formation energy

To calculate the formation energy of the defect, ΔE, we consider the formal reaction:

Perfect Crystal + [Inserted atoms] ——>

——> Defective Crystal + [Displaced atoms] + ΔE (4.4.41)

Some of the terms in square brackets may be absent. For instance, in the case of a vacancy, there are no "inserted atoms", nor are there "displaced atoms" in the case of an interstitial impurity. We can now write:

$$\Delta E = \Delta E^{cry} + \Delta E^{at} \qquad (4.4.42)$$

$$\Delta E^{cry} = E^{perfcry} - E^{defcry} \qquad (4.4.43)$$

$$\Delta E^{at} = \Sigma_{(inserted\ atoms)}\ E^{at} - \Sigma_{(displaced\ atoms)}\ E^{at} \qquad (4.4.44)$$

ΔE^{cry} and ΔE^{at} are total energies, that refer to all the crystal. In order to obtain a manageable expression for ΔE^{cry}, we first write formally the expression for E^{defcry} (and a corresponding one for $E^{perfcry}$):

$$E^{defcry} = 1/2 \sum_{\nu\mu} P_{\nu\mu}(T_{\nu\mu} + Z_{\nu\mu} + F_{\nu\mu}) + E^{repnu} \qquad (4.4.45)$$

where E^{repnu} is the Coulomb repulsion between nuclei. We next note that in the two expressions, the overwhelming majority of terms coincide if account is taken of equation (4.4.34) and if it is assumed that $F_{\nu\mu}=F^{f}_{\nu\mu}$ when both ν and μ belong to D. We shall therefore consider in the following finite pseudo-HF-energies E'^{defcry} and $E'^{perfcry}$, which contain only those terms that do not coincide in the two expressions. The difference

$$\Delta E^{cry} = E'^{perfcry} - E'^{defcry} \qquad (4.4.46)$$

gives the required value *provided that* exactly the same approximations (host-crystal basis set, definition of the indented crystal, truncation criteria, etc.) are adopted in the two calculations, the first one referring to the defective system, the second one to the perfect, but pseudo-defective crystal.

We can distinguish in E' a kinetic (T'), an exchange (E'_{ex}), and a Coulomb contribution (E'_{c}); the latter includes all electron-electron, electron-nuclei, and nuclei-nuclei interactions, except those that remain unchanged on formation of the defect. The short range kinetic and exchange contributions are expressed rather straightforwardly by excluding all negligible terms or those associated with $P_{\mu\nu}$ factors where both μ and ν belong to D. Care must be taken that the correct

weighting factor is associated with each term, corresponding to the number of times it appears in equation (4.4.46):

$$T' = \Sigma^{C}_{\gamma} [\Sigma^{C}_{\mu} + \Sigma^{D^*}_{\mu}] P_{\mu\nu} T_{\mu\nu} \qquad (4.4.47)$$

$$E'_{ex} = -1/2 \Sigma^{C}_{\gamma} [1/2 \Sigma^{C}_{\mu\sigma\tau} + 2\Sigma^{C}_{\mu\sigma} \Sigma^{D^*}_{\tau} + 2\Sigma^{D^*}_{\mu\sigma} \Sigma^{C}_{\tau} + \Sigma^{C}_{\mu} \Sigma^{D}_{\tau\sigma} + 2\Sigma^{D^*}_{\mu\sigma\tau}] P_{\gamma\mu} P_{\sigma\tau} (\gamma\delta | \mu\tau) \qquad (4.4.48)$$

The expression for the Coulomb contribution requires more attention, because interactions to infinity are involved, and because one must account explicitly for the fact that the nuclei in the defective A region are generally different in number, position, and charge with respect to the unperturbed host crystal. We have:

$$E'_C = \Sigma^{A}_{\lambda} \left[(1/2\Sigma^{A}_{\lambda} + \Sigma^{B,Dsr}_{\lambda}) \frac{Z_\lambda Z_{\lambda'}}{R_{\lambda\lambda'}} + Z_\lambda V^{\lambda}_{M} \right] +$$

$$+ \Sigma^{C}_{\gamma} [\Sigma^{C}_{\mu\sigma} (1/2\Sigma^{C}_{\tau} + \Sigma^{D^*}_{\tau}) + 2\Sigma^{D^*}_{\mu\sigma} \Sigma^{C}_{\tau} + (\Sigma^{C}_{\mu} + 2\Sigma^{D^*}_{\mu}) \Sigma^{D^*}_{\sigma\tau}] P_{\gamma\mu} P_{\sigma t} (\gamma\mu|\sigma\tau) +$$

$$+ \Sigma^{C}_{\gamma} [\Sigma^{C}_{\mu} + 2\Sigma^{D^*}_{\mu}] P_{\gamma\mu} (\Sigma^{sr}_{\lambda} Z^{\lambda}_{\gamma\mu} + M_{\gamma\mu}) \qquad (4.4.49)$$

Here V^{λ}_{M} is the Madelung potential due to the long range Coulomb interactions at the location of the nuclear charge Z_λ.

By comparing equation (4.4.46) with equations (4.4.47, 4.4.48, 4.4.49) we have:

$$E' = E'_1 + E'_2 \qquad (4.4.50)$$

with:

$$E'_1 = \Sigma_\gamma^C \left[\Sigma_\mu^C + 2\Sigma_\mu^{D*}\right] P_{\gamma\mu} F^{const}_{\gamma\mu} \qquad (4.4.51)$$

$$E'_2 = \Sigma_\gamma^C \left[1/2\Sigma^C_{\mu\sigma\tau} + 2\Sigma^C_{\mu\sigma}\Sigma^{D*}_\tau + 2\Sigma^{D*}_{\mu\sigma}\Sigma^C_\tau \right] P_{\gamma\mu}P_{\sigma\tau}\left[(\gamma\mu|\sigma\tau) - 1/2(\gamma\sigma|\mu\tau)\right] + \Sigma_\lambda^A\left[\left(1/2\Sigma^A_{\lambda,} + \Sigma^{BDsr}_{\lambda,}\right)\frac{Z_\lambda Z_{\lambda,}}{R_{\lambda\lambda,}} + Z_\lambda V^\lambda_M\right] \qquad (4.4.52)$$

An additional term should be added to the former expressions when the cluster is not neutral. If Q^{net} is the residual charge in the cluster, that is the difference between total (electron+nuclear) charges in the defective and in the perfect crystal, then the contribution to the energy will have the form:

$$E^{pot} = Q^{net} V^{ave} \qquad (4.4.53)$$

where V^{ave} is the average potential inside the host crystal. This quantity may be fixed arbitrarily, as long as one deals with neutral structures. If we assume the overall neutrality of the defective structure, then this term should be compensated by a term of opposite sign that comes from the rest of the crystal. The quantity $-E^{pot}$ will therefore be added to the (4.4.46).

An estimate of the correlation correction to be applied to these expressions can be obtained a posteriori by using, for instance, the semi-local Colle and Salvetti functional (1975,1979,1984), which depends only on the calculated HF charge density. Obviously, also in this case we would have to calculate a "difference" correlation energy:

$$\Delta E_{corr} = E_{corr} - E^f_{corr} \qquad (4.4.54)$$

4.4.2.4 Computational scheme

A general purpose computer program, named "EMBED", has been developed which performs the calculations just described, using as an input the results obtained for the perfect host crystal from the CRYSTAL program. Written in standard FORTRAN, it is about 15000 instructions long, and it has been succesfully implemented on a range of different machines (IBM3090, CRAY-XMP, CONVEX). Its general scheme is as follows:

INITIAL STAGE

1) Read the following items produced by the CRYSTAL code, and characterizing the host crystal: geometry; basis set; point symmetry operators; Fermi level E_f; P^f matrix; DOS expansion coefficients.

2) Read from input the characteristics of the defective region: geometry and basis set of atoms in the A region, C cluster size, computational parameters .

3) Recognize the symmetry subgroup of the defective system; calculate all integrals that are needed; set up the information needed for rapid identification of neighborhood relationships; calculate F^{const} and P^{const}, $S_{CC,CD}$

4) Prepare the initial guess for the density matrix P^0 or read from disk a P' initial guess

SELF-CONSISTENT STAGE

5) Calculate $F_{CC,CD}$, diagonalize F and calculate P_{clust},S_{CC}

6) Calculate the A^j, T^j, M,M' matrices for all cluster levels e_j, hence the P^{coup},$S_{CC,CD}$matrices and E' .

7) If convergence in the P matrix is not reached, restart from step (5).

4.4.3 Comments on the approximations and limitations of the method

4.4.3.1 The "charge problem"

The present embedding scheme differs from molecular or supercell calculations since the number of electrons in the cluster is not fixed, but depends on the nature of the defect.

We define the cluster net charge as:

$$\Delta Q^C = \sum_{\mu\in C} \{ (\sum_{\nu\in C} + 2\sum_{\nu\in D^*}) P_{\mu\nu} S_{\mu\nu} \} - \sum_{a\in C} Z_a - \sum_{\mu\in C'} \{ (\sum_{\nu\in C'} + 2\sum_{\nu\in D^*}) P^f_{\mu\nu} S_{\mu\nu} \} - \sum_{b\in C'} Z_b, \quad (4.4.55)$$

where C' indicates the cluster region before the introduction of the defect and Z_a and Z_b indicate nuclear charges of atoms in the C and C' zone, respectively. From this definition it is clear that the actual 'cluster', intended as the entity whose charge distribution can be perturbed by the defect, is formed by the AOs in C and in D^*. We also note that ΔQ^C can assume non-integral values. In a neutral defect (for example, in the case of an iso-valent substitution, as Na substituting Li in LiF), ΔQ^C must be zero. In principle, if more than one charge state is physically possible, we can fix the cluster charge by varying the position of the Fermi energy (E_f), at least in solids with a finite gap. In order to clarify this point, let us consider first the case where there are no defects in the crystal, and therefore the PC equations are exact. When solving the "molecular" equation (4.3.10) for the cluster, a certain number of pseudo-eigenvalues $\underline{e}_j$ may show up in the gap, associated with dangling-bond states. The cluster density matrix

P_{CC}^{clust} will then depend on E_f that is, on how many dangling-bond states are filled. However, the term P_{CC}^{coup} realizes in all cases the proper correction so as to restore the correct result $P_{CC} = P_{CC}^{f}$, by reducing the population of fully occupied dangling-bond states, and increasing that of virtual ones. Consider now the case of a system with a defect: some of the pseudo-eigenvalues inside the gap could be associated with localized defect states. Suppose that there is one such state with eigenvalue ε', and that the cluster is big enough to ensure that the state is well contained within C. Different situations can now arise according to the position of E_f with respect to ε', that is, if the defect state is unoccupied, or singly or doubly occupied. In practice, we seldom have such favorable, extreme conditions. Due to limited cluster size, defect states and dangling-bond states will mix up in the cluster solution. The total net charge in the local region will vary by fractional quantities according to the position of E_f with respect to the various $\underline{e}_j$ values in the gap. One must also consider the fact that pseudo-eigenvalues and -eigenvectors are changing during the SCF procedure. The value of the Fermi energy should therefore be adjusted self-consistently, according to the physical situation under investigation. This procedure would be very costly and has not been operatively implemented in the code. With reference to a Li vacancy in LiF, we would expect, if the Fermi energy was in the middle of the gap, the cluster charge to be -1; by shifting the Fermi energy near the top valence bands we can depopulate fluorine 2p states, and delocalize an electron vacancy on the fluorine nearest neighbours of the Li vacancy: in this case the cluster charge will become zero. In a true, physical description of the system only these two charge states are meaningful.

In fact, intermediate charge states almost always arise. In particular, two main problems can be identified:

a) when neutral defects are studied (or in auto-embedding calculations), there are often a small, but appreciable, residual charges in the cluster, mainly due to numerical inaccuracies

b) in the case of charged defects an integral cluster charge is never reached. If the Fermi level is left in the middle of the gap in the case of the Li vacancy in LiF, we observe a partial depopulation of the nearest neighbour oxygens, and ΔQ^C assumes a value $-0.2 < \Delta Q^C < -0.5$.

Why do fractional charge states arise, and why does it seem impossible to reach an integer cluster charge? The root of the problems apparently lies in the contrast between the finite/infinite nature of the cluster/host system, to which the finite perturbation is superimposed and by the method we use to treat this perturbation.

We can identify the following factors, of which the first two are numerical, but the third is a true physical effect:

1) the long range polarization of the medium is not correctly accounted for: only a finite number of AOs in the outer region (those included in D^*) can polarize, and therefore generate a dielectric response acting on the cluster. The absence of a correct description of this effect leads not only to an incorrect estimation of the defect formation energy, but can result in a destabilization of a charged defect because of the absence of the stabilizing polarization energy; this, in turn, produces a cumulative error during the self-consistent procedure.

2) The number of AOs in D^* that can be affected by charge transfer effects is, on the other hand, large: small modification of the charge distribution in D^*, due for instance to numerical inaccuracies, may amount to a finite effect on the cluster charge. Also by increasing the cluster size, even small changes in charge on the atoms in region B can result in a non-negligible net charge in C, because of the number of equivalent atoms in the cluster.

3) Anions in the neighbourhood of a charged defect can polarize considerably and their valence electrons displace inwards or outwards, according to the defect charge. These effects will be noted in Chapter 6, with reference to the formation of a bound Schottky pair in LiF. Very large clusters are not treatable, because of the computational cost ; if these displacements arise near the cluster boundary, the response of the neighbours in region D may not be completely taken in account by the Mulliken partition scheme used in (4.4.55), with the result for instance in the failure to count correctly the electron charge associated with the cross terms C-D. It can also be argued that the basis sets used to describe the valence electrons of these anions might be not adequate and, as a result, overestimate the displacement of the electron density.

It must be noted that it is not possible to renormalize the P_{CC} and P_{CD} blocks of the density matrix, by multiplying them by an appropriate constant. By doing that we would multiply by the same amount both valence and core states, and the result would be completely unphysical results.

It appears that the PC equations discussed above are not suitable, in the present formulation, for the study of charged defects; in section 4.5 we present a technique that improves the treatment of the polarization of the medium. The problem of the formal charge of the cluster and of how far the charge associated to the defect can spread remains very much an open question.

4.4.3.2 The self-substitution test

An important test of the correctness of the computational scheme is the so-called self-substitution test. It corresponds to defining a C cluster and a proper defective region A exactly as in the case of a real defect, but with all atoms in A coinciding in species, geometry, and basis set with those of A'. Such a calculation is necessary in any case for defining the reference energy $E^{perfcry}$ [see

equation (4.4.46)]. $P_{CC,CD}$ should in fact coincide at self-consistency with $P^{f}_{CC,CD}$, independent of the C cluster size, because equations (4.4.36, 4.4.37) are exact in the self-substitution case. However, such a result is not as trivial as might appear at first sight. Those equations involve a large number of calculations (and associated numerical approximations) which are completely different from those employed in the solution of the host crystal problem, based on the systematic use of Bloch theorem. For instance, an accurate description of the projected DOSs of the host crystal is here a necessary intermediate step, while it is immaterial in the crystalline calculation, at least when insulators are considered (Pisani et al, 1988).

Moreover we would like to be able to reproduce the correct cluster geometry if the cluster geometry is optimized with respect to the total energy: if one starts from an optimized crystalline geometry, all nuclear displacements within C should lead to an increase in energy. If, however, such displacements take place near the cluster boundary, the effects associated with changes in the overlap matrix, and discussed in Appendix. D, may lead to a different geomety, unless corrective terms are introduced.

4.4.3.3 Self-consistency instabilities

In order to stabilize the SCF process the standard procedure of mixing the F matrix calculated at the n-th cycle with the one evaluated at the (n-1)th cycle is systematically used. If the mixing is high (standard values are 80-95%), this procedure corresponds to averaging over a large number of cycles, quenching oscillations but also slowing down the procedure. The origin of these instabilities can be traced back to some well known problems. First of all we note that there is no response of the outer system to local variations in the density matrix, so that "pathological" solutions may always build up. Moreover, especially with big

clusters, the redistribution of charge within the cluster can encounter the presence of multiple minima, e.g. several slightly different electronic configurations.

The summation over the j cluster eigenvalues that appears in equation (4.4.36,4.4.37) is performed, in fact, over sets of quasi-degenerate eigenvalues, e.g. eigenvalues that differ less than a given threshold. This produces an important reduction in CPU time and prevents quasi-singularities associated with the $(\underline{e}_j-\underline{e}_m)$ denominators. If the grouping scheme changes during the SCF, e.g. if some eigenvalues that were grouped in a pseudo-degenerate set split, the charge distribution in the cluster can change suddenly and catastrophic oscillations be introduced in the convergency process.

In starting the SCF process we usually use a P^0 density matrix that corresponds to using the isolated ion solution for the species in A and the perfect crystal submatrix for the blocks BB and BD. The blocks AB and AD are set to zero. If, however, a converged P' matrix is available, that describes a defective system similar to the one of interest (i.e. a slightly different geometries), it is convenient to adopt it as starting point to start the convergence process. This procedure is usually followed when, for instance, we optimize the cluster geometry.

4.5 DIELECTRIC RESPONSE OF THE MEDIUM AND THE TREATMENT OF CHARGED DEFECTS.

We will now consider how the long-range polarization effects, generated by a charged defect, can be described in our embedding method by means of a simplified, classical model. We aim to describe how the ions in the region D polarize and displace; this result will allow us to calculate how the field generated by region D in the cluster changes, as a result of the displacements in D with respect to the perfect crystal positions. A new contribution to the formation energy, due to the polarization of the outer medium, will also be calculated.

The development of the theory and of a new computer code, 'EMBRYON', that implements these improvements into the framework of the original program 'EMBED', has been an important part of this research work and is presently being pursued in collaboration with M. Leslie and V.R. Saunders at the Daresbury Laboratory.

In the following section we shall describe the theory and how the program EMBED has been modified.

4.5.1 Description of the method and of the program

Following the partition into a C and a D region, as discussed in section 4.3.1, we assume that all the polarization effects in D may be described by the Mott-Littleton method. The atoms in D are treated as polarizable, displaceable entities. Their equilibrium coordinates depend on their mutual interactions and on the electric field $\Delta V_C^P = (V_C^P - V_C^{Pf})$ acting on them, due to the redistribution of charge in C after creating the defect. (where V_C^{Pf} is the field generated by the cluster prior to the introduction of the defect, and V_C^P is the field

generated by the defective cluster). The electron distribution in C is obtained by solving the perturbed cluster equations, as shown in section 4.3, but by adding to the Fock Hamiltonian a corrective term, F^{ML} that describes the effects of the displacements in D on the cluster and that is calculated from the knowledge of the difference potential (and its derivatives) $\Delta V_D^P = (V_D^P - V_D^{Pf})$, where V_D^{Pf} is the potential generated by the outer region with all the atoms in the perfect crystal positions, and V_D^P is the field generated after the displacements have taken place).

If the perturbation introduced by the defect were completely localized in C, then ΔV_C^P would be zero and no displacements would occur in the outer region D, so that ΔV_D^P would also be zero. This becomes true only in the limit of a very large, neutrally charged cluster.

Let us consider a generic ion j in region D. The displacement of j, due to the defect in C, are defined as:

$$\xi_j = \mathbf{r}_j - \mathbf{R}_j \qquad (4.5.1)$$

where $\mathbf{r}_j$ are the (x,y,z) coordinates of the relaxed positions and $\mathbf{R}_j$ the coordinates of the perfect lattice positions. ξ_j can be calculated from:

$$\xi_j = M_j \, D_j \qquad (4.5.2)$$

where D_j is the electric displacement generated by C in j (as defined above) and M_j is the 3x3 Mott-Littleton matrix:

$$M_j = W^{-1} q_j \varepsilon^{-1} \qquad (4.5.3)$$

in which W is the perfect lattice force constant matrix , ε is the trace of the dielectric constant tensor and q_j is the ion charge.

To evaluate $\Delta V_C^P(r_j)$ in the point j of the outer region we need to calculate the potential and its derivative generated by the nuclei and the electrons in C, before and after introducing the defect.

The nuclear contribution is straightforward to calculate, being the problem reduced to the one of calculating the field generated by a finite set of point charges.

The electronic contribution $e_C^P(r_j)$ is given by the equation:

$$[\, e_C^P (r_j)]_{lm} = \sum_{\mu \in C,\, \nu} [\, \{\mu\nu\} \mid \{lm\}; \mathbf{r}_j]\, P_{\mu\nu} \qquad (4.5.4)$$

where $[\, \{\mu\nu\} \mid \{lm\}; r_j]$ is the field integral in $\mathbf{r}_j$ corresponding to the distribution $\{\mu\nu\}$ and m is the component of the multipole of order l-th; the sum is over all the charge distributions that belong to C according to a Mulliken partition of charge

Let now consider how the displacements ξ_j modify the potential V_D^{Pf} acting on a point $\mathbf{r}_i$ that is the centre of a distribution $(\mu\nu)$, with μ in C and ν in C or D.

Following the method outlined in section 4.2.1 we subdivide the outer region D in two sub-regions D_I and D_{II}; D_I is the finite, innermost part of region D, and D_{II} is the outermost part, that extends to infinity. We can then write:

$$\begin{aligned} \Delta V_D^P (\mathbf{r}_i) &= (V_D^P (\mathbf{r}_i) - V_D^{Pf} (\mathbf{r}_i)) = \\ &= (V_{DI}^P (\mathbf{r}_i)) - V_{DI}^{Pf} (\mathbf{r}_i)) + (V_{DII}^P (\mathbf{r}_i) - V_{DII}^{Pf} (\mathbf{r}_i)) = \\ &= \Delta V_{DI}^P (\mathbf{r}_i) + \Delta V_{DII}^P (\mathbf{r}_i) \end{aligned} \qquad (4.5.5)$$

$\Delta V_{DI}^P (\mathbf{r}_i)$ is calculated by explicitly summing over all the ions in D_I:

$$\Delta V_{DI}^P (\mathbf{r}_i) = \sum_{j \in D_I} \left[\frac{q_j}{|\mathbf{r}_i - \mathbf{r}_j|} - \frac{q_j}{|\mathbf{r}_i - \mathbf{R}_j|} \right] \qquad (4.5.6)$$

As regards region D_{II}, it is treated as a dielectric continuum, that interacts with a point charge Q^C located at the origin (where Q^C is the cluster charge, as defined in 4.4.55). The electric field generated by the cluster on a site j in region D_{II} is $(Q^C \frac{\mathbf{R}_j}{|\mathbf{R}_j|^3})$, and the change in potential will be:

$$\Delta V^P_{D_{II}}(j) = \sum_{j \in D_{II}} \left[\frac{q_j}{|\mathbf{r}_i - \mathbf{r}_j|} - \frac{q_j}{|\mathbf{r}_i - \mathbf{R}_j|} \right] = -\sum_{j \in D_{II}} q_j \frac{(\mathbf{r}_i - \mathbf{R}_j) \cdot \xi_j}{|\mathbf{r}_i - \mathbf{R}_j|^3} \tag{4.5.7}$$

where $\mathbf{r}_i$ is at (0,0,0), so that:

$$\Delta V^P_{D_{II}} = -\sum_{j \in D_{II}} q_j \frac{\mathbf{R}^T_j \cdot \xi_j}{|\mathbf{R}_j|^3} \tag{4.5.8}$$

Using (4.5.2):

$$\xi_j = M_j \, D_j = M_j Q^C \frac{\mathbf{R}_j}{|\mathbf{R}_j|^3} \tag{4.5.9}$$

so that the (4.5.8) becomes:

$$\Delta V^P_{D_{II}} = -\sum_{j \in D_{II}} Q^C q_j \frac{\mathbf{R}^T_j \cdot M_j \cdot \mathbf{R}_j}{|\mathbf{R}_j|^6} \tag{4.5.10}$$

To obtain this term we perform a complete lattice sum over C,D and E, using the Ewald technique (as discussed in Appendix E) and then we explicitly subtract the sum over C and D.

The generic element of the corrective matrix that will be added to the Fock matrix is then given by:

$$F^{ML}_{\mu\nu} = \sum_{lm} [\ (lm \mid \mu\nu)]\ \Delta V^{P}_{D}\ (\mathbf{r}_i, lm) \qquad (4.5.11)$$

where we have explicited the components of $\Delta V^{P}_{D}(\mathbf{r}_i)$: m is the m-th component of the multipole of order l-th due to the distribution ($\mu\nu$), whose centre is in $\mathbf{r}_i$.

We can now calculate the contribution to the formation energy of the defect due to the displacement of ions in the outer region. Formally, this quantity is given by:

$$\Delta E^{ML}_{D} = -\ [\Delta V^{P}_{C}(r_j)]^{T} \cdot Q \cdot x\ +\ 1/2\ x^{T} \cdot W \cdot x \qquad (4.5.12)$$

where x are the displacements of the ions in D, ΔV^{P}_{C} the corresponding difference electric field generated by C and acting on them, Q is a vector containing the charges of the ions in D and W is the perfect lattice force constant matrix

$$W = \frac{\partial^2 U_L}{\partial x_i \partial x_j} \qquad (4.5.13)$$

in which U_L is the field-free equilibrium lattice energy.
At equilibrium $\frac{\partial U_L}{\partial x} = 0$, so that, by differentiating (4.5.12), we obtain:

$$-\ [\Delta V^{P}_{C}(r_j)]^{T} \cdot Q\ +\ \cdot\ x \cdot W = 0 \qquad (4.5.14)$$

That yields:

$$x = W^{-1} \cdot Q^{T} \cdot \Delta V^{P}_{C}(r_j) \qquad (4.5.15)$$

We can now substitute this expression in the (4.5.12):

$$\Delta E_D^{ML} = - [\Delta V_C^P(r_j)]^T \cdot Q \cdot W^{-1} \cdot Q^T [\Delta V_C^P(r_j)] +$$

$$+ 1/2 [\Delta V_C^P(r_j)]^T \cdot Q \cdot W^{-1} \cdot W \cdot W^{-1} \cdot Q^T \cdot \Delta V_C^P(r_j) =$$

$$= -1/2 [\Delta V_C^P(r_j)]^T \cdot Q \cdot W^{-1} \cdot Q^T \cdot \Delta V_C^P(r_j) \qquad (4.5.16)$$

Since :

$$\varepsilon \cdot \Delta V_C^P(r_j) = \mathbf{D} \qquad (4.5.17)$$

being ε the dielectric tensor and **D** the electric displacement, with:

$$\varepsilon = \mathbf{I} + \frac{4\pi}{v_c} Q \cdot W^{-1} \cdot Q^T \qquad (4.5.18)$$

(where v_c is the volume of the unit cell), it is possible to rewrite the (4.5.16):

$$\Delta E_D^{ML} = -1/2 \; \mathbf{D}^T \varepsilon^{-1} [(\varepsilon - \mathbf{I}) \frac{v_c}{4\pi}] \varepsilon^{-1} \mathbf{D} =$$

$$= -1/2 \; \frac{v_c}{4\pi} \mathbf{D}^T [\varepsilon^{-1} (\mathbf{I} - \varepsilon^{-1})] \mathbf{D} \qquad (4.5.19)$$

By making explicit the dependence of **D** on the point j (in D) where it is calculated, we have:

$$\Delta E_D^{ML} = -1/2 \; \frac{v_c}{4\pi} \sum_j \mathbf{D}^T{}_j [\varepsilon^{-1} (\mathbf{I} - \varepsilon^{-1})] \mathbf{D}_j \qquad (4.5.20)$$

But : $\mathbf{D}_j = Q^C \frac{R_j}{|R_j|^3} \qquad (4.5.21)$

So that the (4.5.20) becomes:

$$\Delta E_D^{ML} = -1/2 \frac{v_c}{4\pi} \sum_j (Q^C)^2 \frac{[\varepsilon^{-1}(I - \varepsilon^{-1})]}{|R_j|^4} \qquad (4.5.22)$$

This is the expression for the polarization energy used in our procedure. To evaluate this term we perform a lattice sum by Ewald method and then we subtract the terms due to lattice ions in C. This contribution is added to the expression for the energy, as given by the (4.4.51) and (4.4.52). Another term, that corresponds to the interaction of nuclei in C with the polarization field, must be included. It has the form

$$\Sigma_N Z_N \Delta V_D^P(r_N) \qquad (4.5.23)$$

where the sum is over all the N nuclei in C, Z_N is their charge and $V_D^P(r_N)$ is the polarization field generated by the displacements in D calculated in the coordinate r_N of the N-th nucleus.

This new scheme requires a number of modifications in the embedding equations discussed in section 4.4. In particular, since the modifications in the D regions are accounted for by the Mott-Littleton procedure, all the terms that appear in the Fock matrix (equations 4.4.39 and 4.4.40) that correspond to interactions with electronic distributions in D, must refer to the *unperturbed distributions* , calculated for the perfect lattice.

Also the expression for the cluster charge (4.4.55) changes, and will count only half of the bond-charges between regions C and D:

$$\Delta Q^C = \Sigma_{\mu\in C} \{ (\Sigma_{\nu\in C} + \Sigma_{\nu\in D^*}) P_{\mu\nu} S_{\mu\nu} \} - \Sigma_{a\in C} Z_a - \Sigma_{\mu\in C'} \{ (\Sigma_{\nu\in C'} + \Sigma_{\nu\in D^*}) P^f_{\mu\nu} S_{\mu\nu} \} - \Sigma_{b\in C'} Z_b, \qquad (4.5.24)$$

The computational procedure discussed in 4.4.2, will be altered according to the following scheme (changes are indicated by bold characters):

INITIAL STAGE

1) Read the following items produced by the CRYSTAL code, and characterizing the host crystal: geometry; basis set; point symmetry operators; Fermi level E_f; P^f matrix; DOS expansion coefficients.

2) Read from input the characteristics of the defective region: geometry and basis set of atoms in the A region, C cluster size, computational parameters .

***3)** Read from input the radius of region C, D_I and D_{II} for the Mott-Littleton procedure. Read also the force constants matrices for each basis species and the matrix $[\varepsilon^{-1} (\mathbf{I} - \varepsilon^{-1})]$, used in the expression (4.5.11).

4) Recognize the symmetry subgroup of the defective system; calculate all integrals that are needed; set up the information needed for rapid identification of neighborhood relationships; calculate F^{const} and P^{const}, $S_{CC,CD}$

***5)** Calculate the centres of distributions (μ,ν), with μ in C and ν in C or D, where $\Delta V_D^P(\mathbf{r}_i)$ will be calculated

***6)** Determine the net of points in region D where the electric field $\Delta V_C^P(\mathbf{r}_j)$ will be calculated

7) Prepare the initial guess for the density matrix P^0 or read from disk a P' initial guess

SELF-CONSISTENT STAGE

8) Calculate $F_{CC,CD}$, diagonalize F and calculate P_{clust}, S_{CC}

***9)** Calculate $V_C^P(\mathbf{r}_j)$ generated by the electronic distribution in the cluster region.

***10**) Calculate the displacements in region D, the polarization potential (and its derivatives) $V_D^P(\mathbf{r}_i)$.

***11**) Evaluate the correction to the Fock matrix $F_{\mu\nu}^{ML}$ and the energy terms ΔE_D^{ML} that will be added to E' in the step 12.

12) Calculate the A^j, T^j, M,M' matrices for all cluster levels e_j, hence the P^{coup},$S_{CC,CD}$matrices and the energy E' .

13) If convergence on the P matrix is not reached, restart from step (5).

The procedure discussed above improves the original embedding theory, by explicitly taking into account the polarization of the medium and by making more explicit the different approximations used for the cluster and the outer region. On the other hand, the treatment of charged defects remains a formidable problem: preliminary calculations using EMBRYON show that the flow of charge to/from the cluster, in the case of charged defects, is almost always a cause of instabilities in the self-convergence procedure; further work will be necessary in order to find feasible and theoretically sound solutions to this problem.

REFERENCES

Almlof J and Wahlgren U (1973), Theor Chim Acta, 28, 161

Ballantine LE and Kolar M (1986), J Phys C: Solid State Phys, 19, 981

Baraff GA and Schluter M (1984), J Phys B, 30, 1853

Barandiaran Z and Seijo L (1988), J Chem Phys, 89, 5739

Bar-Yam. Y and Joannopoulos JD (1984), Phys Rev B, 30, 1844

Catlow CRA and Mackrodt WC (1982), Lecture Notes in Physics, Vol 166, Springer-Verlag, Berlin

Colbourn EA and Mackrodt WC (1982), Surf Sci, 117, 571

Colle R and Salvetti O (1975), Theor Chim Acta, 37, 329

Colle R and Salvetti O (1979), Theor Chim Acta, 53, 55

Colle R, Fortunelli A and Salvetti O (1984), J Chem Phys, 80, 2654

Dick BG and Overhauser AW (1958), Phys Rev, 112, 90

Ewald PP (1921), Ann Physik, 64(4), 253

Fisher AJ (1988), J Phys C: Solid State Phys, 21, 3229

Fowler PW and Tole P (1988), Surf Sci, 197,457

Grimes RW, Catlow CRA, Stoneham AM (1989), J Phys Condensed Matter, 1, 7367

Harding JH, Harker AH, Keegstra PB, Pandey R, Vail JM and Woodward C (1985), Physica B, 131,151

Inglesfield JE (1981), J Phys C: Sol State Phys, 14, 3795

Kaufman JVR and Clark CD (1963), J Chem Phys, 38, 6 , 1388

Kenton AC and Ribarsky MW (1981), Phys Rev B,23,2897

Koster GF and Slater JC (1954), Phys Rev, 95, 1167

Kunz AB and Klein DL (1987), Phys Rev B, 17, 4614

Leslie M (1981), SERC Daresbury Laboratory Report D1/SCI/TM31T

Lewis GV and Catlow CRA (1985), J Phys C, 18(6), 1149

Lidiard AB (1976) in Henderson B and Hughes AE, (eds), Defects and their structure in non-metallic solids, Plenum, NY

Mott NF and Littleton MJ (1938), Trans Farad Soc, 34, 489

Nichols CS, Van de Walle CG, Denteneer PJH, Bar-Yam Y and Pantelides ST (1989), Phys Rev B,39,10791

Pisani C, Dovesi R and Ugliengo P (1983), Phys Stat Sol (b), 116, 249

Pisani C, Dovesi R, Nada R and Kantorovich L N (1990), J Chem Phys, 92, 7448

Pisani C, Dovesi R, Nada R and Tamiro S (1989), Surf Sci, 216, 489

Pisani C, Dovesi R, Roetti C (1988), Lecture Notes in Chemistry, Springer-Verlag, Heidelberg

Shangda X, Changxin C, Libin L and Ellis DE (1987), Phys Rev B, 35, 7671

Shluger A, Grimes RW, Catlow CRA (1991), to be published

Simonetta M (1986), Int J Quantum Chem,17,501

Surratt GT and Goddard WA III (1978), Phys Rev B, 18,2831

Vail JM, Harker AH, Harding JH, Saul P (1984), J Phys C,17,3401

Vail JM (1990), J Phys Chem Solids, Vol 51, no 7, 589

Chapter 5.
Ab-initio Hartree-Fock calculations on silicates and magnesium silicates

5.1 INTRODUCTION

Silicates are one of the most abundant and widespread mineral groups on Earth, comprising more than 95% by weight of the crust and mantle of the planet. Silicon is also important for life on Earth: clay minerals absorb and release water and several cations important for plant nutrition; silicon compounds play a substantial rôle in the cells of living organism. In the human body silicon is present in the cells of connective tissues and is involved in the biosynthesis of collagen, the substance that forms hair and nails, and in the formation of bony tissue (Carlisle, 1970). Silicon forms, second to carbon, the largest number of compounds with other elements and plays a crucial rôle in the chemistry of our planet and of the creatures living on it.

Simple molecular compounds of silicon, such as SiO and SiS, have been detected by radiowave studies as interstellar material (Zuckermann, 1977). Although in most regions of space the density of these gaseous compounds is extremely low (less than about 10^5 molecules per cm^3) the total amount of silicon in the interstellar gas may reach a level equivalent to several percent of that concentrated in the stars. Silicon plays also a very important technological rôle: in addition to being widely used as building materials, silicon compounds have found widespread use in the manufacture of glasses, ceramics, molecular sieves, selective sorbents, adsorbents, catalysts, silicone products and electronic devices.

A better understanding of the properties of the Si-O bond is therefore of great importance: on the one hand it will lead to improvements in our understanding of

the geochemistry of the Earth; on the other it will allow applied scientists to improve present technology. Moreover, due to their enormous variability, silicates are ideally suited for the study of general chemical and crystallographic principles.

To understand the reason why silicon is found in such a large number of different structures, we must take a closer look at the properties of the chemical bonds that silicon can form. In contrast to the C-O, C-C and C-H bonds, the bond energy of the Si-O bond is considerably higher than that of the Si-Si and Si-H bonds. Therefore the Si-O bond is dominant in silicon chemistry; and only a rather small number of silicon compounds are known which are the analogues of the organic carbon compounds.

In section 5.2 the properties of the Si-O bond (and of the cation - O bond that occurs in compounds of general formula $M_sSi_tO_v$) are reviewed. Then, in section 5.3, we present the results of a study on the SiO_2 polymorphs stishovite and α-quartz. In section 5.4 the results of a similar study on $MgSiO_3$ - ilmenite are discussed, with particular attention to the basis set problem.

5.2 CHEMICAL BONDING IN SILICATES

5.2.1 The Si-O bond

The nature of the Si-O bond has been extensively studied by means of experimental techniques (infrared spectroscopy, X-ray fluorescence spectroscopy, photoelectron spectroscopy) and with theoretical methods. Examples of experimental investigations aimed to the study of the Si-O bond can be found, for instance, in Brytov et al. (1979), Gupta (1985), Wiech and Zurmaev (1985) and Gibbs (1982). In the following we shall discuss some of these results in more detail.

The bond between silicon and oxygen is usually considered to be partly ionic and partly covalent. In a purely *ionic* model, Si is described as an Si^{4+} ion and O as a O^{2-} ion, kept together by electrostatic forces, so that the bonds are nondirectional. According to this model the oxygen ions tend to be close-packed, the Si ions filling tetrahedral (or octahedral) sites between the oxygens. In fact, with the exception of the high-pressure SiO_2 -stishovite, only few silicates have a density anywhere near to that of a closed-packed oxygen ions arrangement.

In a *covalent* model, the Si-O bond is described in terms of the valence bond theory. The electron configuration of a silicon atom in its ground state is

$$1s^2\ 2s^2\ 2p^6\ 3s^2\ 3p_{xyz}^{\ 2}$$

An energy of about 6eV is required to promote an electron from the 3s level to the 3p level. Also the energy difference between the 3s and the 3d levels is relatevely small (~ 11 eV) and about the same size as that between the Si 3d and

2p level of oxygen. Thus all nine orbitals in the outer valence shell of silicon can participate in bonding. The degree of participation of the Si 3d orbitals in the bond has always been the subject of controversy, as will be discussed in the following sections.

In a **tetrahedrally coordinated** systems there is an sp^3 hybrid with four equivalent orbitals pointing towards the corners of the tetrahedron. Each lobe of a Si sp^3 orbital overlaps an O 2p orbital to form a σ bond. Considerations purely of symmetry show that there can also be some overlap between O 2p and Si 3d orbitals, resulting in the formation of a π bond. By assuming a purely covalent model that includes only the σ bonds, the predicted Si-O distance is 1.76 Å (calculated as the difference between the sum of the covalent single bond radii of silicon and oxygen), much longer than the experimentally determined average distance, that is 1.63 Å . Another discrepancy is the deviation from the theoretical value of 109.47° of the Si-O-Si angle, that is experimentally found to be scattered, for most silicates, in a small range near 140 °.

The experimental evidence has been explained taking in account the partially ionic character of the Si-O bond (Schomaker and Stevenson, 1941) that would shorten the bond length. A double bond character, resulting from the participation of the Si 3d orbitals in the bonding, would not only strengthen the Si-O bond (making the bond length shorter) but also justify the widening of the bond angle. This possibility was suggested for the first time, more than fifty years ago, by Pauling (1939). A different interpretation suggests that the Si - Si repulsion alone can explain why the Si-O-Si angle is wider than what would expected (O'Keeffe and Hyde, 1978; Glidewell, 1977, 1978). In fact an indication of an important rôle for the d orbitals on Si is also given by comparisons between the calculated density of states and the fluorescence spectra of different forms of silica: agreement is found only when the Si d orbitals are included in the calculation (Collins et al., 1972). Nevertheless, for more than two decades, the real extent of

the contribution of d orbitals on Si has been debated, mainly because their rôle cannot be accurately pinpointed experimentally, and most of the calculations were performed on molecular fragments (for example Gibbs, 1982) or using poor basis sets (Dovesi et al., 1987).

When **octahedrally coordinated** we may propose sp^3d^2 hybrids for the bonding of the silicon, with the six orbitals pointing towards the corners of the octahedron. These hybrids overlap with the 2p orbitals of the surrounding oxygens, forming six σ type bonds. Silicon shows this coordination number in high pressure silicates, such as the rutile structured SiO_2 (stishovite), $MgSiO_3$ (ilmenite and perovskite) and in some low pressure structures in which the oxygens are bonded to species, such as phosphorous (as in e.g. SiP_2O_7), that are more electronegative than Si. According to Edge and Taylor (1971) and Liebau (1971), these atoms drain electrons from the Si-O bonds, thus weakening and lengthening them and reducing their mutual repulsions to the extent that the four coordinated Si is destabilized. Again, the rôle of Si 3d orbitals has been discussed at length (Gibbs, 1982) and the degree of participation of the d orbitals in the bonding is still unclear.

5.2.2 The cation-oxygen bond M-O

In silicates of general formula $M_rSi_sO_t$ the electronegativity of M can vary considerably, and so can affect the ionicity and the strength of the Si-O bond.

If we consider a bond system Si - O_1 - Si - O_2 - M, where M is an electro-positive cation (such as magnesium), then M transfers more electrons to its neighbouring oxygen atom than does Si, due to its lower electronegativity. As a result, the slightly more negative O_2 atom transfers part of its electron density to the adjacent silicon atom, thus shifting the electron density maximum further

towards Si than does the less negative oxygen atom O_1. The terminal oxygens are therefore slightly more charged than the bridging ones.

While the influence of cations of different electronegativity on the ionicity of the Si-O bond seems to be well-established, their influence on Si-O bond lengths and Si-O-Si angles is less obvious, and can be revealed only by keeping the other parameters as constant as possible, which is often difficult to achieve.

For all the above mentioned reasons it is important to clarify the properties of the Si-O bond by means of ab-initio electronic structure calculations, correctly taking in account the periodic crystalline environment and using a basis set rich enough to describe the polarization effects.

In the following sections we present the results of two studies, using state-of-the-art all-electron Hartree Fock calculations on minerals. First we consider two SiO_2 polymorphs, α-quartz and stishovite. The calculations accurately reproduce the structural properties of the two crystals; the density of states and electron charge density maps allow us to understand better the differences that occur in the bonding due to the different coordination number of silicon. The importance of d orbitals is also stressed by our calculations and we propose an interpretation of their rôle in the Si-O bond. Next we discuss the ilmenite structured $MgSiO_3$, a mineral that may play an important rôle in the geochemistry of the Earth. Its relatively small unit cell makes it possible to carry out a detailed study of basis set effects. Because of the lack of experimental results on the electronic properties of the bonding in this mineral (e.g. X-ray emission spectra and electron deformation maps) we exploited the *predictive* capability of our calculations to study the effect of an ionic environment on the Si-O bond and to compare the bonding in ilmenite and stishovite.

5.3 AN AB INITIO HARTREE-FOCK STUDY OF α-QUARTZ AND STISHOVITE

5.3.1 Introduction

The development in the early sixties of a range of reliable experimental techniques, especially X-ray emission, X-ray Photoemission Spectra (XPS) and Ultraviolet Photoemission Spectra (UPS), provided detailed insights into the chemical nature of SiO_2 polymorphs. In response to these results, there has been an increasing interest in the use of quantum chemical methods to investigate the properties of Si-O bond in order to provide information about electronic and structural properties.

In all but one of the SiO_2 polymorphs silicon has a tetrahedral coordination; they differ in the way in which the tetrahedra are connected together. The only exception is the rutile-structure mineral stishovite, where silicon has octahedral coordination and each oxygen is linked to three silicon atoms. This mineral is not found on the Earth's surface, except in an impact breccia at Meteor Crater, Arizona, (Chao et al., 1962) and was synthesized at high pressure and temperature (Stishov and Popova, 1961): it has a density higher than α-quartz and a longer Si-O bond. Stishovite clearly has intrinsic interest as the only octahedrally coordinated SiO_2 polymorph; moreover it can be used as a model for more complex compounds where silicon has the same coordination number (e.g. $MgSiO_3$, perovskite). Indeed, the latter material forms the major proportion of the lower part of the Earth's mantle. Moreover it has also been suggested that stishovite can be present in large amounts in the deep mantle, where it can be produced by disproportion of other silicates or by transformation of α-quartz at

high pressure (Ringwood 1975). Theoretical approaches can provide information that is otherwise inaccessible on these important materials.

Several calculations have been performed on both α-quartz and stishovite in order to describe their electronic and structural properties. Considerable success has been achieved using semi-classical simulations, in which effective potentials are used to describe the interatomic forces (Sanders et al., 1984; Cohen, 1987; Jackson and Gordon, 1988), as recently reviewed by Catlow and Price (1990). Many studies have been reported using electronic structure calculations employing tight-binding theory or with molecules as models for the real systems (Pantelides and Harrison 1976, Li and Ching 1985 , Gupta 1985 , Hill et al. 1983, Lasaga and Gibbs, 1988).

Preliminary results on α-quartz obtained with a minimal basis set (five atomic orbitals for oxygen and nine for silicon) have been reported by Dovesi et al. (1987). Structural properties of other silicates have been investigated by adopting pseudopotentials (in order to reduce the problem only to the valence electrons) and using a minimal basis set (Silvi 1990 , Silvi and Dovesi 1990). Recent improvements in reliability and generality of the code now allow more sophisticated basis sets and better computational conditions to be used.

We present here the first attempt to study and compare α-quartz and stishovite at an ab-initio all-electron Hartree Fock level using an extended basis set. The calculations have been performed using CRYSTAL, the code discussed in Chapter 3. This approach is intrinsically more powerful than cluster methods, since the long range crystalline field is correctly taken in account and the problems due to the cluster termination are absent.

We aim, first, to evaluate the effect of the basis set and of d-type polarization functions, and secondly to characterize the chemical and electronic properties of the two minerals, especially as regards differences due to the different coordination number.

In the following we investigate how different quality basis sets reproduce the experimental structure and we discuss the rôle played by d-orbitals in influencing the relative energies of the two structures. Then the electronic properties are considered: the band structure, the density of states and deformation maps of electronic charge density are used to discuss the relative ionicity and the nature of the Si-O bond.

5.3.2 Geometry and Structural Data

Since 1935 the positional parameters of α-quartz have been known with three-figure precision (Wei 1935). The structure of α-quartz has been refined by diffraction techniques, both X-ray (Smith and Alexander 1963 , Levien at al. 1980) and neutron (Wright and Lehmann 1981). These methods have also been used to establish the response of the structure to compression and to study the nature of the pressure and temperature induced phase-transitions (Jorgensen 1978 , Grimm and Dorner 1975). The crystallographic data of Jorgensen were used in the present study and are given in Table 5.1.

Stishovite has the rutile-type structure and a number of structure determinations are available, so that all the cell parameters are reliably known (Sinclair 1978 , Baur and Khan 1971 , Hill et al. 1983 , Spackman et al, 1987). The positional parameters are reported in Table 5.1. Because of the higher coordination number of Si, the density of stishovite is higher than that of α-quartz or any of the 4-coordinated polymorphs.

The effect of this higher density on the dynamical properties of stishovite has still to be fully investigated.

5.3.3 Basis set effects and geometry optimization

Since the basis set plays a crucial rôle in the description of the system, care is necessary in order to satisfy the bonding requirements for both O and Si. A molecular basis set is usually an acceptable starting point, but it need to be reoptimized for the bulk structure. We started by using for both species the 6-21G basis set proposed by Pople and coworkers (Binkley et al. 1980 , Gordon et al. 1982). According to this basis, core electrons are described using atomic-like orbitals resulting from a combination of 6 GTOs (Gaussian Type Orbitals). A split-valence basis set of sp functions is used for valence electrons in order to allow more variational freedom: a combination of two GTOs describes the valence region closer to the nuclei and an independent, individual GTO is used for the outer region. Only the exponent of the latter GTO was variationally reoptimized in order to take in account the effects of the crystalline field: the adopted exponents are 0.17 a.u. for Si and 0.36 a.u. for O. Such an approach is not satisfactory if the system possesses a highly ionic character, as, for example, in MgO (Causa' et al. 1986) or in magnesium silicates; but we may be confident that it will perform better for the more covalent compounds considered here. An optimization of some selected geometrical parameters can be considered as a valid test of the quality of the basis set (since errors in the calculated equilibrium geometries due to the intrinsic limits of the Hartree Fock approximation are usually within 1%). If the simple 6-21G basis set is not adequate, it is possible to determine if that inadequacy is due only to a poor description of the anisotropic distortion of the valence shells, in which case added d-functions can dramatically improve the calculation or if a more sophisticated basis set has to be chosen in order to describe the isotropic distortions of valence shells more accurately.

The split valence 6-21G basis set can be enriched by single gaussian d-type functions added to silicon (6-21G* basis set) or to both silicon and

oxygen (6-21G ** basis set). We used an exponent of 0.45 a.u. for silicon and of 0.65 a.u. for oxygen. Since Pauling (1939) it has often been suggested that 3d orbitals are used by Si in forming double bonds with the oxygen atoms of a silicate tetrahedral group as well as in the hexacoordinated state. The present calculations aim to determine if that assumption is valid; we note that an extensive discussion of the rôle played by these orbitals in the case of molecules containing silicon is given by Gibbs (1982). The additional variational freedom due to the polarization functions can account for the distorted electronic distribution on Si due to the external crystalline field which acts on partially occupied valence shells and for the formation of semi-covalent bonds; for fuller ionicity that distribution would be spherical, and therefore there would be no need for added orbitals with a high angular quantum number. The importance of d-functions can therefore be used as a qualitative indicator of the asphericity of the bonding in the system.

The geometrical parameters chosen for the optimization are first the cell volume (which is varied maintaining the c/a ratio constant); the second derivative of the energy with respect to this parameter (after allowing all the structure to relax during the compression) yields the bulk modulus ; secondly we studied the c/a ratio (at constant volume), a critical structural variable which in the case of stishovite (and other rutile structured crystals) is difficult to reproduce using semi-classical simulations; moreover the interatomic bond angles are directly related to this parameter. The internal coordinates were fixed at the experimental values given in Tab. 5.1.

The total Hartree-Fock energy and the results of the optimisation are presented in Table 5.2. Table 5.3 presents the Mulliken Population Analysis in the different cases (net charges, bond population and d-orbital population). It is important to recall that Mulliken Populations can sometimes be misleading, being strongly dependent on the basis set and on the partition scheme adopted; on the other hand, if the same conditions are used, this quantity can provide a useful comparison of different systems.

The results obtained with the three basis sets are as follows:

1) In both polymorphs, the 6-21G basis set leads to an overestimation of the volume, particularly in the case of α-quartz; also the c/a ratio is overestimated for stishovite, although it is almost exact for α-quartz.

2) As expected, after adding d-orbitals on Si (6-21G* basis set) a contraction of the unit cell volume was found (-6% in α-quartz and -1.8% in stishovite). As shown in Table 5.3 there is also an increase in the Si-O bond population and a decrease of the relative ionicity of Si and O due to the fraction of electrons transferred from oxygen to the Si-O bond because of the added orbitals; these effects are greater in α-quartz (where the bond population increases from 0.198 to 0.325) than in stishovite (where the increase is from 0.104 to 0.161). In both systems the population of the d orbitals is quite high (0.483 electrons in α-quartz and 0.434 in stishovite), showing that these orbitals play an important rôle and are extensively used by silicon in both minerals

3) If d orbitals are also added to oxygen (6-21G** basis set) there is a further, small contraction in the volume of α-quartz (which is now only 1% larger than the experimental value) and no variation as regards stishovite. Due to the availability of an extra function, oxygen gains charge (and the bond population slightly decreases because of the increased ionicity), but it must be stressed that the population of the oxygen d-functions is extremely small in both systems, being 0.015 electrons in α-quartz and 0.022 electrons in stishovite. With the enhanced basis sets the c/a ratio is very well reproduced in stishovite, where the error is lower than 1%; in the case of α-quartz the enrichment of the basis set causes a slight overestimation of the ratio: the total error is however less than 1.5%.

These preliminary indications are supported by the calculated energies: the presence of d orbitals on silicon causes a considerable drop in the total HF

energy, which is more important in α-quartz than in stishovite (0.28 and 0.13 a.u per SiO_2 unit respectively). The further addition of d orbitals on oxygen reduces the total energy by 0.06 and 0.03 a.u. per SiO_2 unit in quartz and stishovite respectively.

A crucial factor is the relative stability of the two minerals : at a 6-21G level stishovite is incorrectly found to be more stable than α-quartz (0.009 a.u.) but this result is reversed when the better 6-21G* and 6-21G** basis sets are used for which α-quartz is more stable by 0.007 a.u and 0.012 a.u. respectively (i.e. 18 kJ and 31 kJ). This result shows the inadequacy of the 6-21G basis set, but comparisons at the 6-21G** level appears to be substantially more reliable. The significant changes in energy point out that it is possible that an additional set of d orbitals on Si could give an appreciable contribution. It is not at present possible to verify this hypothesis because such calculations would have excessive computational requirements.

It is therefore possible to conclude the following:

1) The presence of d orbitals on Si has an important effect on the wave function of α-quartz and stishovite, as found by other authors. The correct reproduction of the experimental geometry of stishovite and α-quartz is not possible if the polarization effects described by these extra functions are not taken into account. d-orbitals added on oxygen do not seem to be very important; they do not modify the description of the geometry as much as the d orbitals on Si, and their energetic contribution is modest.

2) Polarization effects described by these orbitals are more important in α-quartz than in stishovite: in the tetrahedrally coordinated silicon a more substantial energetic gain is associated to Si 3d orbitals. Although the total energy of the two systems is far less affected by d-orbitals on oxygen, which are left essentially empty, they still seem to play some rôle in modelling the valence shell

in α-quartz, because of their effect on the unit cell volume, which on the other hand is negligible for stishovite.

A comparison between α-quartz and stishovite corroborates earlier evidence (Gibbs 1982) indicating that the latter is more ionic: net charges of Si and O are higher in stishovite than in α-quartz regardless of the basis set used, with stishovite being around 20% more ionic than α-quartz when the 6-21G** basis set is used, so that it is possible to conclude that the higher coordination number of silicon leads to a substantial reduction in the covalency of the Si-O bond. This result is in good agreement with Gibbs (1982) and Hill et al. (1983) where similar conclusions were found, although there are substantial differences in assigning fractional atomic charges, probably due to the different basis set and computational framework used. The increased covalent bonding character found by Li and Ching (1985) in stishovite is contradicted by the present results.

In the following sections all the results will refer to the 6-21G** basis set.

5.3.4 Electronic properties

In this section we consider the Density of States (DOS) and the electron charge density of α-quartz and stishovite. First we discuss the structure of the calculated DOS, and our theoretical results are compared with X-ray emission spectra for α-quartz. Next we show deformation electronic density maps (i.e. the density in the crystal minus the densities of non-interacting atoms), in order to get a better insight into the nature of the Si-O bond in the two systems and to understand the rôle played by the d orbitals, which proved to be so important in the description of the structural properties.

Since the zero of the one-electron energy levels is arbitrarily defined, we set the zero at the top of the valence bands (at the beginning of the gap) in both systems.

5.3.4.1 Density of States of α-quartz

The total and Projected Density of States (PDOS) into the O 2p, 2s and Si 3s, 3p and 3d orbitals is presented in Figure 5.1 (only valence bands are shown). We note that the actual scale for the Y-axis is not the same for the projections in the O and Si orbitals. The general features are those observed in all ionic oxides. In particular, two series of peaks are found in the valence band: at higher energy, just close to the gap, characterized by O 2p states and, at lower energy, by O 2s states.

The detailed features are as follows:

a) A first band, between 0 and -4.2 eV, with a predominant contribution from the oxygen lone-pair (2p non bonding orbitals); smaller contributions from Si 3p and 3d fall in this region.

b) A band located between -5.0 and -12 eV, due to O 2p and Si 3s, 3p, 3d orbitals: in this structure two sub-peaks can be identified: the Si contribution is mainly due to 3p states in the top one and to 3s states in the bottom one.

c) Between -23 and -26 eV a peak is found, due to the O 2s states that overlap Si 3p and 3s states.

It is interesting to note that there is no mixing between oxygen s and p orbitals, while the contribution due to silicon s,p and d orbitals is spread more uniformly over all the valence bands. This is particularly evident in the sub-band at about -5 eV, where partially covalent bonds are formed between O 2p orbitals and Si sp hybrids. No contribution due to d orbitals on O was found in the range of energy considered.

5.3.4.2 Density of states of stishovite

The PDOS of stishovite into the sets of valence orbitals is given in Figure 5.2 together with the total density of states. Two band structures can be identified: an upper valence band, between 0 and -14 eV and a lower bottom valence band between -24 and -30 eV.

a) The upper valence band does not have a two-peak structure as in α-quartz, nor is there the small intra-band gap as in the latter case. It is still possible to identify a main contribution , due to O 2p orbitals overlapping the Si 3d orbital, and at lower energies due to Si 3s orbitals and O 2p orbitals. The broad peak due to Si 3p orbitals extends from 0 to -14 eV, with a maximum at about -7 eV.

b) The sharp peak in the lower valence band at -25 eV is nearly totally due to O 2s states with contributions from Si 3p and Si 3d states and, at about -27 eV, from Si 3s states.

On comparing these results with those for quartz the following differences are clear: first we note that the valence bands are wider in stishovite and the gap between s and p bands is also larger. These effects are probably due to the higher density and ionicity of stishovite: the Madelung field acting on oxygen is higher and there is a stronger interaction between the electron clouds of next neighbour O atoms.

Secondly the upper valence band, which in quartz is resolved in two sub-peaks separated by a small gap, is continuous in stishovite. This effect can again be explained by taking into account the more covalent nature of the bonding in quartz: the non-bonding O Π states lie higher in energy than the bonding Σ states (corresponding to bonding contributions between O p orbitals and Si sp hybrids).

We also note (in Figure 5.1 and 5.2) that in quartz Si 3s and 3d states are much lesser populated than Si 3p states; this is not the case in stishovite: Si 3p

states are lesser populated than in quartz and their population is comparable with that of the 3s and 3d states.

5.3.4.3 Comparison with experimental data: α-quartz

There is a wide range of techniques which give information about electronic structure and the nature of bonding: X-ray emission spectra seem to be particularly suitable for a comparison with the present theoretical results, because they sample the different contributions to the bond from different sets of valence orbitals. Therefore they can be directly compared to the projected density of states, although some caution should be observed, since there is some arbitrariness in fixing the zero energy in the experimental results. In the present case we have fixed the end of the calculated valence band so that it coincides with the higher energy limit of the uppermost peak in the Si K emission spectrum. Furthermore theoretical data should be convoluted, usually by using gaussian-type functions, so that the relative height and width of each peak can be compared with experimental predictions.

All the possible emission spectra in α-quartz (Si K and L2,3 and O K) have been measured (Klein and Chun 1972), (Wiech 1984) and are shown in Figure 5.3, where dotted lines are used for the theoretical PDOS and full lines for the experimental spectra. Because arbitrary units are used for the Y-axis the scale of the theoretical results has been adjusted in order to fit as much as possible the experimental data.

The following comparisons can be made:

a) Oxygen K emission vs. calculated 2p states.

The experimental spectrum shows a sharp peak at about -3 eV followed by a shoulder localized between -5 and -10 eV, and the same features are reproduced by our calculations, although the sharp peak is reproduced as a high plateau and

the lower peak is resolved in many sub-peaks. There is no experimental evidence for the gap of less than 1 eV calculated between the two sub peaks. This gap has been found in previous theoretical studies (Wiech and Zurmaev 1984, Gupta 1985) and its occurrence has still to be experimentally verified; the width of the gap given by our calculation is of the same order as the resolution of the experimental spectra (about 0.6 eV), so that the problem is unresolved.

b) Si K emission vs. calculated 3p states.

The experimental Si K spectrum displays a sharp peak at about -6 eV followed by a shoulder from -5 eV to 0. Another peak is found at about -18 eV, in the lowest part of the valence band. The bottom peak is shifted toward more negative values by the present calculation (the exaggeration of band widths and band gaps is a well known feature of Hartree-Fock calculations (Pisani et al. 1988)). The top peak and the shoulder are reproduced by our calculations, although the previous comments on the presence of a small gap at 4.5 eV, which is not observed experimentally, apply here as well.

c) Si L2,3 emission vs. calculated 3s and 3d states.

The experimental curve displays a two-peak structure, with maxima at -3 and -8 eV in the upper valence band and a smaller peak at -20 eV. In the PDOS of the Si 3s orbitals (see Figure 5.1), the peak at -3 eV is completely absent, while the other peaks are correctly found (the peak at -20 eV is shifted towards more negative values, but the experimental peak is very broad, spanning from -15 up to -25 eV).

The absence of the upper sub-peak was observed in other theoretical simulations and it was suggested that Si 3d orbitals (that contribute to this spectrum because of the dipole transition rules) can be present in the valence band and that the peak in the non-bonding region can be, at least in part, reproduced by taking in account these orbitals (Collins et al. 1972, Urch 1969).

If Si 3s and 3d PDOS's are allowed to overlap, this suggestion is confirmed: a peak due to Si 3d non-bonding states is clearly localized between 0 and -4 eV, and a two-peak, symmetrical structure is restored. From this argument we may conclude that the present results are in good agreement with experiment, and that d orbitals on Si give a substantial contribution to the Si L2,3 emission spectrum.

5.3.4.4 Comparison with experimental data: stishovite

A similar comparison can be made as regards stishovite, whose emission spectra were collected and discussed by Brytov et al. (1979) and by Wiech (1984). The spectra are shown in Figure 5.4. Because of the lack of extensive experimental studies and of previous theoretical calculations, some caution is necessary in trying to make a comparison.

The lower valence band (lower peak in the PDOS of Si 3s and 3p) is shifted by our calculation toward more negative values;the experimental results confirm the substantially different nature of Si 3p electrons in stishovite, in particular the Si K emission is a broad peak localized at about -7 eV which is remarkably different from that in quartz. This peak is very well reproduced by the calculations. The experimental oxygen K spectra of stishovite and quartz are less different than the corresponding calculated PDOS's, and it is questionable whether this is due to a lack of resolution in the experimental data or to inadequacies in the theoretical description.

The ad-mixture of Si 3s and 3d states in the Si L2,3 spectrum is confirmed again by the calculations .

5.3.4.5 Electron Charge Density (ECHD) maps for α-quartz and stishovite

Deformation maps (crystal electron density-isolated atom electron density) are extremely useful in order to investigate the charge transfer that takes place when

chemical bonds are formed, and they give valuable information about the important contributions to the bonding (e.g. whether ionic or covalent bonding is dominant). Figures 5.5 and 5.6 show total density maps corresponding to a plane cutting the O-Si-O bond plane in the two systems, so that the two non-equivalent oxygens are included; and in Figure 5.7 and 5.8 the corresponding deformation maps are displayed.

In quartz it is possible to observe first the presence of non bonding electrons on oxygen, localised into a p-type orbital, pointing away from silicon. These electrons can therefore be associated with the non-bonding band found in the DOS, due to oxygen p orbitals Secondly we see an increase of electron density in the interatomic region between Si and O, corresponding to the covalent bonding. Thirdly, there is a net loss of electron density from regions close to the O; this loss seems to be associated with a back-donation process from O to Si, due to the instability of the ion O^{2-} in this crystalline environment. The effect of the back-donation is reflected by the shape of the electron distribution of Si, which is very asymmetric indeed, with a long tail pointing toward the O-O interatomic region. There is therefore a significant fraction of electrons involved in a charge transfer between the two species, which is not localized in the neighbourhood of the nuclei, but rather used in creating a Si-O bond, with covalent character, mainly due to an overlap between the p orbitals of silicon and oxygen, as previously noted in the Density of States.

It is also of interest to characterise the effect of d orbitals added on silicon. We plotted difference maps corresponding to the crystal described by the basis sets with and without d orbitals respectively; Figure 5.9 shows the resulting map; it appears that the predominant effect is a net charge transfer from the non-bonding oxygen p-orbitals to the bonding ones: d orbitals on Si, therefore, increase the strength of the Si-O bond, by increasing the fraction of oxygen electrons involved; the covalency is therefore also enhanced. Similar effects are found by

Gibbs et al. (1987) and Geisinger et al. (1987). This interpretation is supported by the Mulliken Population Analysis results discussed in the previous section.

For stishovite the picture turns out to be quite different: the lone-pair is much bigger than in quartz and the back-donation process is now less important, so that less charge is transferred to silicon and O preserves more of its ionic character. Therefore the distortion of the Si electron distribution is smaller, and its shape is more spherical than in quartz. The directional increase of electron density in the interatomic region between Si-O is smaller than in quartz. Note that the apparent difference between the two oxygens, despite the fact that they are crystallographically equivalent, is due to the hybridation of this species (sp_2), so that one oxygen lone-pair is coplanar to the O-Si_3 plane but the other is perpendicular to this and is not shown.

Fig.5.10, in which the effect of d-orbitals on Si is displayed, supports these observations: the charge transfer induced by d orbitals on Si is in this case much smaller than in quartz, although there is no doubt that these orbitals play a rôle in the hexa-coordinated structure as well.

Comparisons with experimental deformation density maps are in principle possible. In practice such comparisons are not generally useful, due to the fact that the experimental maps are strongly dependent on the models adopted in refining the data. Moreover many details in the valence shells are not accurately described by X-ray diffraction, since the core electrons dominate the scattering. Examples of experimental maps for quartz and stishovite are given by several authors (Hill et al., 1983 , Gibbs 1982, Geisinger et al., 1987 , Spackman et al., 1987).

5.3.5 Conclusion

In this section the electronic properties of stishovite and quartz have been studied at an ab-initio Hartree-Fock level, in order to interpret the chemical nature of the Si-O bond in the two crystalline environments. A good agreement with the experimental geometry has been found, suggesting that other structural properties could also be studied. The results concerning relative stabilities, Mulliken analysis, density of states and electron charge density, give an homogeneous, consistent picture of the two structures. In particular, it has been possible to stress the importance of silicon 3d orbitals in the Si-O bond in quartz and stishovite, where they contribute to the back-donation of electrons from oxygen to silicon, therefore stabilising the oxygen ion. A covalent character has been found in the Si-O bond of quartz, while stishovite is more ionic, although covalency is appreciable in this structure too.

5.4 AN AB INITIO HARTREE-FOCK STUDY OF $MgSiO_3$ - ILMENITE

5.4.1 Introduction

Magnesium-rich silicates form the major proportion of the Earth's mantle, a region of depth varying from 100 km to about 2800 km and which is characterized by high pressures (up to 1.4 Mbar) and temperature (up to 4000 K). A number of interesting reactions and phase transformations occur in this exceptional environment; not all of them are yet fully understood. Depending on the details of P and T and stoichiometry, magnesium silicate can adopt the spinel, ilmenite, garnet and perovskite structure. Some physical data are available on these systems. The stability relations of the magnesium silicate form of spinel, ilmenite and perovskite were investigated by Ito and Yamada (1982). Horiuchi et al. (1982) have refined the crystal structure of the ilmenite-type by single crystal X-ray analysis; the elastic constants have been determined by Weidner and Ito (1985), while heat capacity, thermal expansivity and enthalpy of transformation were measured by Ashida et al. (1988). However, because of the problems involved in the synthesis of sufficiently large quantities of sample to enable experimental studies, information on these materials is limited. Theoretical simulations of electronic and structural properties of these material are therefore of great importance.

Simulations, in which effective potentials are used to describe the interatomic forces, have been successful in reproducing structural and thermodynamical properties of these phases, and in predicting observables not yet determined by

experiments (Wall and Price, 1988; Matsui et al., 1987; Catlow and Price, 1990). Such methods are, however, unable to provide information about the electronic properties. Knowledge of the electronic structure and of the chemical nature of the bonding requires techniques that explicitly solve the Schroendiger equation. The purpose of such calculations is to investigate the nature of the bonding, especially as regards the Si-O bond, in terms of relative ionicity, electron charge distribution and density of states. This information can then be used to explain (or predict) experimental measurements, such as electron charge density maps and electronic spectra.

We present in this section the first attempt to study the ilmenite structured $MgSiO_3$ at an ab-initio periodic all-electron Hartree-Fock level, using an extended basis-set. A previous study was carried out by B. Silvi (1990) using pseudo-potentials for the description of the core electrons and a split valence basis set for the valence orbitals. The present calculations have been performed using the program CRYSTAL, as discussed in Chapter 3. In this section we will focus on the problem of choosing a reliable and balanced basis set, able to provide an accurate description of the geometry and of the electronic structure. We show that it is possible to reproduce the unit cell volume to within 1.5% of the experimental value. The eventual goal is to assess the technical needs for calculations of this type on silicates in general, which will then lead to a systematic study of the magnesium silicate polymorphs.

5.4.2 Structural data

The structure of ilmenite-type MgSiO3 was first identified by Kaway et. al. (1974). It has been shown to be stable in the pressure range from 210 to 250 kbar at 1700 °C (Ito and Yamada, 1982). The positional parameters of the atoms have

been accurately determined by Horiuchi (1982) using single-crystal X-ray diffraction techniques. The structure (space group $R\bar{3}$ is obtained by substituting Mg for Fe and Si for Ti in the ilmenite-type mineral $FeTiO_3$. Mg and Si are octahedrally coordinated and completely ordered; the oxygen atoms are arranged in an approximately close-packed hexagonal array. The positional parameters and the distances between atoms are given in Table 5.4 and the structure shown in Figure 5.11

5.4.3 Basis set effects

The establishment of a reliable, well balanced set of basis functions to describe the atomic species of the system under investigation, is an essential preliminary step of the calculation. Success in the optimization of selected geometrical parameters can be considered a good test of its quality. The optimization of the unit cell volume (varied maintaining a constant c/a ratio) with respect to the total energy is usually a reliable indicator of the quality of the basis set under test; an optimization of all the independent coordinates is at present too expensive to perform. Changes in the total energy should also be taken in account in order to evaluate the usefulness of increasing the quality of a given basis set.

In the previous section we showed that Si and O, in α-quartz and stishovite, can be described by a split-valence 6-21 G basis set enriched by polarization d-type functions. The starting point was the molecular basis sets optimized by Pople and co-workers (Binkley et al., 1980; Gordon et al., 1982). According to this basis, core electrons are described using atomic-like orbitals, resulting from a combination of 6 GTOs. A split-valence set of sp orbitals is used for valence electrons: a combination of 2 GTOs describes the inner valence region and an independent, single GTO is used for the outer region. In our earlier study only the exponent of the latter GTO was variationally reoptimized in order to take in

account the crystalline environment. The rôle of d-orbitals on Si proved to be crucial in describing correctly the two systems.

In the case of ilmenite-$MgSiO_3$ six different basis sets, of increasing quality, were investigated. For convenience these will be labelled BS1....BS6 (see Table 5.5) and are discussed below. In each case the exponent of the most external sp-type (and d-type if present) GTO on both oxygen and silicon was re-optimized: the optimized exponents are reported in Table 5.5.

For magnesium we used thoughout the basis set that had been optimized for bulk MgO by Causa' et al. (1986). The 1s and 2sp functions are described by 8 and 6 GTOs, respectively; this corresponds to a very accurate solution for the isolated Mg^{2+} ion. The basis set was then enriched by a single sp-type GTO (with exponent 0.40), that allows us to describe the contraction of the ion due to the crystalline field. This choice for Mg is justified on the basis of the highly ionic nature of Mg in this structure. Moreover the assumption of high ionicity can be tested by making the outer sp-shell more diffuse or by adding another valence function as will be discussed in the following section.

For oxygen and silicon a range of options was available. The same 6-21 G basis sets used in the case of SiO_2 were tested, with and without d-type orbitals on Si (labelled BS1 and BS2 respectively); we then adopted for oxygen the same basis set that was optimized for this species in the calculation on bulk MgO (where the 1s function is described by 8 GTOs, the 2sp function by 5 GTOs plus an additional sp-type single GTO), without changing the quality of the silicon basis set (BS4 and BS3, with and without d orbitals on silicon respectively). With reference to the latter we also checked the effects of a more sophisticated basis set on silicon (Dovesi, 1990), namely a 8-31 G (BS5), whose valence was then enriched by d-orbitals (BS6). It was not possible to test the effects of d-orbitals on oxygen because of the excessive additional computational costs: we

expect their rôle to be far less important, as our previous investigations have shown.

We note that by moving from BS1 to BS3 and BS5 we mainly improve the description of *core and lower valence states*. On the other hand, the use of polarization functions on silicon (BS2, BS4, BS6) can account for polarization effects and for the formation of covalent bonds: they improve the description of the *outer valence and of the bonding electron density*. In some extent the two problems can be considered independent.

5.4.4 Results

The calculation will be presented and discussed in the following sequence: first the effects of the different basis sets on the cell volume, energy and Mulliken population is analysed. Then we compare the influence of the basis set used for Mg in MgO, and for Si in quartz and stishovite, with the present study.

Table 5.6 presents the Mulliken population analysis for the different basis sets, the results of the volume optimization and the total Hartree-Fock energy; the Mulliken data provides useful preliminary insights into the nature of the bonding, while the energy (reported with respect to the total HF energy calculated with the first basis set BS1) allows the effects of the different basis sets on the energies to be evaluated. The HF prediction of the cell volume, which refers to 0 K, must be corrected to yield a room temperature volume, if we are to compare with experiment. We therefore used the expansion coefficient proposed by Ashida (Ashida et al., 1988) to correct our calculated 0 K volumes:

$$V(cm^3\ mol^{-1}) = V_0 + 6.427 \times 10^{-4} \times T(K)$$

The results obtained with the six basis sets are as follows:

Using a 6-21 G basis set for silicon and oxygen the volume is underestimated by -0.7 % ; the addition of d-orbitals on Si increases the contraction (-2.3 %); this result is not satisfactory, since we get a less accurate estimation of the volume by employing a better basis set. It suggests that the basis sets may be unbalanced. By adopting a richer basis set for oxygen (BS3) the volume is overestimated (+2.4 %), d-orbitals (BS4) produce a contraction (-1.1 %) that leads to a very accurate estimation of the volume. The 8-31 G basis set for silicon, with and without added d-orbitals added (BS6 and BS5), does not introduce an improvement: the error is, respectively, +2.1 % and -1.3% . We should then consider that the 0 K experimental volume we are comparing with should also be corrected to take in account the zero-point energy contraction. Simulation techniques based on effective potentials estimate this quantity as a further contraction by about 1.5% of the volume. This correction would reduce the error on the predicted volume in the cases BS3 and BS5 to below -1%, which is probably below the numerical inaccuracies of our procedure.

It is useful to consider the differences in charge and total energy produced by the different basis sets. In the first case (BS1) Mg is highly, but not completely ionic (+1.86), O is considerably ionic (-1.45 electron) and silicon shows a semi- ionic nature (+2.49 electron). The Mg-O bonds has a small, but not completely negligible bond population (0.016). A richer basis set for the oxygen (BS3) lowers the total energy by 0.475 hartree, and increases the ionicity of all the species. It should be noted that the Mg-O bond population becomes negative, indicating the completely ionic nature of the bonding; the important change in energy is due to the better description of low energy oxygen core orbitals. The population of the Si-O bond is higher in the case of BS1 (where oxygen core electrons are less strongly localized). By improving the description of the core on silicon (BS5) the gain in energy is much smaller (0.042 hartree); charges and bond-populations are very slighty affected. In all three cases, d-orbitals added on silicon lower the total energy and reduce the relative ionicity of Si and O, because

of the fraction of electrons transferred from oxygen to the Si-O bond (whose Mulliken population increases considerably); magnesium is left almost unaffected. As expected, notwithstanding the nature of the basis set used for the core electrons, the population of the d-orbitals on silicon is very similar in the three cases (about 0.4 electrons); likewise the bond population between Si and O (about 0.17 ~ 0.18 electrons)is unaffected. This confirms that the quality of the description of lower-lying energy states only slightly affects the chemical bonding.

These results show that core electrons on the oxygen are not adequately described by a 6-21 G basis set, that is unbalanced with respect to the one used for magnesium; moreover it does not allow the valence distribution to relax enough in the presence of about 1.5 extra electrons. A better basis set for oxygen considerably stabilizes the system and improves the optimized unit cell volume (case BS3). For silicon the situation is more favorable: the 6-21 G basis set appears to be adequate in describing the low-lying states; the description of the valence electrons, that are involved in weak covalent bonding with the six neighbouring oxygens, is quite satisfactory and can easily be improved by the addition of localized d-functions (case BS4). The use of a richer basis set for the silicon core (e.g. the 8-31 G tested in this study, case BS5) does not seem to be justified on the basis of the present results. Therefore in the following sections we shall concentrate on results obtained with BS3 and BS4.

It is interesting to compare the effect on the energies and populations, of the addition of more external sp-function and of d-orbitals on Mg, for MgO and $MgSiO_3$. Polarization functions are expected to play a minor rôle in a fully ionic system and their importance is expected to increase with the increasing covalent character of the bonds. In Table 5.7 we present the Mulliken Population analysis and the total energy (per Mg atom in the unit cell, with reference to the case in which the sp-functions are removed (corresponding to the fully ionic Mg basis

set)). Increasingly diffuse sp-functions are tested and a set of d-functions, described by a single GTO with exponent a=0.50 is also added. In both MgO and $MgSiO_3$ a more diffuse sp-function on Mg produces an almost linear decrease in the energy, while the population of the sp-orbitals regularly increases (but always remains very small). This effect is about 10 times greater in $MgSiO_3$ than in MgO. The presence of d-orbitals is twice as important in the ilmenite-structure as in MgO; and Mg in the former crystal is less ionic by 0.1 electron than in MgO, regardless on the basis set that is used. Although the Mg^{2+} ion appears to be less stable in the ilmenite structure, the essentially ionic nature of Mg in this structure is confirmed.

It is interesting to compare the silicon species in $MgSiO_3$-ilmenite, stishovite and α-quartz. We performed calculations on the latter two systems using the basis sets labelled BS3 and BS4 for oxygen and silicon. We note that in stishovite this basis set produced dangerous linear dependencies in the HF eigenvectors, so that stricter computational conditions, and slightly more localized valence functions on silicon were necessary (the most external sp-functions, described by a single GTO, use an exponent of 0.16; an exponent of 0.55 was used for the d-functions). In Table 5.8 we present the Mulliken Population data and the effect on the energy due to the presence of d-functions on Si in the three systems (per Si atom in the unit cell).

If we adopt the Si-O bond population and the energetic changes induced by the d-functions as an indicator of the relative covalent nature of the bonding, we find that the ionicity-scale is as follows: stishovite > ilmenite > α-quartz. It is particularly interesting to note that the effect of d-orbitals on Si in quartz is one third greater than in ilmenite and that these orbitals are twice as important in α-quartz as in stishovite. The slightly different basis set adopted for stishovite does not affect this result, since its effect on the energy is probably one order of magnitude lower than the actual differences found amongst the three systems. If we consider the individual atomic species, we note that Si is more covalent and

oxygen is more ionic in ilmenite than in stishovite, as the electrostatic potential on the Mg ions promotes greater ionicity in the oxygen.

5.4.5 Electronic properties

The total density of states (DOS), and its projections (PDOS) into sets of orbitals (O 2s and 2p and the Si 3s,3p and 3d) is presented in Figure 5.12 (where only valence bands are shown). We note that the actual scale for the y-axis is not the same for the projection in the O and Si orbitals. The general features are those observed in many other ionic oxides, in particularly there is a striking similarities with the DOS of stishovite . Two bands are found in the valence region: at higher energies, just close to the gap, characterized by O 2p and, at a lower energy, by O 2s states. In the first band, located between 0 and -9 eV, two contributions can be identified: a peak at -2 eV with a predominant contribution from the oxygen lone-pair (2p non-bonding orbitals); smaller contributions from Si 3p and 3d also fall in this region; another peak, at about -5 eV is due to O 2p and Si 3s, 3p and an almost negligible contribution from Si 3d orbitals. We note that the Si 3p and 3s states do not overlap with each other.

Between -20 and -25 eV another band is found, due to O 2s states that overlap Si 3s,3p and 3d orbitals. Again, there is no significant overlap between the Si 3s and 3p states.

Deformation maps (crystal electron density - isolated atoms electron density) provide a useful insight into the bonding. It is possible to investigate the charge transfer that takes place when the bonds are formed and the polarization effects on the charge distribution. Fig 5.13 and 5.14 show the deformation maps corresponding to a plane cutting the O-Si-O and O-Mg-O bond plane respectively. It is possible to observe the presence of non-bonding electrons on oxygen,

localised into a p-type orbital. This orbital points away from silicon, and it is strongly polarized towards the magnesium ion. These electrons are associated with the non-bonding sub-band found in the DOS, due to oxygen p orbitals. There is an increase of electron density in the interatomic region between Si and O, corresponding to the formation of a covalent bond; this effect is associated with the loss of charge from a region close to the O, that can be explained by considering that O^{2-} is unstable in this crystalline environment. We also observe the highly distorted and polarized shape of the charge distribution on Si, with an increase of electron density, with respect to the ideal cation, in the direction of the Si-O bond. We can therefore conclude that there is a significant fraction of charge used in creating a Si-O bond (as found in the Mulliken analysis); as indicated by the density of states this is mainly due to an overlap between p orbitals of silicon and oxygen. Magnesium is remarkably different from silicon: the shape of the cation is almost spherical and there is no evidence of an increase in charge between Mg and O. This indicates again the completely ionic nature of Mg. It has indeed an electrostatic effect on oxygen, that results in a polarization of the lone-pair.

5.4.6 Conclusion

In this chapter we have presented the first study of a magnesium-silicate ($MgSiO_3$-ilmenite) at an HF periodic ab-initio level, using an extended basis set. Different basis sets have been carefully tested and compared.The importance of correctly taking into account the ionicity of oxygen has been shown. The rôle of d-orbitals on silicon has also been stressed. We showed that it is possible to reproduce the unit cell volume with great accuracy. The Si-O bond appears to be more covalent in $MgSiO_3$ than in SiO_2-stishovite, while the oxygen atoms are

more ionic and more polarized in the ilmenite structure, because of the presence of the Mg ions.

Further studies are in progress, in particular on $MgSiO_3$-perovskite and Mg_2SiO_4-forsterite, in order to check if the basis set adopted in this study can be easily transferred to other structures.

TABLE 5.1

Experimental positional parameters, unit cell volume and average Si-O bond length in α-quartz and stishovite (taken from Jorgensen, 1978).

	α-quartz	**stishovite**
a / Å	4.9147	4.1772
c / Å	5.4065	2.6651
x (Si)	0.467	0.000
x (O)	0.415	0.306
y (O)	0.268	0.306
z (O)	0.214	0.000
volume / $Å^3$	113.10	46.50
Average Si-O bond lenght / Å	1.608	1.774

TABLE 5.2

Energy (in a.u. per SiO_2 unit) and results of the geometry optimization for α-quartz and stishovite using different basis sets. ΔE is the difference between the energy of α-quartz and stishovite.

	Basis set	**α-quartz**	**stishovite**	**ΔE**
	6-21G	-438.6372	-438.6459	0.009
ENERGY	6-21G*	-438.7176	-438.7108	-0.007
	6-21G**	-438.7376	-438.7261	-0.012
	6-21G	1.082	1.023	
V / V0	6-21G*	1.019	1.004	
	6-21G**	1.010	1.004	
	6-21G	1.097	0.666	
c/a	6-21G*	1.090	0.647	
	6-21G**	1.086	0.643	
	(experimental)	1.100	0.638	

TABLE 5.3

Mulliken Population analysis for different basis sets: net charges on Si and O, population of d-orbitals (where used) and average Si-O bond population.

	6-21 G		**6-21 G***		**6-21 G****	
	quartz	**stishovite**	**quartz**	**stishovite**	**quartz**	**stishovite**
q(Si)	2.38	2.70	1.75	2.28	1.94	2.42
q(O)	-1.19	-1.35	-0.88	-1.14	-0.97	-1.20
q d(Si)	--	--	0.483	0.434	0.423	0.415
q d(O)	--	--	--	--	0.015	0.022
q(Si-O)	0.198	0.104	0.325	0.161	0.305	0.151

TABLE 5.4

Positional and cell parameters of the ilmenite-structured $MgSiO_3$ (after Horiuchi et al., 1982)

	x	y	z
Mg	0	0	.35970
Si	0	0	.15768
O	.3214	.0361	.24077

a = 4.7284 Å
c =13.5591 Å
Volume = 262.54 $Å^3$

TABLE 5.5

Basis Sets for Si and O, with the optimized exponent (a) used for the external sp-functions and (if present) the extra set of d-functions. In all the cases Mg is described by an 8-61 G basis set, as optimized for MgO bulk.

	Si	O
BS1	6-21g (a=.130)	6-21g (a=.350)
BS2	6-21g (a=.130) +d (a=.450)	6-21g (a=.350)
BS3	6-21g (a=.134)	8-51g (a=.244)
BS4	6-21g (a=.134) +d (a=.490)	8-51g (a=.244)
BS5	8-31g (a=.130)	8-51g (a=.244)
BS5	8-31g (a=.130) +d (a=.540)	8-51g (a=.244)

TABLE 5.6

Mulliken Population Analysis (net charges and bond populations), total energy and optimized unit cell volume (V) for the different basis sets tested. The energy (in a.u.) is given as a difference with respect to the total HF energy obtained using the basis sets (BS1). V/V_0 refers to the experimental V_0, corrected in order to take in account the effects of the crystal expansion and the zero-point energy from 298 K to 0 K.

	BS1	BS2	BS3	BS4	BS5	BS6
q(Si)	2.42	2.17	2.60	2.25	2.52	2.22
q(O)	-1.42	-1.34	-1.51	-1.39	-1.49	-1.38
q(Mg)	1.85	1.84	1.93	1.92	1.93	1.92
q(Si-O)	.130	.170	.115	.172	.119	.171
q d(Si)	----	.35	----	.39	----	.35
q (Mg-O)	.016	.018	-.004	.000	-.004	-.001
Energy	----	-.1262	-.4752	-.6257	-.5171	-.6671
V/V0	.993	.977	1.024	.989	1.021	.987

TABLE 5.7

Influence of the basis set of magnesium on the Mg net charge, the total HF energy (in a.u.) and the population of the d orbitals (if present). Reference is made to the 'fully-ionic' basis set, where the set of external sp-functions is removed. a is the exponent of the single GTO used to describe this set of function.

Mg Basis Set	MgO			$MgSiO_3$		
	qMg	q(d)	ΔE	qMg	q(d)	ΔE
no sp	2.00		----	-2.01		----
sp(a=0.40)	-1.98		-.0030	-1.92		-.013
sp(a=0.35)	-1.97		-.0031	-1.89		-.0152
sp(a=0.30)	-1.96		-.0033	-1.85		-.0167
sp(a=0.30) + d(a=0.50)	-1.90	.041	-.0035	-1.81	.058	-.0299

TABLE 5.8

Comparison between quartz, stishovite and ilmenite. Mulliken charges and the descrease in energy (ΔE, in a.u.) produced by d-functions on Si are reported. All data were obtained using a 6-21G basis set on Si and a 8-51G basis set on O (cases BS3 and BS4, as explained in Table 5.5)

Si Basis Set	**no d orbitals on Si**			**with d orbitals on Si**				
	q(Si)	q(O)	q(Si-O)	q(Si)	q(O)	q(Si-O)	q(d)	ΔE
quartz	2.61	-1.31	.170	1.77	-0.88	0.328	.470	1.01
stishovite	2.89	-1.45	.060	2.50	-1.25	0.108	.352	-.494
ilmenite	2.60	-1.51	.115	2.25	-1.39	0.172	.390	-.753

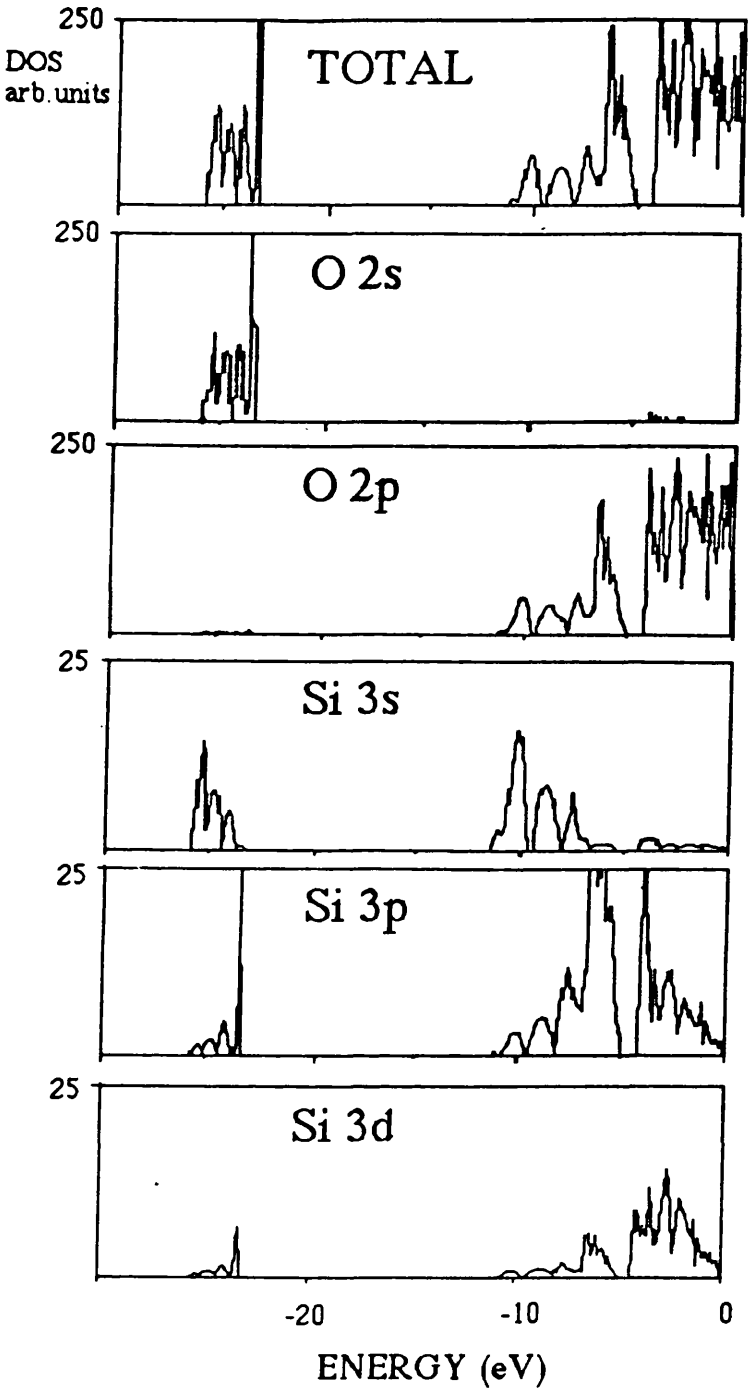

Figure 5.1. Total and Projected Density of States of α-quartz. The vertical scale in the case of Si states is expanded by a factor of ten.

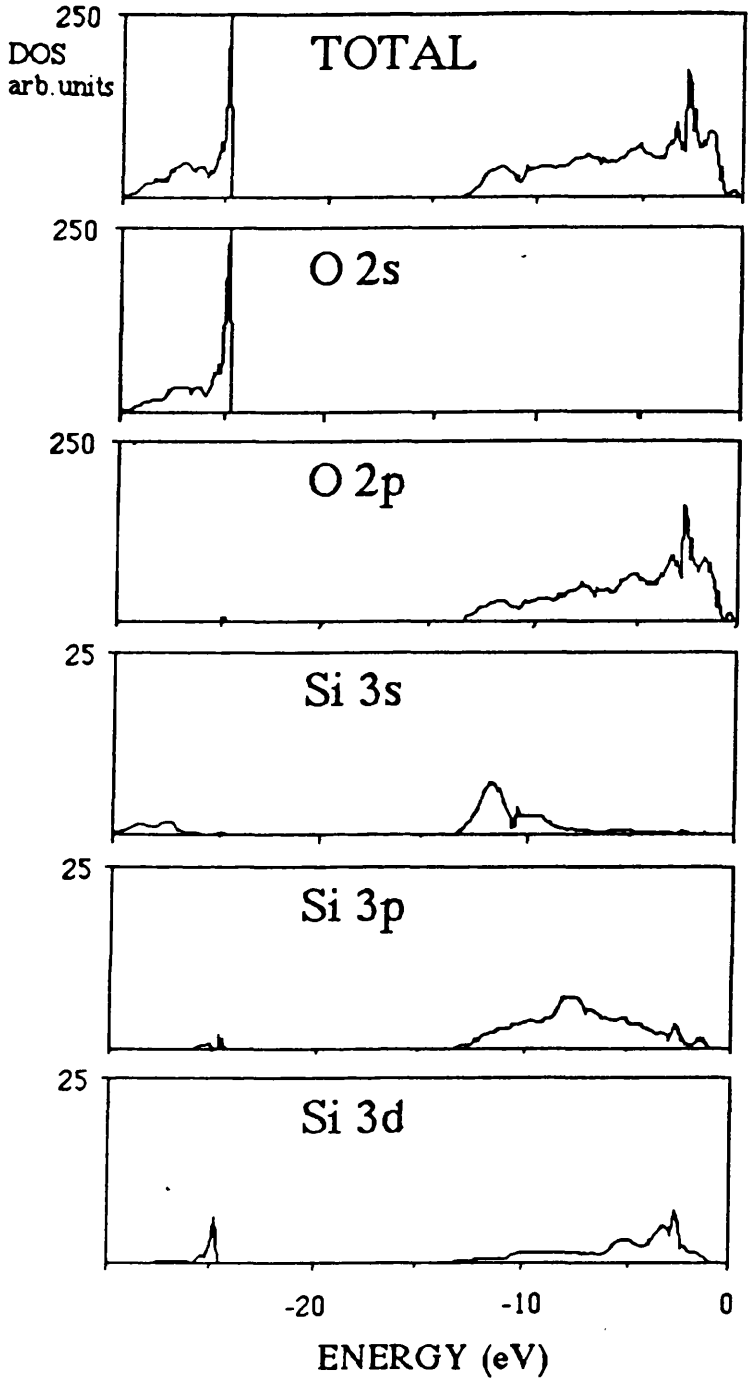

Figure 5.2. Total and Projected Density of States of stishovite. The vertical scale in the case of Si states is expanded by a factor of ten.

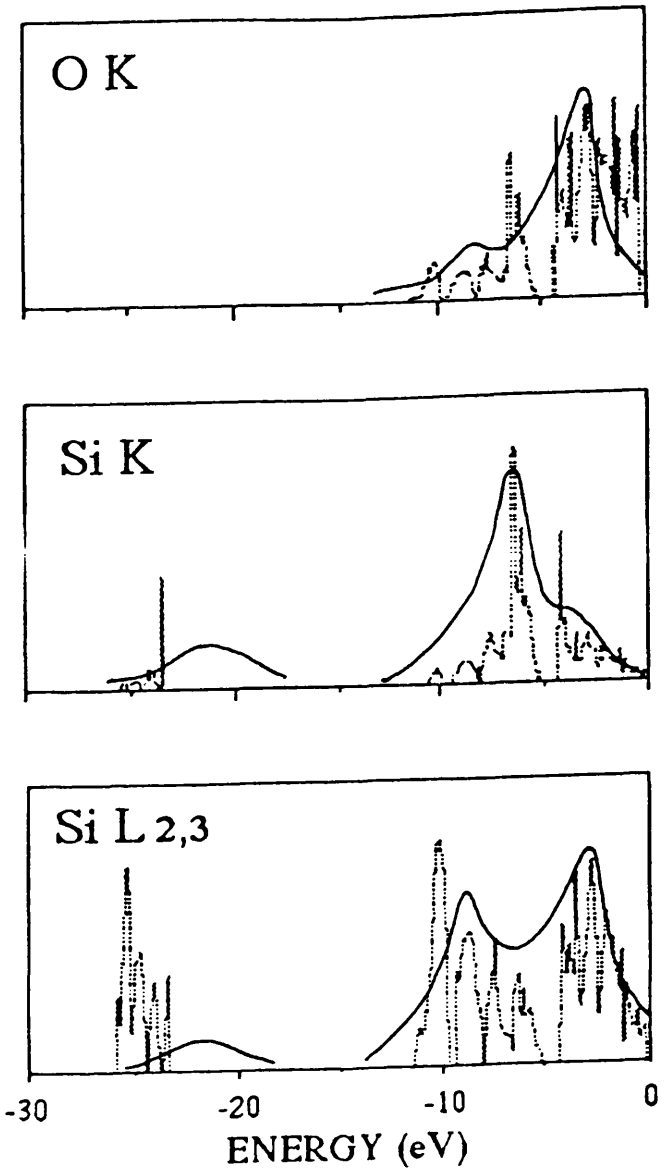

Figure 5.3. X-ray emission spectra of α-quartz. Experimental data are plotted in full lines; theoretical results are in dotted lines. The vertical scale is in arbitrary units.

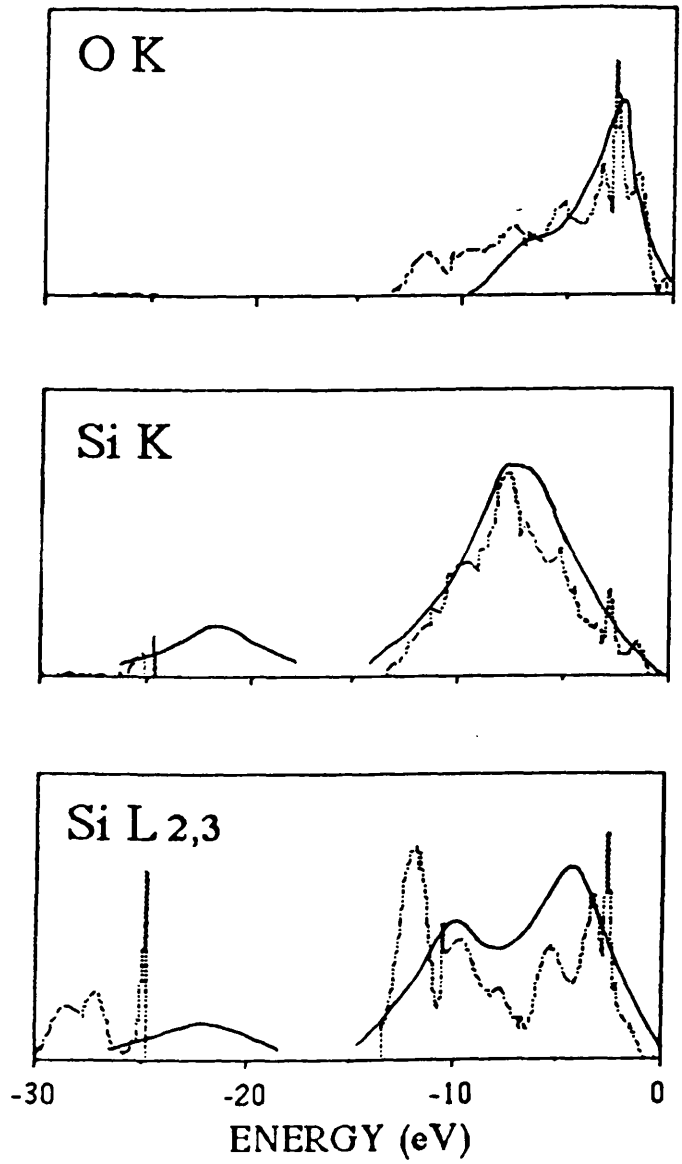

Figure 5.4. X-ray emission spectra of stishovite. Experimental data are plotted in full lines; theoretical results are in dotted lines. The vertical scale is in arbitrary units.

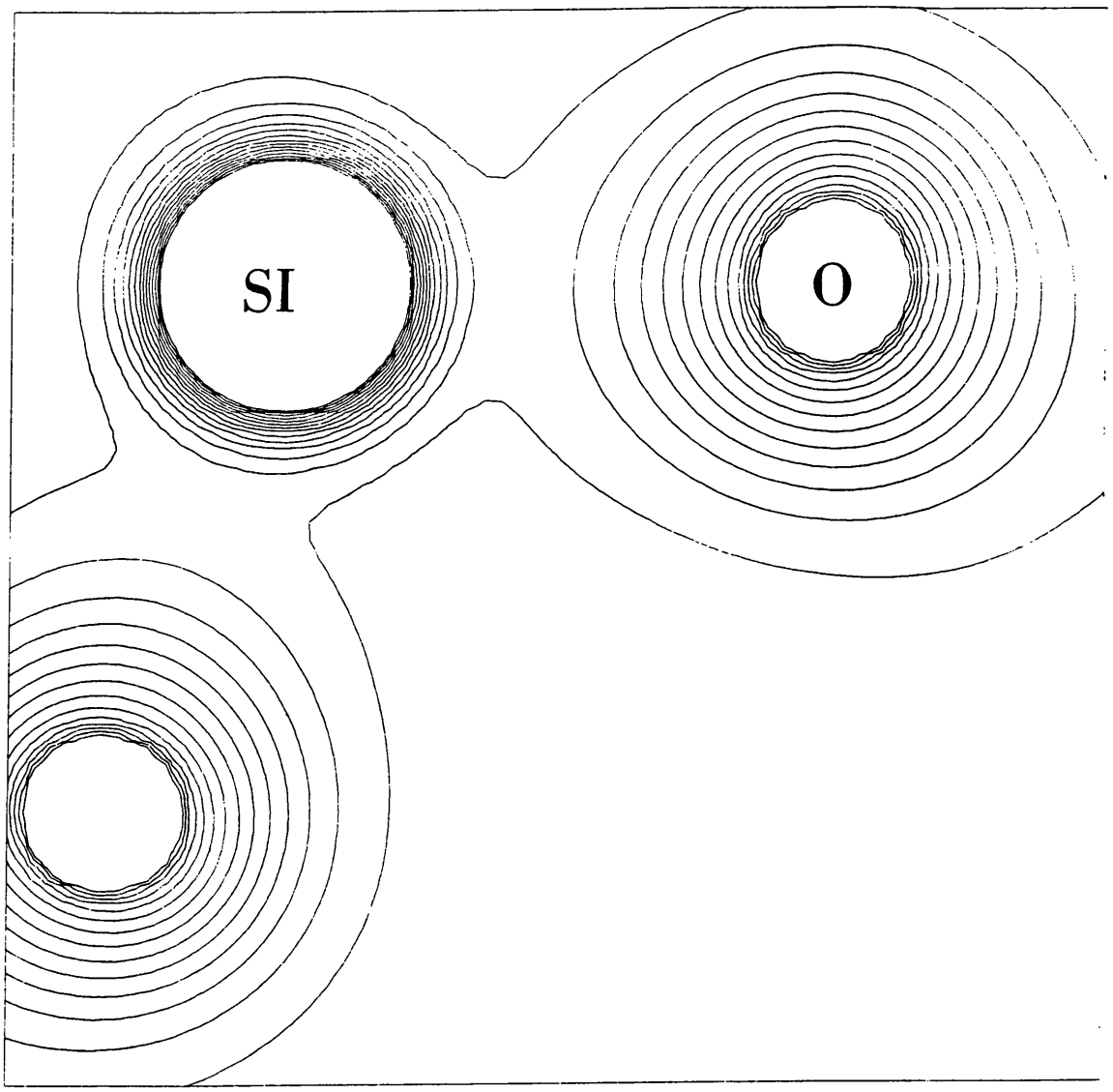

Figure 5.5. Electronic total charge density map corresponding to a plane cutting the O-Si-O plane in quartz. Contour intervals correspond to increases of 0.10 el/(a.u.)^3

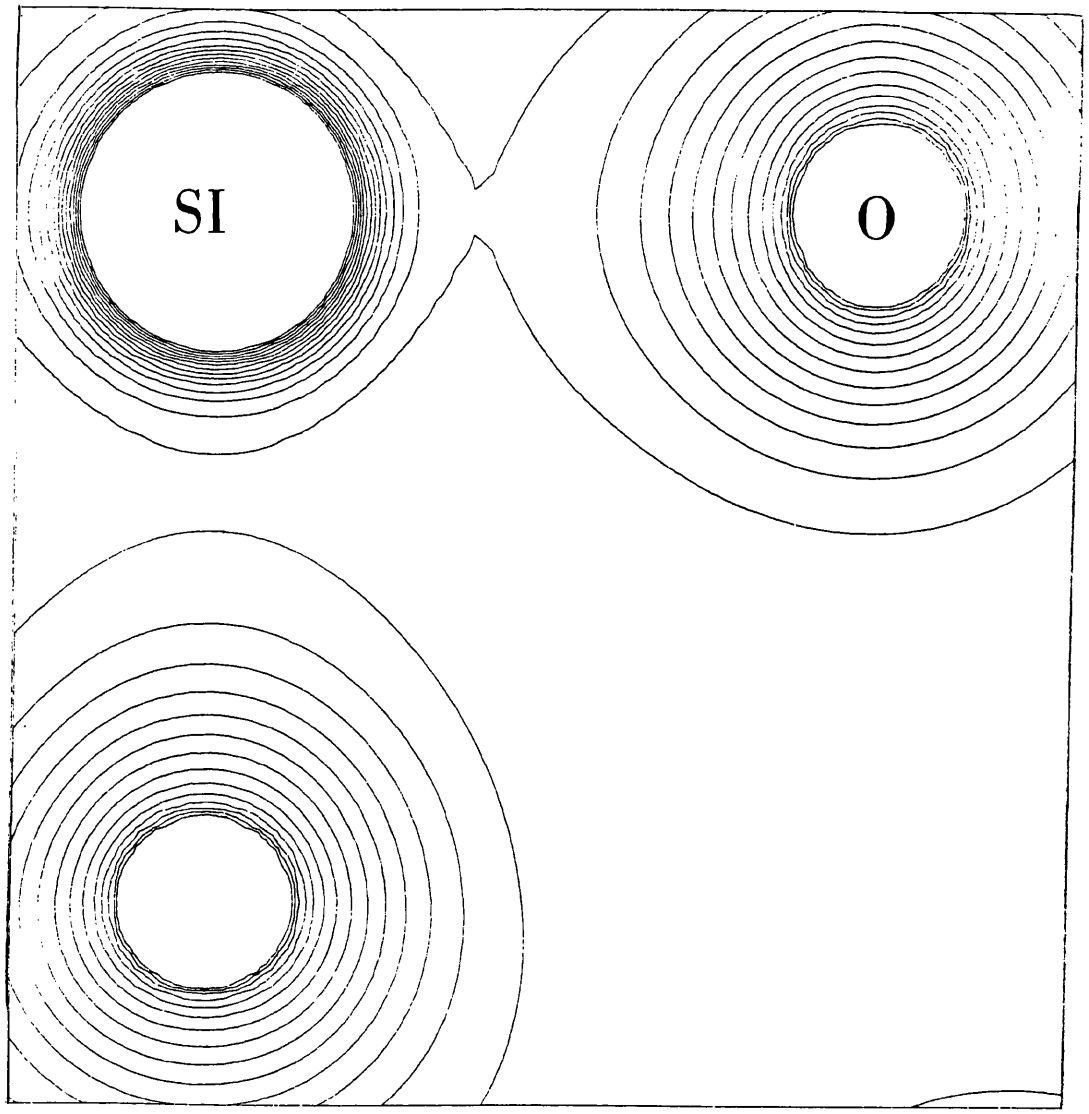

Figure 5.6. Electronic total charge density map corresponding to a plane cutting the O-Si-O plane in stishovite.Contour intervals correspond to increases of 0.10 el/(a.u.)^3

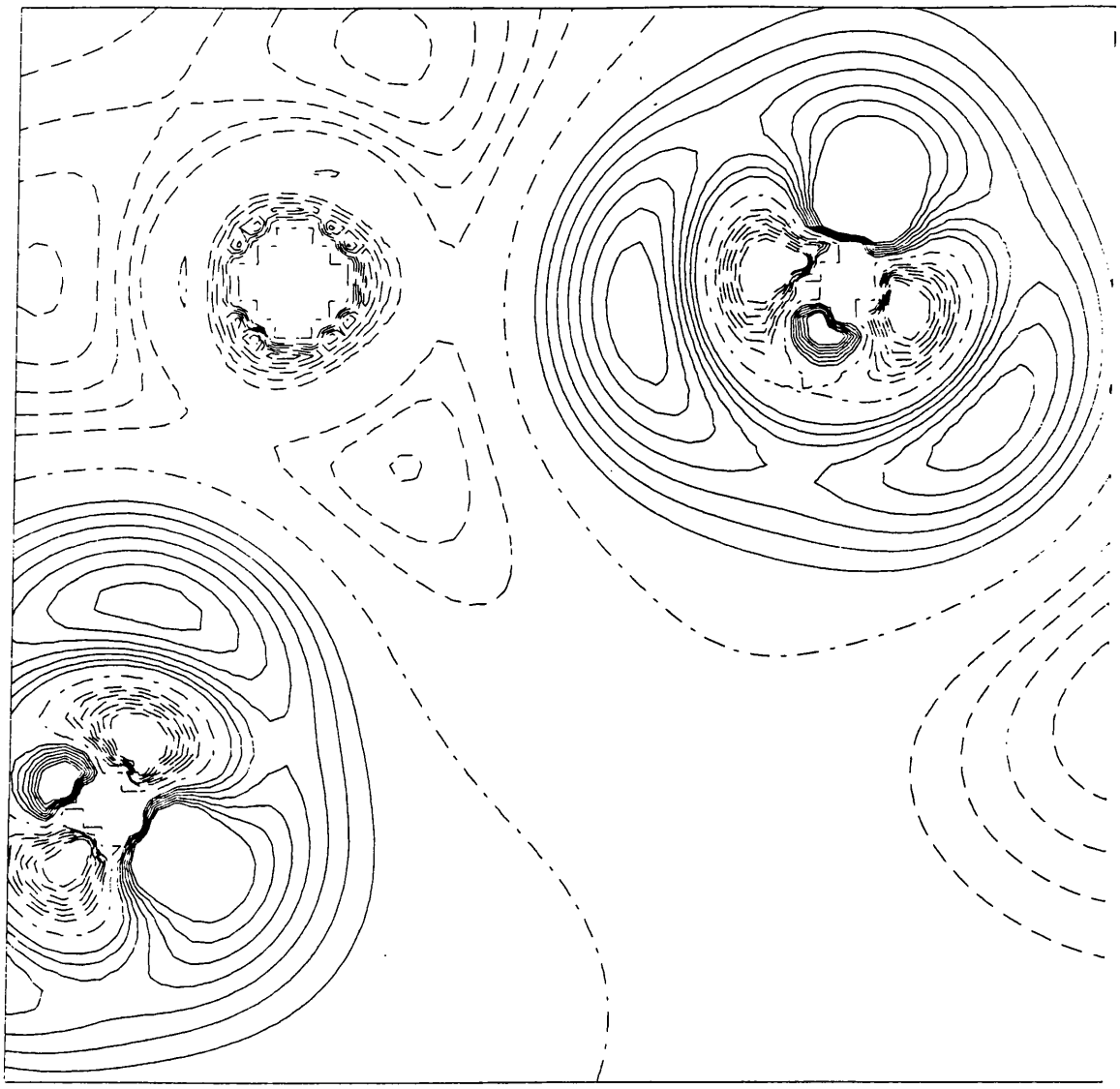

Figure 5.7. Electronic charge deformation map (crystal - isolated atoms) for quartz. Atomic positions as in figure 5.5. Full and dashed lines indicate positive and negative values respectively; dot-dashed line corresponds to the zero-level.Contour intervals correspond to increases of 0.010 el/(a.u.)^3

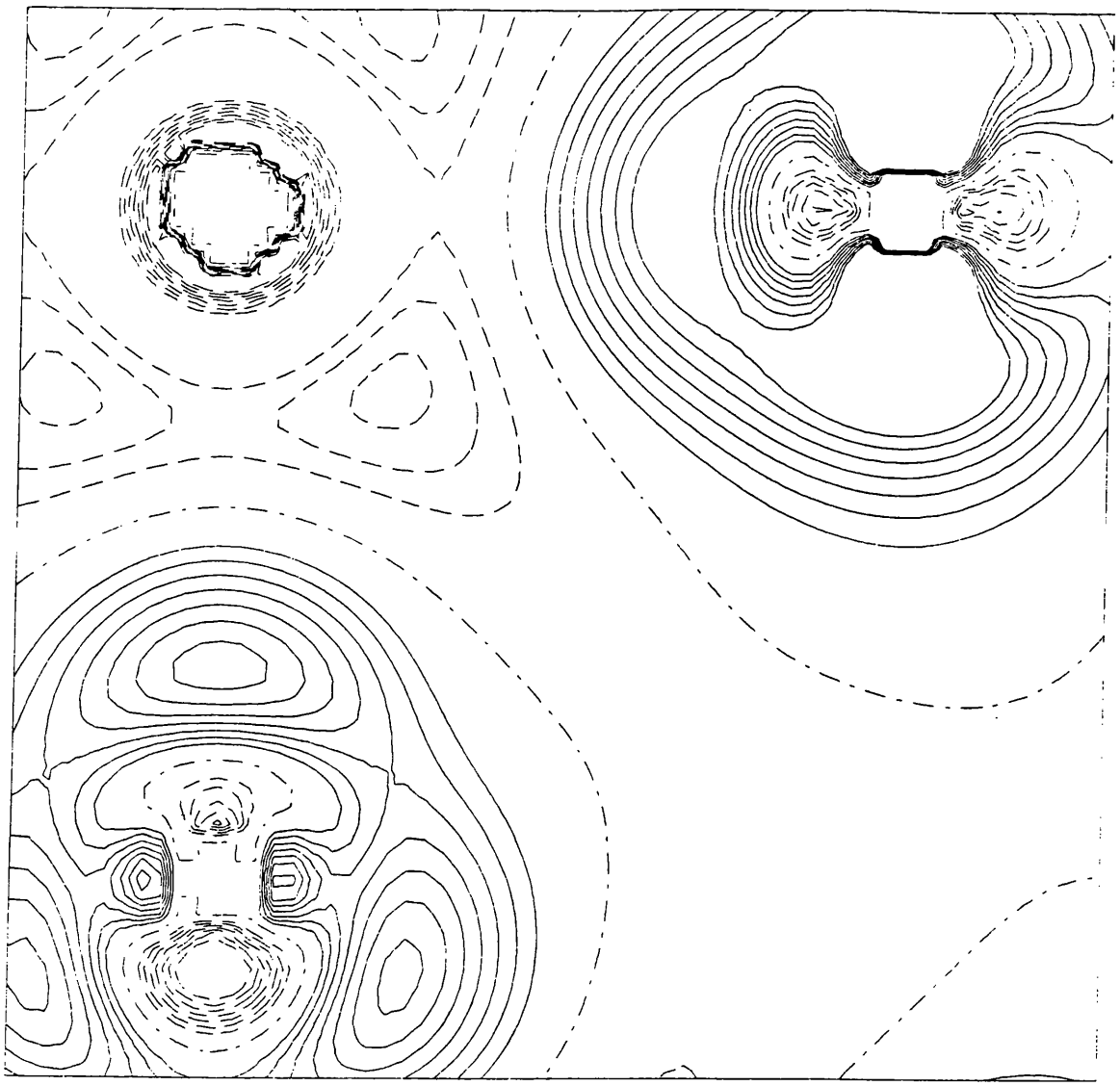

Figure 5.8. Electronic charge deformation map (crystal - isolated atoms) for stishovite. Atomic positions as in figure 5.6 and intervals as in Figure 5.7. Full and dashed lines indicate positive and negative values respectively; dot-dashed line corresponds to the zero-level.

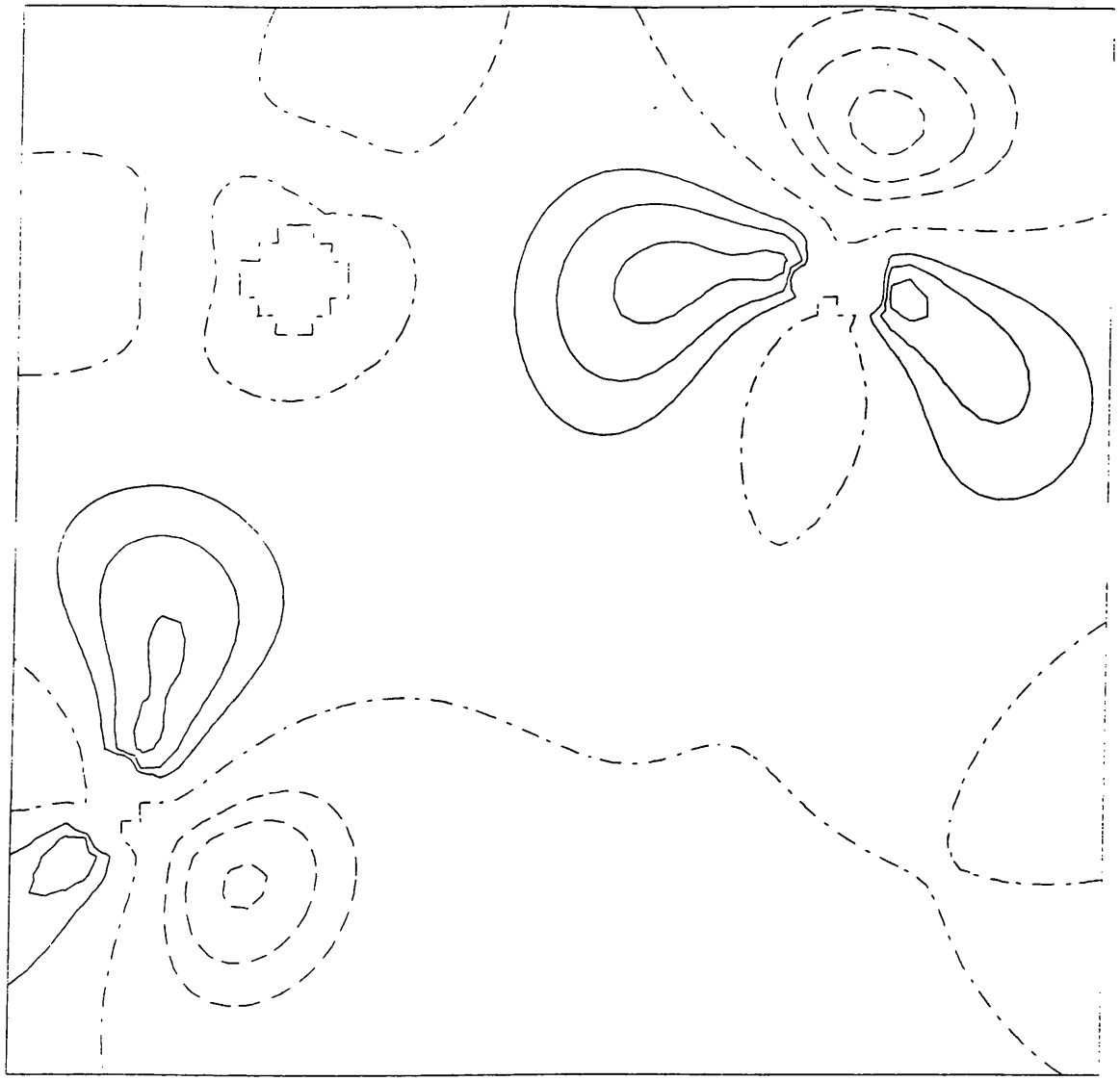

Figure 5.9. Electronic charge difference map corresponding to quartz described by a basis set with and without d orbitals respectively (6-21G**-6-21g). Atomic positions as in figure 5.5 and intervals as in Figure 5.7. Full and dashed lines correspond to positive and negative values respectively; dot-dashed line corresponds to the zero-level.

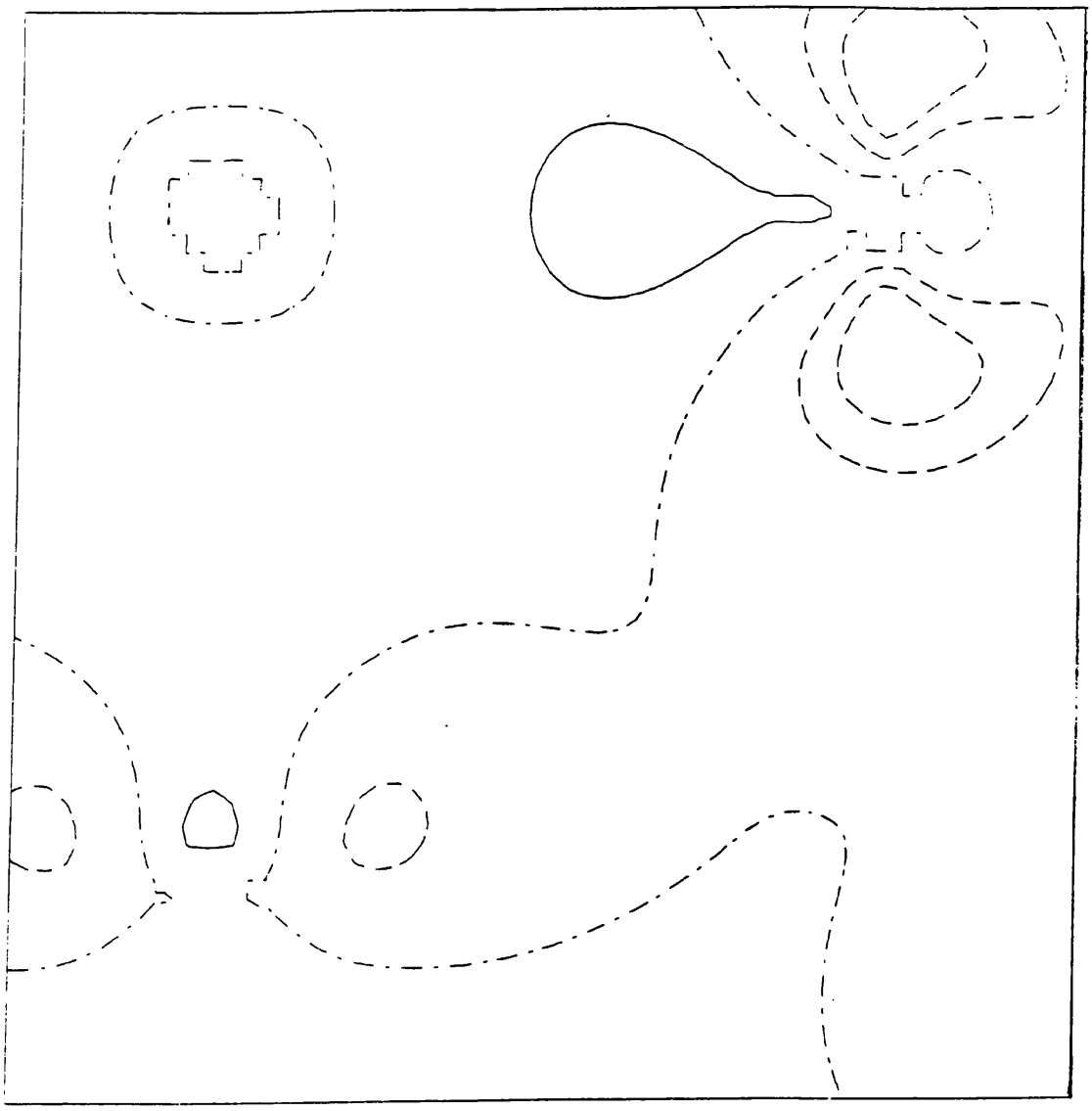

Figure 5.10. Electronic charge difference map corresponding to stishovite described by a basis set with and wihout d orbitals respectively (6-21G**-6-21g). Atomic positions as in figure 5.6 and intervals as in Figure 5.7. Full and dashed lines correspond to positive and negative values respectively; dot-dashed line corresponds to the zero-level.

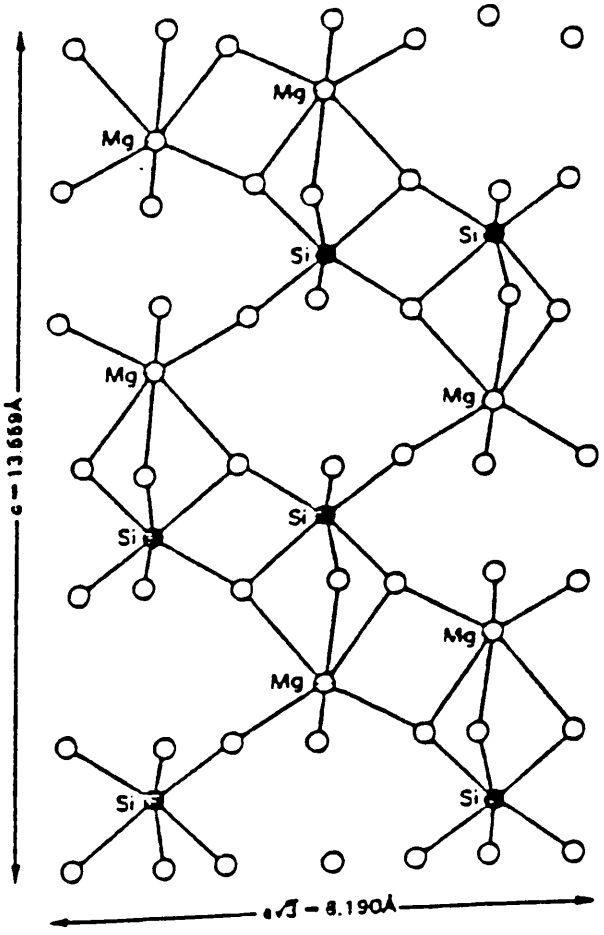

Figure 5.11 A perspective view of the ilmenite structured $MgSiO_3$ after Horiuchi et al. (1982). Open circles, oxygen; shaded circles, Mg; black circles, Si.

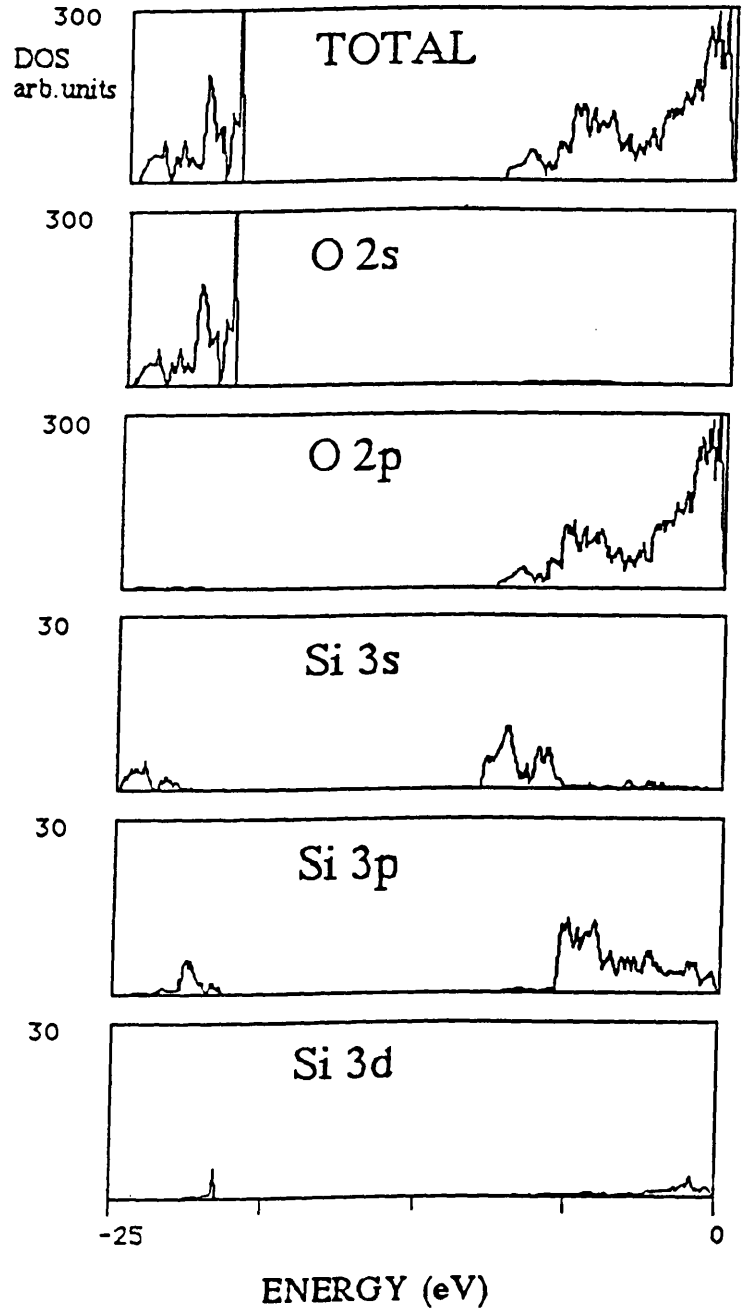

Figure 5.12 Total and projected density of states of $MgSiO_3$. The vertical scale in the case of Si states is expanded by a factor of ten.

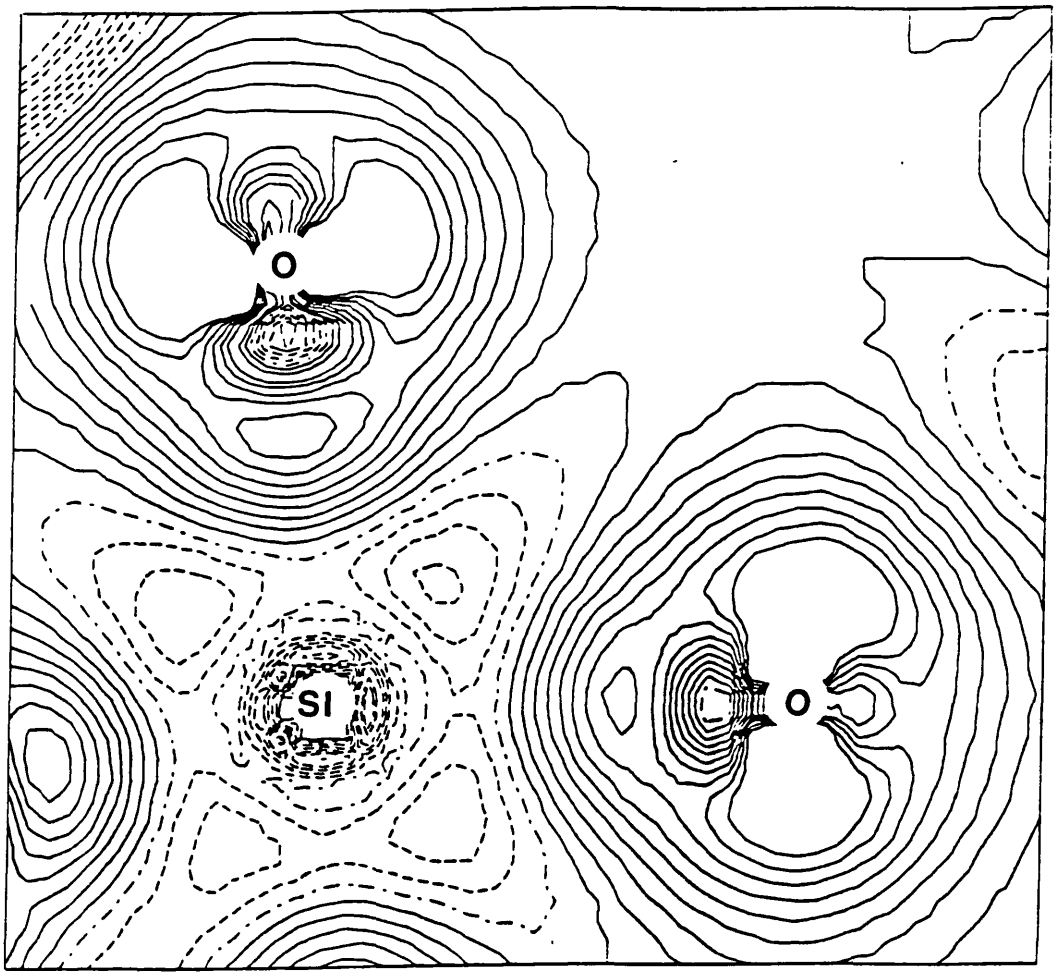

Figure 5.13 Electron charge deformation map (crystal - isoalted atoms) corresponding to a plane cutting the O-Si-O plane. Full and dashed lines indicate positive and negative values respectively; dot-dashed line corresponds to the zero-level.Contour intervals correspond to increases of 0.010 el/(a.u.)3

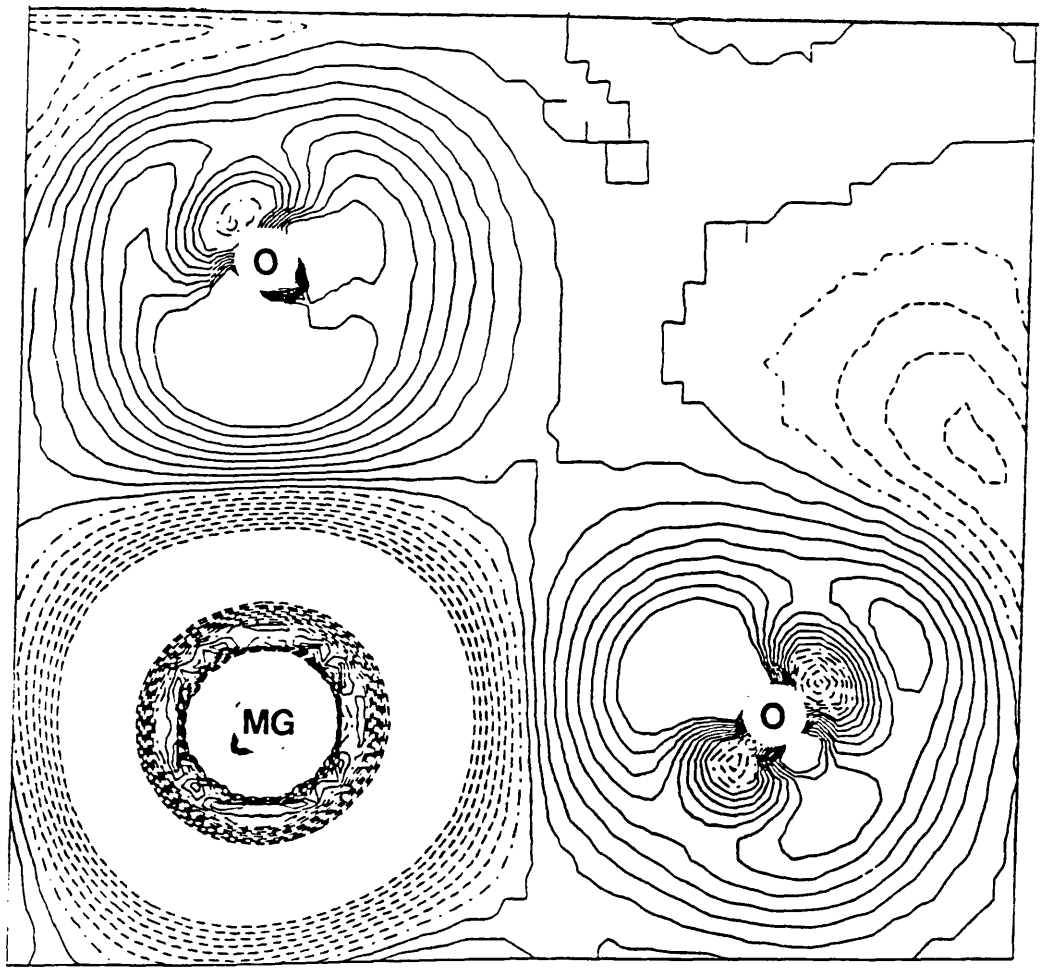

Figure 5.14 Electron charge deformation map (crystal - isoalted atoms) corresponding to a plane cutting the O-Mg-O plane. Full and dashed lines indicate positive and negative values respectively; dot-dashed line corresponds to the zero-level.Contour intervals correspond to increases of 0.010 el/(a.u.)3

REFERENCES

Agullo-Lopez F, Catlow CRA and Townsend PD (1988), Point defects in materials, Academic Press

Ashida T , Kume S , Ito E and Navrotsky A (1988), Phys Chem Minerals, 16, 239

Baur HW and Khan AA (1971) Acta Cryst B, 27,2133

Binkley JS, Pople JA and Hehre WJ (1980), J Am Chem Soc ,102, 939

Brytov IA, Romashchenko YN and Shchegolev BF (1979), J Structural Chem, 20,190

Carlisle EM (1970), Sciences (NY), 167, 279

Catlow CRA and Price GD (1990), Nature, 6290, 243

Causa' M, Dovesi R, Pisani C, Roetti C (1986), Phys Rev B, 33,1308

Causa' M, Dovesi R, Roetti C, Kotomin E and Saunders VR (1987), Chem Phys Letters , 140,120

Chao ECT, Fahey JJ, Littler J and Milton DJ (1962), J Geophys Res, 67,419

Cohen RE (1987), Geophys Res Lett ,14,37

Collins GDA, Cruickshank DWJ and Breeze A (1972), J Chem Soc Faraday Trans, 68,1189

Dovesi R, Pisani C , Roetti C and Silvi B (1987), J Chem Phys , 86,6967

Dovesi R, Pisani C, Roetti C, Causa' M and Saunders VR (1988), QCPE Program N.577, Quantum Chemistry Program Exchange, Indiana University, Bloomington, Indiana, U.S.A.

Dovesi R, Pisani C, Roetti C, Silvi B (1987), J Chem Phys, 86, 6967

Edge RA and Taylor HFW (1971), Acta Crystallogr B, 27, 594

Geisinger KL, Spackman MA and GV Gibbs (1987), J Phys Chem ,91,3237

Gibbs GV (1982), Am Min, 67,421

Gibbs GV, D'Arco P and MB Boisen Jr (1987), J Phys Chem, 91,5347

Glidewell C (1977), Inorg Chim Acta, 25, 77

Glidewell C (1978), Inorg Chim Acta ,29, L283

Gordon MS, Binkley JS, Pople JA, Pietro WJ and Hehre WJ (1982), J Am Chem Soc, 104, 2797

Grimm H and Dorner B (1975), J Phys Chem Solids, 36,407

Gupta PR (1985), Phys Rev B, 32,8278

Hehre WJ Stewart RF and Pople JA (1969), J Chem Phys, 51(6),2657

Hill RJ, Newton MD and Gibbs GV (1983), J Sol State Chem, 47,185

Horiuchi H, Hirano M, Ito E and Matsui Y (1982), Am Min, 67, 78??

Ito E and Yamada H (1982), Stability relations of silicate spinels, ilmenites and perovskites In S Akimoto and M H Manghnani, Eds., High-pressure research in geophysics, p.405-419, Centre for Academic Publications, Tokyo, Japan

Jackson MD Gordon RG (1988), Phys Chem Minerals, 16,212

Jorgensen JD (1978), J Appl Phys, 49,5473

Kawai N, Tachimori M and Ito E (1974), Proceedings of the Japan Academy, 50, 378

Klein G and Chun HU (1972), Phys Stat Sol (b), 49,167

Lasaga AC and Gibbs GV (1988), Phys Chem Minerals, 16, 29

Levien L, Prewitt CT and Weidner DJ (1980), Am Min , 65, 920

Li YP, Ching WY (1985), Phys Rev B, 31,2172

Liebau F (1971), Bulletin Societe Francaise de Mineralogie et de Cristallographie , 94, 239

Matsui M , Akaogi M and Matsumoto T (1987), Phys Chem Minerals, 14, 101

Nada R, Catlow CRA, Dovesi R and Pisani C (1990), Phys Chem Minerals, 17, 353

Nizam M, Bouteiller Y, Silvi B, Pisani C, Causa' M and Dovesi R (1988), J Phys C ,21,5351

O'Keeffe M, Hyde BG (1978), Acta Crystallogr B, 34, 27

Pantelides ST and Harrison WA (1976), Phys Rev B ,13,2667

Pauling L (1939), The nature of the chemical bond, 1st ed. Cornell University Press, Ithaca, New York

Pisani C, Dovesi R, Roetti C (1988), Hartree-Fock ab-initio treatment of crystalline systems Lecture Notes in Chemistry. Springer Verlag, Heidelberg

Ringwood AE (1975), Composition and Petrology of the Earth's mantle, Mac Graw Hill

Sanders MJ, Leslie M and Catlow CRA (1984), JCS Chem Commun, 1271

Shomaker V, Stevenson DP (1941), J Am Chem Soc, 63,37

Silvi B (1990), to be published

Silvi B and Dovesi R (1990), to be published

Sinclair W, Ringwood AE (1978), Nature ,272,714

Smith SG Alexander LE (1963), Acta Cryst ,16,462

Spackman MA, Hill RJ and Gibbs GV (1987), Phys Chem Minerals ,14,139

Stishov SM and Popova SV (1961), Geochemistry ,10,923

Urch DS (1969), J Chem Soc (A) ,32,3026

Wall A and Price G D (1988), Am Min, 73, 224

Wei PH (1935), Z Kristallogr 92,355

Weidner D J and Ito E (1985), Physics of the Earth and Planetary interiors, 40, 65

Wiech G (1984), Solid State Comm , 52,807

Wiech G and Zurmaev EZ (1985), J Phys C ,18,4393

Wright AF, Lehmann MS (1981), J Solid State Chem ,36,371

Zuckermann B (1977), Nature, 168, 491

Chapter 6.
An ab-initio Hartree-Fock Perturbed Cluster embedding study of neutral defects in LiF

6.1 INTRODUCTION

In this section we will apply the perturbed-cluster embedding technique discussed in section 4.3 (and the resulting program EMBED) to the problem of neutral defects in LiF.

LiF is a well known, rock-salt structured, alkali halide, with a lattice parameter of 3.99 Å. It is fully ionic and its structure and elastic properties can be modelled at a high level of accuracy by semi-classical modelling techniques. Cation impurities constitute major contaminants in LiF, as in the other alkali halides. Electrons trapped at lattice defects result in colour centres (Lidiard, 1976), (Kaufman and Clark, 1963); they are often paramagnetic and can be identified by means of EPR and ENDOR techniques. Hole centres, commonly referred to as V centres are also found in LiF and their absorption spectra and paramagnetic properties have been investigated. A review of work on these defect centres is given by Agullo-Lopez,Catlow and Townsend (1988)

Defects in this structure have been extensively studied using computational techniques. Special attention has been paid to the modelling of the properties of colour and hole centres. Semi-empirical INDO cluster calculations were used by Shluger et al. (1988) to model the self trapped holes in LiF; using the same semi-empirical approach, Kantorovich (1987) studied F centres, holes and their pairs with a self-consistent inclusion of polarizability. Pandey and Kunz studied the V_K centre using a hierarchy of models, namely a free F_2^- ion, the same ion embedded in a perfect point-ion LiF lattice, the F_2^- ion embedded in a relaxed shell-model lattice and a molecular cluster that includes the 10 nearest-neighbour Li^+

embedded in a relaxed shell-model lattice (Pandey and Kunz, 1988); the relaxed-lattice calculations were performed using ICECAP (the program discussed in section 4.2.2) and are reviewed by Vail (1990). The V_K centre was also modelled using the Mott-Littleton approximation by Cade, Stoneham and Tasker (1984). Using the same approach Shluger, Grimes and Catlow (1991) studied the self-trapped exciton in alkali halides, comparing their results with Mott-Littleton calculations and experimental optical absorption energies.

The electronic and structural properties of perfect LiF are described accurately using periodic HF techniques (Dovesi, 1991), with relatively inexpensive basis sets. The high point symmetry (O_h) makes the calculations relatively cheap in computational terms. Since many point defects do not alter the local point symmetry (as when only one atom belonging to the perfect lattice is removed or substituted, resulting in a symmetrical relaxation of the first neighbours), large clusters can be tested (for example, in this work, we have included up to 33 atoms in the inner region). This system appears to be ideal to test and refine the computational technique. We are also particularly interested in comparing our results with those obtained within a classical framework, by for example the use of Mott-Littleton techniques. We have focused our attention on neutral defects, to avoid the problems associated with charged states, that have been discussed in section 4.4.3. The case of neutral defects is an important test for the validity of our approach, as they induce a local perturbation that causes a relaxation of the neighbouring atoms. Local polarization fields and dipole moments are also created and their effects are appreciable.

Two defects were studied: the Na impurity that substitutes for a Li ion and the bound Schottky pair (BSP), where two neighbouring Li and F ions are removed, producing two coupled vacancies, that neutralize each other net charge.

We will first discuss, for each cluster size employed, the results of the auto-embedding test (that was outlined in 4.4.3), with particular attention to the calculated cluster geometry. We will use these results to correct the plots of

energy vs. displacement relating to the defect nearest-neighbour relaxation, in order to take into account the error introduced in the elements of the overlap matrix (as discussed in subsection 4.4.3 and in appendix D). The predictions of EMBED for the geometry and the formation energy are compared with those of CASCADE. Changes in the electronic structure induced by the defect will then be investigated; this information is, of course, inaccessible by standard simulation techniques. Mulliken charges, electron charge density maps and analyses of the defect electronic levels will be discussed.

6.2 BASIS SET AND CLUSTER SIZE

6.2.1 Host crystal solution

Table 6.1 shows the basis set for Li which derives from a basis set originally optimized for LiH; the core electrons are described by an s-type AO resulting from the contraction of 6 GTO's. Two outer s-type and p-type GTO's are added to describe better the polarization effects and allow the ion to expand or contract under the effect of the crystalline field. This set may be denoted as 6-11. For the F^- anion, reference to the isolated solution is still possible, because in the case of the halides the anions X^- are stable and correctly described at the HF level. Table 6.1 presents the 7-311 basis set adopted, that was variationally optimized: the core is described by an s-type shell of 7 GTO's; the valence by a 3 GTO's sp-type shell enriched by two additional single gaussian sp-shells that allow a better description of the valence electrons.

The experience gained using basis sets of this quality suggests that they are able to reproduce accurately the electronic and the geometric structure of the periodic lattice. The full ionicity of this structure is confirmed by the Mulliken population analysis: Li and F net charges are +0.981e and -0.981e respectively. The experimental bulk geometry is correctly reproduced by this set of basis functions: the calculated lattice parameter is 4.010 A (experimental: 3.99 A). The former value will be adopted in all the calculation discussed in this chapter.

The primary information concerning the host crystal necessary to solve the embedding equations, are the projected densities of states, as was discussed earlier. The accuracy needed in their description depends on the width of each corresponding band and on its proximity to the Fermi level. The number of

polynomials used in the expansion (see Appendix C) was 1 for 1s core bands, 2 for 2s fluorine bands and 9 for all the others.

6.2.2 Basis set for the defects

For the Na impurity a 8-51 GTO basis set was adopted; its coefficients are shown in Table 6.2. This basis set was optimized (Saunders, 1991) for Na^+ in NaCl, and correctly reproduces the electronic properties of the sodium ion in a fully ionic environment. For this reason we consider it adequate for the purposes of the present study.

More care is necessary in the case of the BSP: formally, the basis functions of neighbouring Li and F should be removed from the set C', so that C will contain only the basis functions used to describe the neighbouring atoms in the cluster. In practice it is usual to add "ghost" functions, centred on the vacancy, that improve the description of local distortions of the electronic distribution on the nearest neighbours and to allow charge to be re-distributed in the vacancy sites. Therefore we placed a single GTO sp-type function centred on each vacancy. It should be noted that an exponent in the range of 0.20 ~ 0.30 a.u. is usually adopted to describe the vacancy states . Unfortunately, we encountered serious convergence problems when exponents in this range were tested, and only a value of 0.55 guaranteed a stable SCF.

6.2.3 Geometry and cluster size for the defect calculations

Three clusters were considered for the Na substitutional impurity. For two of them the six nearest neighbouring F^- ions were allowed to relax. In the case of the largest cluster, because of the computational costs, it was not possible to optimize

the geometry and the predicted relaxed positions calculated by CASCADE were used.

Fig. 6.1a shows the atoms included in the C regions: the actual defective region contains the impurity and the first shell of six fluorine ions in all the cases; the B region contains the 6 fourth-neighbouring Li ions in cluster I, the 12 second-neighbouring Li atoms in cluster II, and, in cluster III, the 12 second-neighbouring Li ions, the 8 third-neighbouring F ions and the 6 fourth-neighbouring Li ions (for a total of 26 atoms in region B, 33 atoms in region C). The unusual cluster I was tested in order to verify the results found by Grimes (Grimes et al., 1989) in the case of the Li impurity in MgO. In that study it was shown that the relaxation of the first shell of neighbours take them closer to the ions along the axis of movement (in this case the Li). They are more polarized than other ions closer to the defect and play, as a result, a more important role in describing the local environment of the defect. We note that in Grimes's calculations the model was simplified: the region surrounding the cluster was described by a finite lattice of point charges, without any description of short-range repulsion between the relaxed ions in the inner region and the point charges. Therefore the problem in that case was somewhat more serious than just an incorrect description of polarization effects (e.g. there was no counterbalance to the attractive electrostatic interaction between the relaxed ions and the point charges). This is not the case in the present study. On the other hand, it is important to test if it is possible to use the relatively inexpensive and manageable cluster I to mimic correctly most of the polarization effects and changes in charge density in the defect region. It was not possible to use a smaller cluster, containing only the central atom plus six F^- (with no atoms in the B region): the relaxation of the self-substituted cluster, in this case, fails completely. The fluoride ions tend to relax unrealistically towards the central atom and it is impossible to find an energy minimum, since the SCF procedure becomes

unstable when the geometry becomes too distorted with respect to the perfect lattice.

The BSP was first simulated using a small cluster (cluster IV, shown in Fig. 6.1b), that contains the BSP and the 5 neighbouring Li only. In this case we have optimized the V(F) - Li^C distance. We have also considered cluster V that contains the two vacancies and the 10 first neighbours (5 Li and 5 F). A number of problems are associated with this cluster, if one aims to optimize the positions of the 12 ions. Computational costs are high, because of the low symmetry of the point group (only 8 operations are left). Furthermore it is difficult to evaluate the corrections to the overlap matrix, since the coordinates of four sets of equivalent atoms are to be optimized. Therefore, for this cluster, we considered only two configurations: the unrelaxed one and the one relaxed according to CASCADE.

6.2.4 Computational conditions: CPU time vs. cluster size

Throughout the study, the investigation has been limited by the need to reach a compromise between, on one hand, the quality and quantity of information to be collected, and on the other, the computer time needed.

The time required to evaluate the two-electron integrals strongly depends on the cluster dimensions, the basis set used and the tolerances adopted for the truncation of the two-electron series. These factors also determine the dimensions of the ($C.D^*$) matrices (see subsection 4.4.2.1) that are multiplied and manipulated in the SCF procedure. The latter step becomes also increasingly expensive with the number of cluster pseudo-eigenvalues (see summation over j in equation (4.30, 4.31)). In Table 6.3 we report, for each defective cluster, the number of atomic orbitals in C (N_C), the number of atomic orbitals in the D^* region (N_{D*}), the number of integrals (in millions) (N_I), the CPU time to evaluate them (t_1, in seconds) and the CPU time necessary for each SCF cycle (about 20-30 cycles are usually needed to reach

converged solutions). All the jobs were run on the IBM3090 computer at the SERC Rutherford Laboratory. Computational tolerances used to study the BSP are less strict than those adopted in the case of the Na substitutional, because of the higher cost of the latter calculations; we note the steep increase in cost due to the lower point symmetry in cluster IV and V. It is also evident that both clusters III and V are too expensive for any sort of systematic study.

6.3 RESULTS: SELF-SUBSTITUTION

One of the means of verifying the correctness of the formulae and of the computational scheme employed, is the so-called self-substitution test. It consists in defining a cluster C and a defective region A exactly as in the case of a real defect, but with all the atoms in A coinciding in species, geometry and basis set with those in A'. The density matrix elements, at convergence, must coincide with the corresponding elements calculated by CRYSTAL for the perfect, periodic lattice. Such a result is not trivial: the two schemes are actually different; they employ different approximations and different equations to reach, in principle, the same description of the atoms in C. Moreover it is possible to relax locally the atoms in the cluster from their perfect lattice positions. This can be used to calculate phonon frequencies or for parameterizing atom-atom interaction potentials. If one starts from the optimized bulk geometry, all the displacements should lead to an increase in energy. As discussed above, if these displacements affect atoms near the cluster boundaries, the effects associated with changes in the overlap matrix may lead to a different minimum in the variation of energy with displacement.

In Table 6.4 we present the Mulliken populations obtained from EMBED and CRYSTAL for all the clusters considered. We note a very good agreement between the two. We note that by increasing the cluster size even small changes in charge can result in a non-negligible net charge in C, because of the number of equivalent atoms in the cluster. This effect is particularly evident in the case of cluster III. These fluctuations can be explained as numerical noise due to the computational conditions and the approximations introduced with respect to the periodic case.

Fig. 6.2 shows the total electron charge density for cluster II (similar results are obtained for the other clusters). We note that there is no difference between

the electron distribution on atoms in C and on atoms in the indented lattice (for instance the Li and F at the top right). The six neighbouring F atoms in cluster I, II and III and the Li^C atom in cluster IV are then allowed to relax, while the other atoms in C are kept at their perfect crystal positions. We found that the more the ions are relaxed, the more unstable becomes the convergence procedure: these difficulties, that are in part related to the problems discussed in section 6.2.4, produce a numerical noise that affects the results and the quality of the interpolation. Fig.6.3 reports the formation energies (in hartree) in the three cases, as a function of the F-Li distance (d , in a.u.). Two energy curves are shown: the triangles correspond to total defect energies, as calculated by EMBED at convergency. In all cases the minimum corresponds to a very large decrease of d . We note that cluster I, that includes the six coaxial Li ions, is the one that better reproduces the correct value, while clusters II and IV, where the atoms relaxed are near to the cluster boundary, yield the most unsatisfactory results. This is due largely to the neglect of changes in the P_D elements associated with modifications of the overlap matrix at the cluster border. This effect is more important when the cluster is smaller. In particular, the elements of the overlap matrix that are more affected by a relaxation of the six F^- are those corresponding to the interaction with the coaxial outer Li. It is therefore not unexpected to find that cluster I, where these Li are included in C, reproduces the Li-F distance more accurately. It can also be suggested that cluster I better describes the polarization of these coaxial Li ions, which must be an important factor in determining the equilibrium distance.

As discussed in Appendix D, we conclude that for small changes in d the overlap effect on P_D is linear in the relaxation parameter. The curves identified by circles in Fig 6.3, are obtained by adding a term $E^{ovl}(d) = \alpha \Delta d$, such that the minimum energy coincides with $\Delta d = 0$. The same correction will then be applied to the corresponding defective clusters, to obtain the estimated relaxed atomic positions and total energy.

6.4 RESULTS: Na IMPURITY AND THE BOUND SCHOTTKY PAIR (BSP)

Our discussion of the results for the two defects will refer throughout to the clusters and the relaxation mechanisms considered in the previous sub-section. In Fig.6.4 we show the effect of relaxation of the nearest neighbouring F^- ions on the defect energies in clusters CI and CII (Na substitutional) and of Li^C in the cluster C IV (BSP), respectively. The curves are corrected taking into account the linear term E^{ovl} evaluated in the auto-embedding case and derived from the curves in Fig.6.3

Table 6.5 presents the equilibrium distances (in a.u.) calculated by EMBED (when available, e.g. in cluster I,II,IV), the defect formation energies (in eV) and the corresponding Mulliken charges. The energies (in square brackets) reported for cluster III (Na substitutional) and V (BSP) are not corrected to include the term E^{ovl}, which could not be evaluated in the auto-embedding case owing to the excessive computational costs. For cluster III, the Na-F distance used was 3.98 a.u. (as we can expect that relaxation in this case will yield a result similar to cluster I). In cluster V, for which no quantum mechanical estimation of the relaxation effects was available, we used the atomic positions predicted by CASCADE. Energies and relaxed distances for all the clusters can be compared with results obtained by performing a CASCADE calculation, defining an inner region that coincides with the largest C region defined by EMBED (e.g. with cluster III and V).

For LiF and Na we used the first set of potentials described by Catlow, Diller and Norgett (1977). Because of the completely different techniques used to simulate the system in the two methods, which are respectively semi-classical and quantum-mechanical models and which have different treatments of the

polarizability of the ions, non-equivalent definitions of "inner" and "outer" regions and with a much larger number of ions being allowed to relax in CASCADE compared with EMBED, the results should be compared with great care. It is, however, encouraging that the two approaches give comparable results for the equilibrium geometries and defect formation energies. Finally, difference electron charge density maps (crystal - isolated ions) are shown in Fig.6.5, 6.6, 6.7, 6.9, 6.10 for C I, CII, CIII, CIV and CV respectively; they refer to the relaxed geometries listed in Table.6.4. Fig. 6.11 refers to the unrelaxed cluster CV. All these results and plots will be discussed in the following subsection. The maps are shown along a plane containing the defect and the nearest neighbours, with the x,y axes coinciding with the (100) and (010) crystalline directions.

6.5 DISCUSSION

6.5.1 Na substitutional

The substitution of Li by Na causes a relaxation outwards of the first neighbours that can be simply explained on the basis of the larger radius of the impurity with respect to Li. Charge transfer from Na to F is suggested by the Mulliken analysis: in all the clusters F ions are more negative than in the host crystal, and Na has a net charge of about +1.02. The net charge of the different clusters is always slightly negative, consistent with the auto-embedding results, so we suggest that this effect is partially due to numerical inaccuracies in the treatment of the atoms in C and of the matching of the cluster to the outer region, regardless of the presence of the defect. This residual charge is, however, small, and almost constant during the relaxation of the first neighbour F. By allowing the coaxial Li to polarize, the fluoride ions can further relax outwards, and reach a more stable configuration, so that the introduction of the defects requires less energy. In cluster II, the F^- relax towards the Li ions that are much more rigid so that the displacement is energetically less favourable. Moreover, the elements $S_{\mu\nu}$ of the overlap matrix, with μ corresponding to an AO centred on F and ν to an AO centred on the corresponding coaxial Li, are considerably affected by the relaxation process.Cluster I yields a slightly larger displacement of the six F ions, and a lower formation energy than cluster II (the formation energy of cluster III is certainly overestimated, since the overlap correction E^{ovl} was not calculated for this cluster size). The improved treatment of the polarization effects, and of the changes in the overlap matrix (as discussed before) in cluster I may explain the difference.

The relaxed Na-F distance predicted by the quantum mechanical procedure is lower than in CASCADE. However taking in account the differences between the two procedures and the larger number of ions allowed to relax in the CASCADE calculations, we consider the results from EMBED are satisfactory.

More detailed information is given by the electron charge density maps. The most notable feature is that all the ions contract (with respect to the isolated ion) under the effect of the crystalline field . This effect is particularly evident in the case of Na. The larger radius of Na^+ with respect to Li^+ causes an important distortion in the outer shells of F, that are relaxed outwards. Moreover, the presence of net dipole moments on these ions is shown by the polarization of their electronic distributions, that are distorted and egg-shaped. The distortion is also evident in the core region. The ECHD maps show clearly that the polarization effects are not limited to the first neighbours: in all the clusters, the six coaxial Li ions are perturbed with respect to the perfect crystal. This effect is more evident in cluster I and III, where they are included in the cluster. The second neighbour Li are, if included in region C, affected as well by the polarization effects. This is particularly clear in Fig. 6.7, that shows the similarity between the polarization effects of the coaxial Li and those of the twelve Li^+ second neighbours of the defect. Nevertheless the polarization of the coaxial Li ions affects the relaxation of the fluorines much more and will have a greater effect on the energy of the defect.

Fig. 6.8 presents the contributions to the total electron charge density, for cluster II, that arises from the terms P^{CLUST}, P^{CONST} and P^{COUPL}, as shown in eq. 4.4.36 and 4.4.37. The cluster term corresponds to an essentially isolated cluster (Fig. 6.8a); the P^{CONST} term (Fig. 6.8.b) is negligible inside C though at its frontier the orthogonality correction deforms the electron density distribution. The coupling term (Fig. 6.8c) is very important in the border region, with positive and negative contributions that affect atoms outside the cluster as well.

Fig. 6.8d shows the total charge density that results from the sum of the three terms. It is clear that the final result is the product of important corrections to the cluster solution and cancellation of big terms (see for example Fig. 6.8b and 6.8c).

Fig. 6.13 shows the position of the 2p HF levels of the F^B anion as calculated for the ion in the "auto-embedded" cluster CI, CII and CIII and for F in the defective clusters (containing the substitutional Na) CI, CII and CIII respectively. The introduction of the Na defect destabilize the F 2p levels, because of the increased compression of these ions due to the larger radius of Na. By relaxing the fluorines, the O 2p levels are stabilized. This results underlines, again, the importance of the relaxation effects in stabilizing defects in the lattice.

6.5.2 The Bound Schottky Pair (BSP)

The removal of two nearest neighbour ions provides a considerable local perturbation of the LiF lattice. CASCADE predicts an appreciable displacement of all the nearest neighbours of the coupled-vacancies (5 Li and 5 F). With reference to the labels used in Fig. 6.1b (cluster V) the calculated displacements from CASCADE are as follows (Δx and Δy in a.u.):

ATOM	Δx	Δy
F^B	-.076	.250
F^C	-.242	.0
Li^B	-.136	.349
Li^C	-.348	.0

Although in cluster IV only one Li is allowed to relax, and in cluster V all the 10 neighbours are relaxed according to CASCADE, we note that the effects on the

Mulliken populations (reported in Table 6.4) are relatively small. The ghost functions centred at the vacancy sites allow some charge to be re-distributed: the vacant Li site becomes slightly positive and the fluorine site slightly negative. The nearest Li ions become less positive than in the perfect lattice, while the fluoride ions become less negative. It is quite clear that if the fluorines are not included in the cluster the latter charge transfer is less important and their polarization is almost negligible. Both clusters are almost neutral, as they were in the corresponding auto-embedding calculations, and by relaxing cluster IV we did not find a significant change in the residual charge. These considerations are in part supported by the electron charge density maps (Fig.6.9-6.11).By comparing Fig. 6.9 and 6.10 (corresponding to clusters CIV and C V respectively) it is clear that the five Li ions polarize in a very similar manner in the two clusters; on the other hand the five fluoride ions that are not included in cluster C IV and that, in this case, appear completely unperturbed, are indeed polarized and distorted in cluster V. It appears that the density matrix cross-terms P_{CD} are unable to describe these effects, that should be considered as a truly electrostatic polarization of the F^- ion rather than a chemical coupling (i.e. an effect similar to the shell polarization described by Mott-Littleton calculations). The polarization of the fluorines has two components: a distortion of the outer valence, that becomes egg-shaped and expands outwards and a polarization of electrons closer to the nuclei, with an increase of charge density towards the Li vacancy and a reduction towards the outer nearest neighbour. In Fig. 6.11 we present the charge density for cluster C V <u>without</u> relaxing the ions: it is evident that the polarization effects are quite independent of the relaxation and are mainly due to the presence of the BSP.

The calculated dipole moment (defined as a vector that points towards the more negative pole) on the F^B ions, along the [010] direction is +0.01a.u., pointing towards the vacancy (by analyzing the single contributions we note that the dipole moment is +.006, +.026 and -.022 a.u. on the 2sp, 3sp and 4sp shell

respectively; the different behaviour of the inner and outer valence electrons is so confirmed). On the other hand, the dipole moment on F^C, along the [100] axes, is -0.036 a.u. (single contributions are +0.0098, +0.023 and -0.069). As expected the polarization effects are stronger along the axes of the V(F)-V(Li) bond.

It is interesting to note that an effect similar to that found for F^- in the presence of a Li vacancy ,was found in preliminary calculations on the Li substitutional in MgO, where a Mg^{2+} is substituted by a Li^+ ion with a resulting deficiency of charge in the cluster. In Fig. 6.12 the corresponding charge density map is shown; the two features discussed above are clearly present. The outer valence of the surrounding oxygen ions expand outwards, while there is an opposite effect in a region nearer to the oxygen core, with an increase of charge density pointing towards the Li defect.

It can be suggested that this result arises from a balance of different forces; the removal of Li induces two effects on the fluoride electronic clouds : on one hand the unbalanced electrostatic field on the latter ion will produce a displacement outwards of its electronic cloud; on the other, the absence of the Pauli repulsion will allow the fluorine's electron to expand towards the vacant site. This effect was noted, for example, on the surface of lithium oxide (Lichanot et al., 1991) and was discussed by Fowler (1988). The outer valence electrons are more sensitive to the electrostatic field (being more weakly bound) than the inner valence electrons (using a classical terminology we would say that the outer valence and the inner valence charge distribution are coupled to the core by different spring constants). As the valence shell polarizes, it "over-screens" the core, i.e. the valence moves so much that the core sees a dipole in the opposite direction to the applied field; this effect is formally described in terms of the Lindhard theory for the electrostatic screening of a field (p. 297, Kittel, 1963).

Unfortunately it is not possible to compare the predicted geometries and formation energies for different cluster sizes but, assuming that the displacements only depend on the presence of the defect and do not strongly

couple (so that each can be considered as an "independent mode"), the V(F)-Li^C distance predicted by EMBED is in good agreement with CASCADE. The formation energy of this defect predicted by cluster IV is close to the CASCADE result, although the small magnitude of the discrepancy ma be partly fortuitous. Cluster V yields a higher formation energy, as expected, since the E^{ovl} correction is not included. We note that, comparing the EMBED results for the Na substitutional and the BSP, the formation energy for the latter defect is consistently higher as would be expected, and as is obtained in the CASCADE calculations.

6.6 CONCLUSIONS

In this section we have presented the results of a study of neutral defects in LiF, carried out by using the program EMBED. For both the Na substitutional and the Bound Schottky Pair, our method yields useful insights into the nature of the defect, which are consistent with the picture provided by simulation techniques. Disagreements between the two methods, for instance as regards formation energies, are due both to the different underlying *Ansatz* and to the numerical inaccuracies in the quantum procedure. The use of tighter tolerances to improve the numerical quality of the results will require a further optimization of the code to boost performance.

On the other hand, the nature of the defects discussed above does not require very large clusters; the perturbation introduced by these defects is localized, and relatively small cluster sizes yield satisfactory results. Although polarization effects, especially in the case of the BSP, are very important, our results suggest that they are localized on the first neighbours of the defect.

Techniques such as those discussed in section 4.4 will hopefully allows us to study charged defects and to describe the effect of polarization more accurately, therefore extending the limits of applicability of the method.

TABLE 6.1

Basis set adopted for Li and F in the perfect bulk and defect calculations. Exponent (α) and coefficients are in a.u. The contraction coefficients multiply normalized individual gaussians.

ATOM	SHELL	α	s-coeff	p-coeff
Li	s	840.	0.00264	----
		217.5	0.00850	----
		72.3	0.0335	----
		19.66	0.1824	----
		5.044	0.6379	----
		1.5	1.0000	----
	sp	0.65	.00001	1.0000
		0.51	1.0000	.00001
F	s	13770.	0.00088	----
		1590.0	0.00915	----
		326.5	0.0486	----
		91.66	0.1691	----
		30.46	0.3708	----
		11.50	0.41649	----
		4.76	0.1306	----
	sp	19.00	-0.1094	0.1244
		4.530	-0.1289	0.5323
		1.370	1.0000	1.0000
	sp	0.45	1.0000	1.0000
	sp	0.21	1.0000	1.0000

TABLE 6.2

Basis set adopted for Na in the defect calculations. Units are as in Tab. 6.1

ATOM	SHELL	α	s-coeff	p-coeff
Na	s	56700.	0.000225	----
		8060.0	0.00191	----
		1704.0	0.01105	----
		443.6	0.05006	----
		133.1	0.1691	----
		45.8	0.3658	----
		17.75	0.3998	----
		7.380	0.1494	----
	sp	119.0	-0.00673	0.00803
		25.33	-0.07980	0.06390
		7.800	-0.0793	0.20740
		3.000	0.305600	0.33980
		1.289	0.5639	0.3726
	sp	0.504	1.000000	1.00000

TABLE 6.3

Cluster size vs. cost: we report the number of atomic orbitals in C (N_C), the number of atomic orbitals in the D^* region (N_{D^*}), the number of integrals (in millions) (N_I), the CPU time to evaluate them (t_1, in seconds) and the CPU time necessary for each SCF cycle.

CLUSTER	N_C	N_{D^*}	N_I	t_1	t_2
C I	117	1118	69	553	120
C II	147	1280	74	591	139
C III	281	2122	122	996	200
C IV	32	706	43	320	27
C V	97	1106	151	1069	337

TABLE 6.4

Atomic Mulliken net charges for the different clusters considered in the self-substitution case compared to the LiF bulk calculated by CRYSTAL. Clusters are labelled as discussed in the text. Atoms in clusters C I, C II, C III are labelled with reference to Fig.6.1a.

Atoms in clusters C IV and CV are numbered with reference to Fig.6.1b. Q(C) is the residual cluster charge, as defined in section 4.3.

	Li^A	F^B	Li^C	F^D	Li^E		Q (C)
C I	.980	-.976	.979	-.984	.981		-.055
C II	.980	-.981	.981	-.981	.981		-.079
C III	.981	-.979	.981	-.976	.980		-.151
	Li^A	Li^B	Li^C	F^A	F^B	F^C	Q (C)
C IV	.979	.975	.979	-.960	-.979	-.979.	-.015
C V	.980	.979	.981	-.982	-.976	-.976	.073
	Li	F					Q (C)
LiF bulk (from CRYSTAL)	.981	-.981					.000

TABLE 6.5

Optimized interatomic displacements (Δd, in a.u.), formation energies (ΔE, in eV) and Mulliken net charges on the defect and nearest neighbours) for the Na substitutional and the BSP. Clusters CI..CV are labelled according to Fig.6.1a,b. The corresponding Δd and ΔE predicted by CASCADE are also reported. The energies in square brackets are not corrected to include the term E^{ovl} (see text).

Na substitutional	**C I**	**C II**	**C III**	**CASCADE**
Δd(Na-F)	0.15	0.12	----	0.23
ΔE (eV)	1.28	2.15	[4.98]	1.78
q(Na)	1.018	1.020	1.020	
q(F)	-.993	-.997	-.989	
q(Cluster)	-.080	-.097	-.152	
BSP	**C IV**	**C V**		**CASCADE**
$\Delta d[V(F)-Li^C]$	.45	----		.35
ΔE (eV)	13.22	[16.79]		13.25
q(V(Li))	.022	.002		
q(V(F))	-.001	-.002		
$q(Li^B)$	.971	.974		
$q(Li^C)$	.970	.968		
$q(F^B)$	-.984	-.967		
$q(F^C)$	-.977	-.940		
q(Cluster)	.004	-.006		

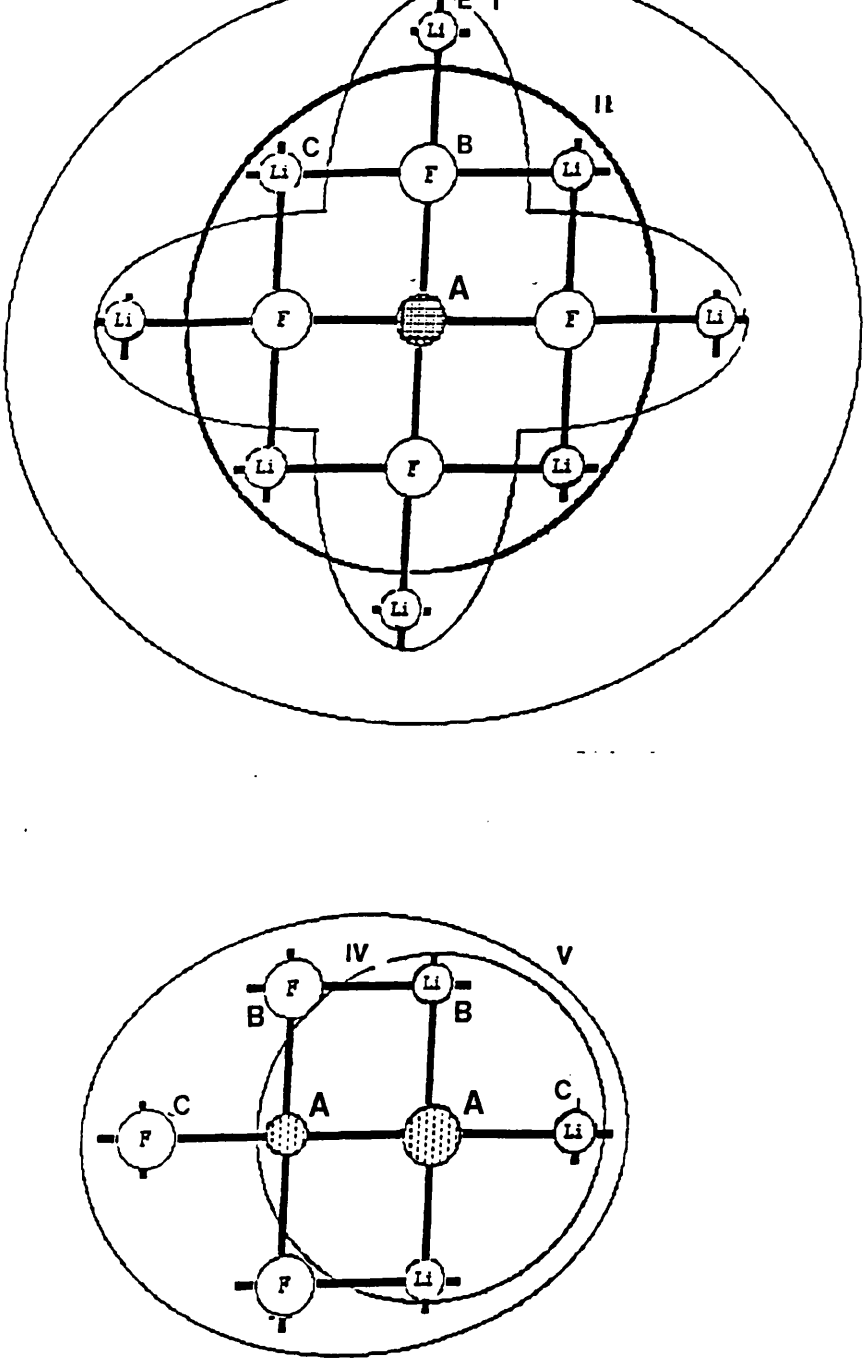

Figure 6.1. (a) Clusters used to study the Na substitutional in LiF: the actual defective region contains the impurity and the first shell of six fluorine ions in all the cases; the B region contains the 6 fourth-neighbouring Li ions in cluster I, the 12 second-neighbouring Li atoms in cluster II, and, in cluster III, the 12 second-neighbouring Li ions, the 8 third-neighbouring F ions and the 6 fourth-neighbouring Li ions (for a total of 26 atoms in region B, 33 atoms in region C). (b) Cluster used to study the Bound Schottky Pair (BSP) in LiF: cluster IV contains the BSP and the 5 neighbouring Li only; cluster V contains the two vacancies and the 10 first neighbours (5 Li and 5 F).

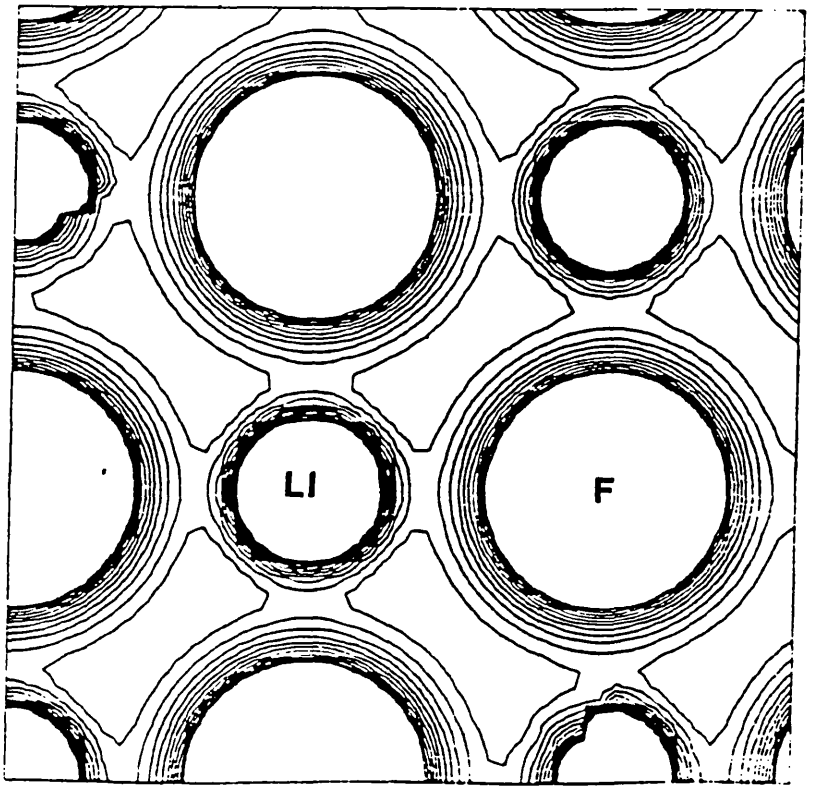

Figure 6.2. Total electron charge density for cluster II in the autoembedding case. The map is drawn in the (100) plane. The interval between the isodensity lines is .005 e/bohr^3.

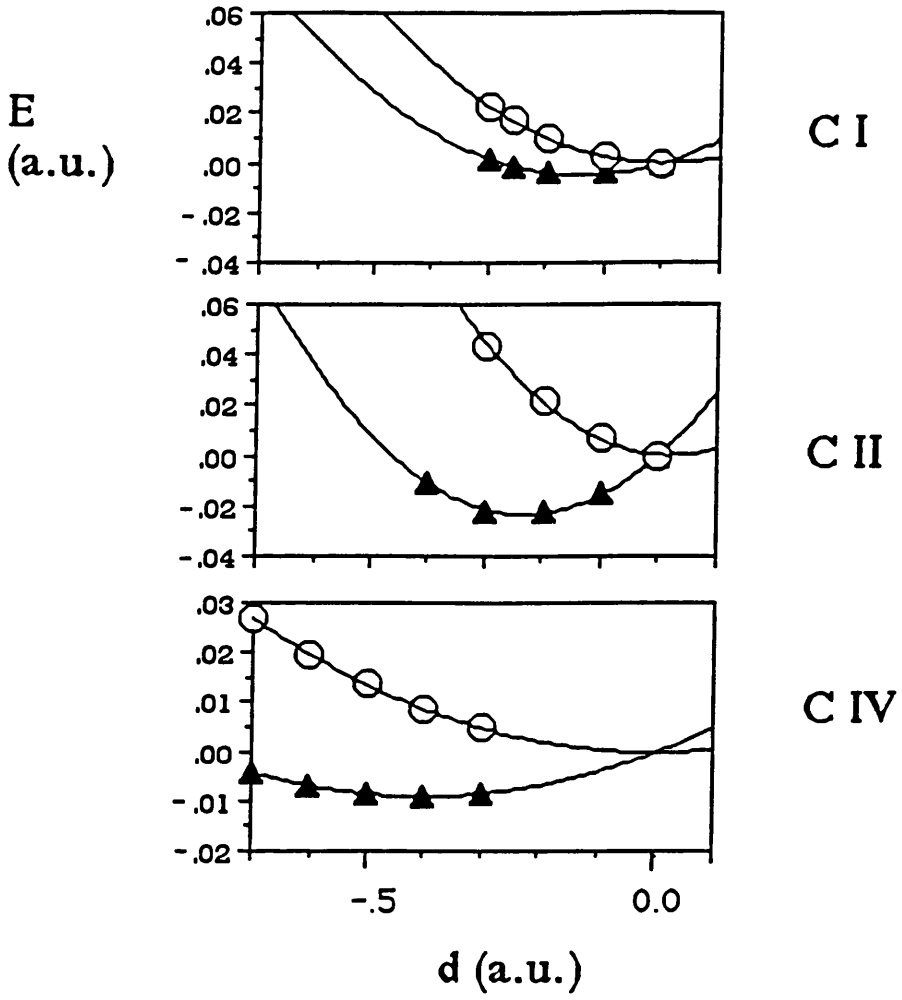

Figure 6.3. Formation energies (in hartree) in the autoembedding clusters I,II and IV, as a function of the F-Li distance (d , in a.u.). Two energy curves are shown: the triangles correspond to total defect energies, as calculated by EMBED at convergency. The curves identified by circles are obtained by adding a term $E^{ovl}(d) = a\ d$ (see text).

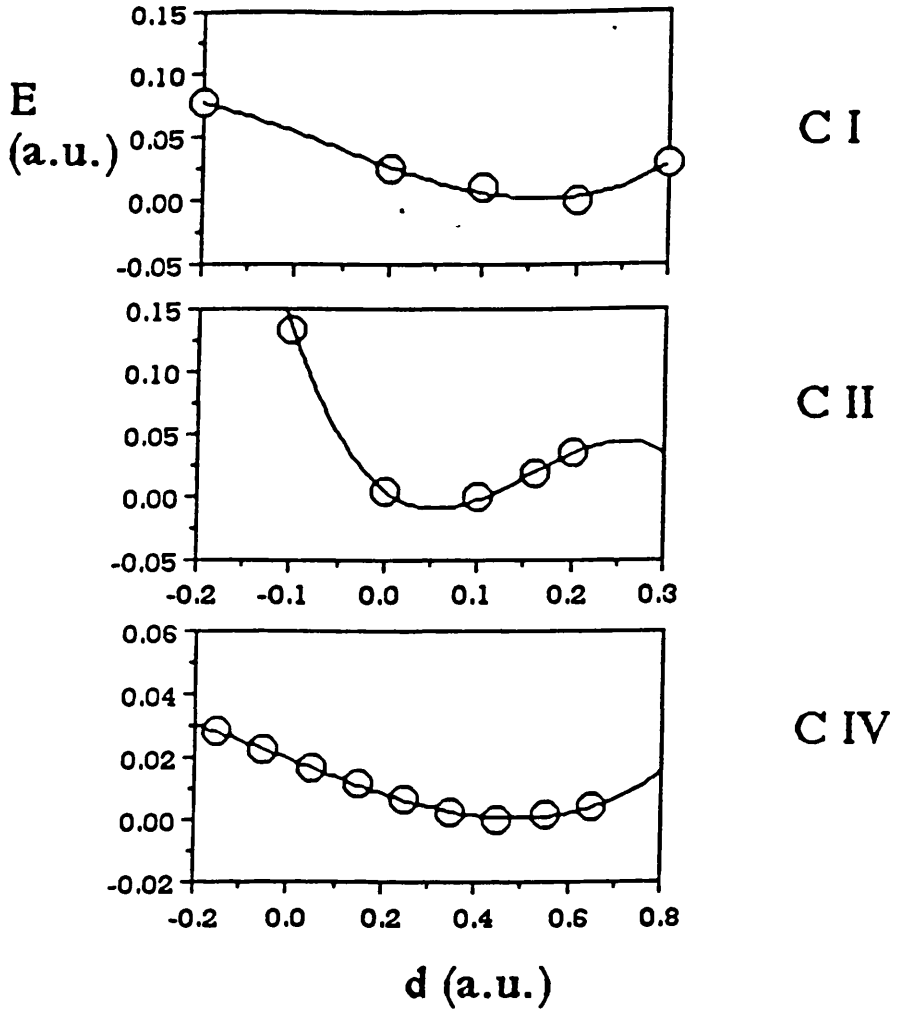

Figure 6.4. Effect of the relaxation of the nearest neighbouring F^- ions on the defect energies in cluster CI and CII (Na substitutional) and C IV (BSP), respectively. The curves are corrected taking into account the linear term E^{ovl} evaluated in the auto-embedding case and derived from the curves in Fig.6.3

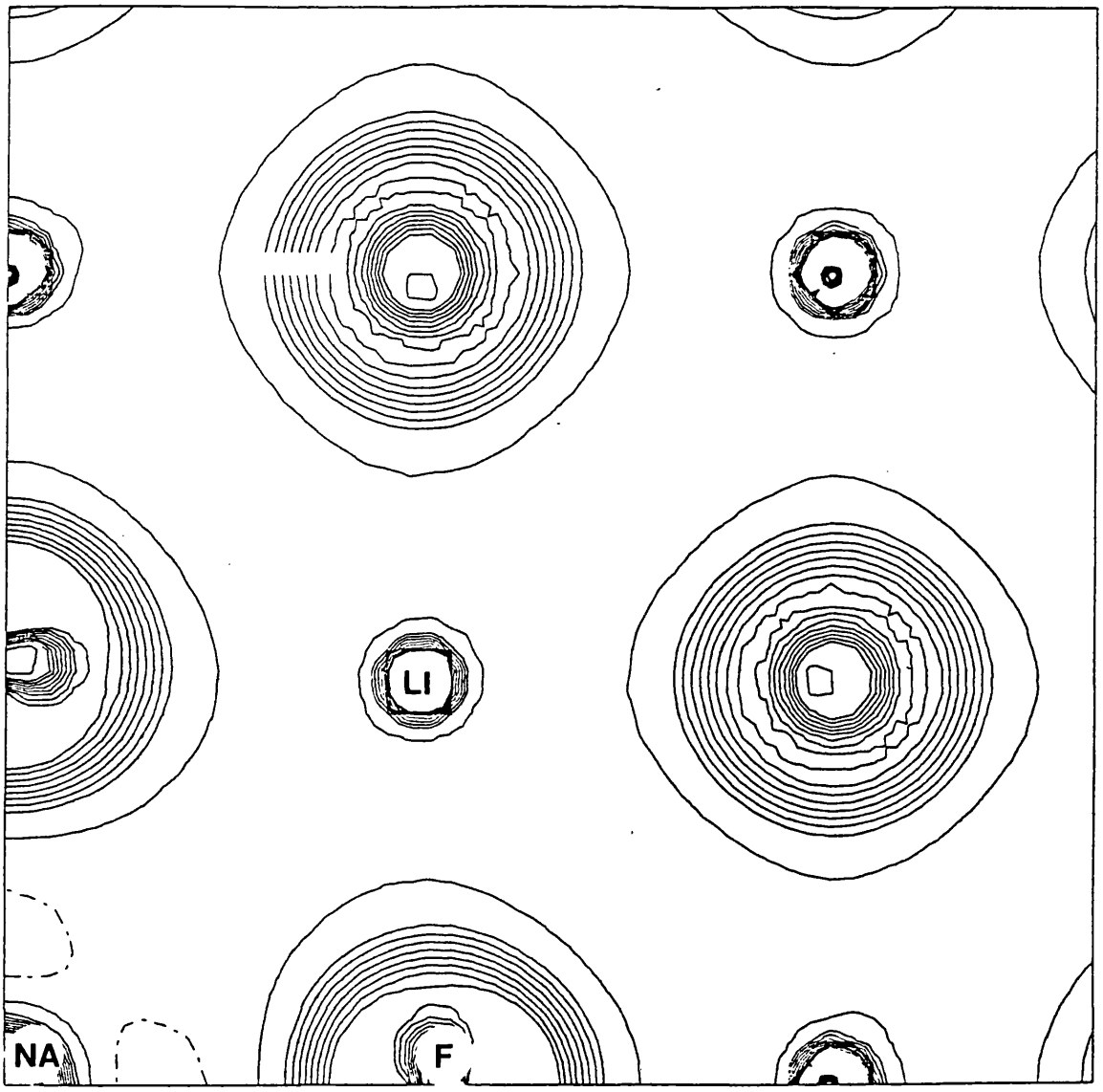

Figure 6.5 Difference electron density maps of the relaxed cluster I (Na+6F+6Li). The map is drawn in the (100) plane. The interval between the isodensity lines is .005 e/bohr^3. Positive, negative and zero isodensity lines are represented by continuous, dashed and dot-dashed lines.

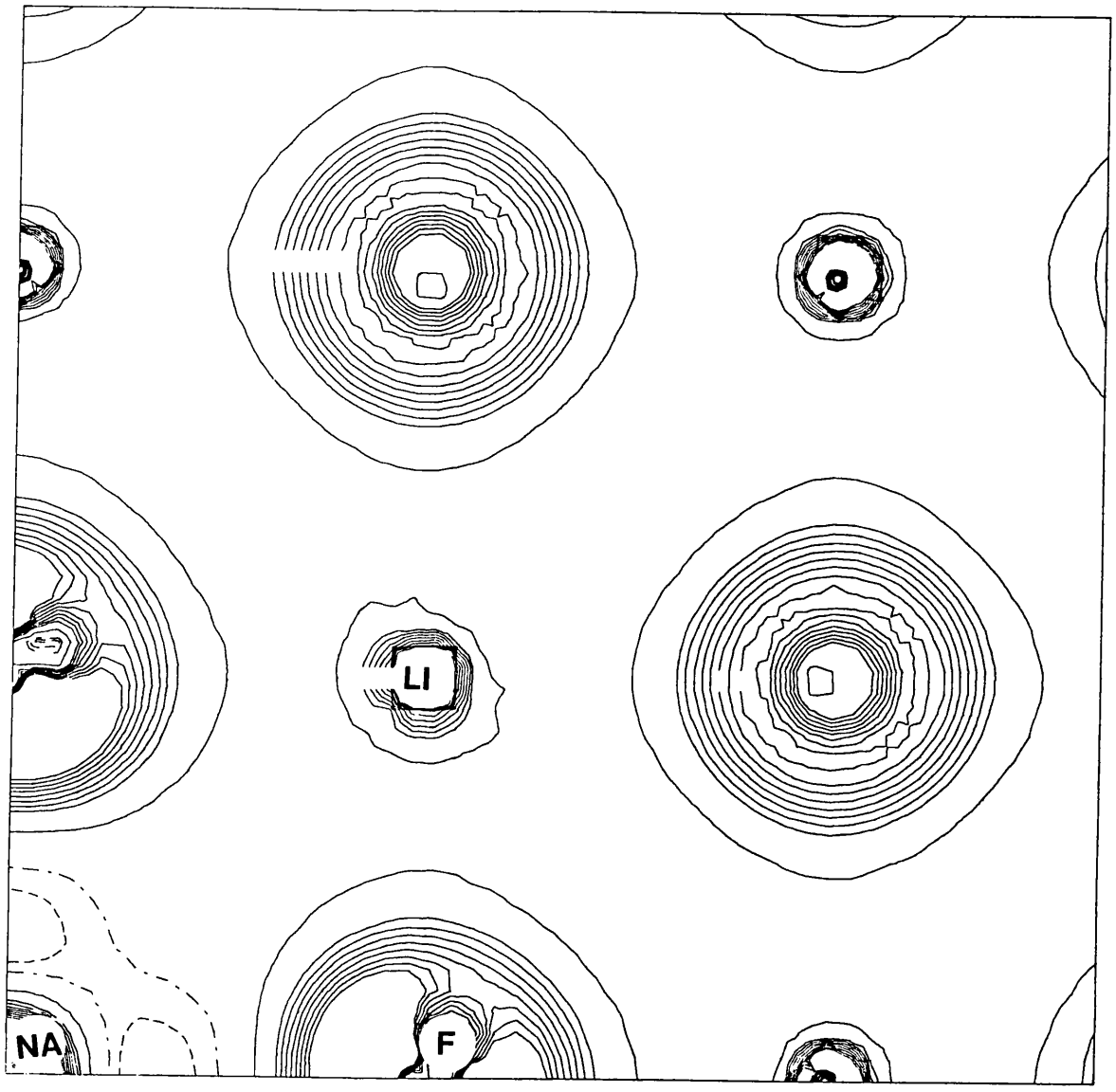

Figure 6.6 Difference electron density maps of the relaxed cluster II (Na+6F+12Li). The map is drawn in the (100) plane. All the conventions are as in Fig.6.5

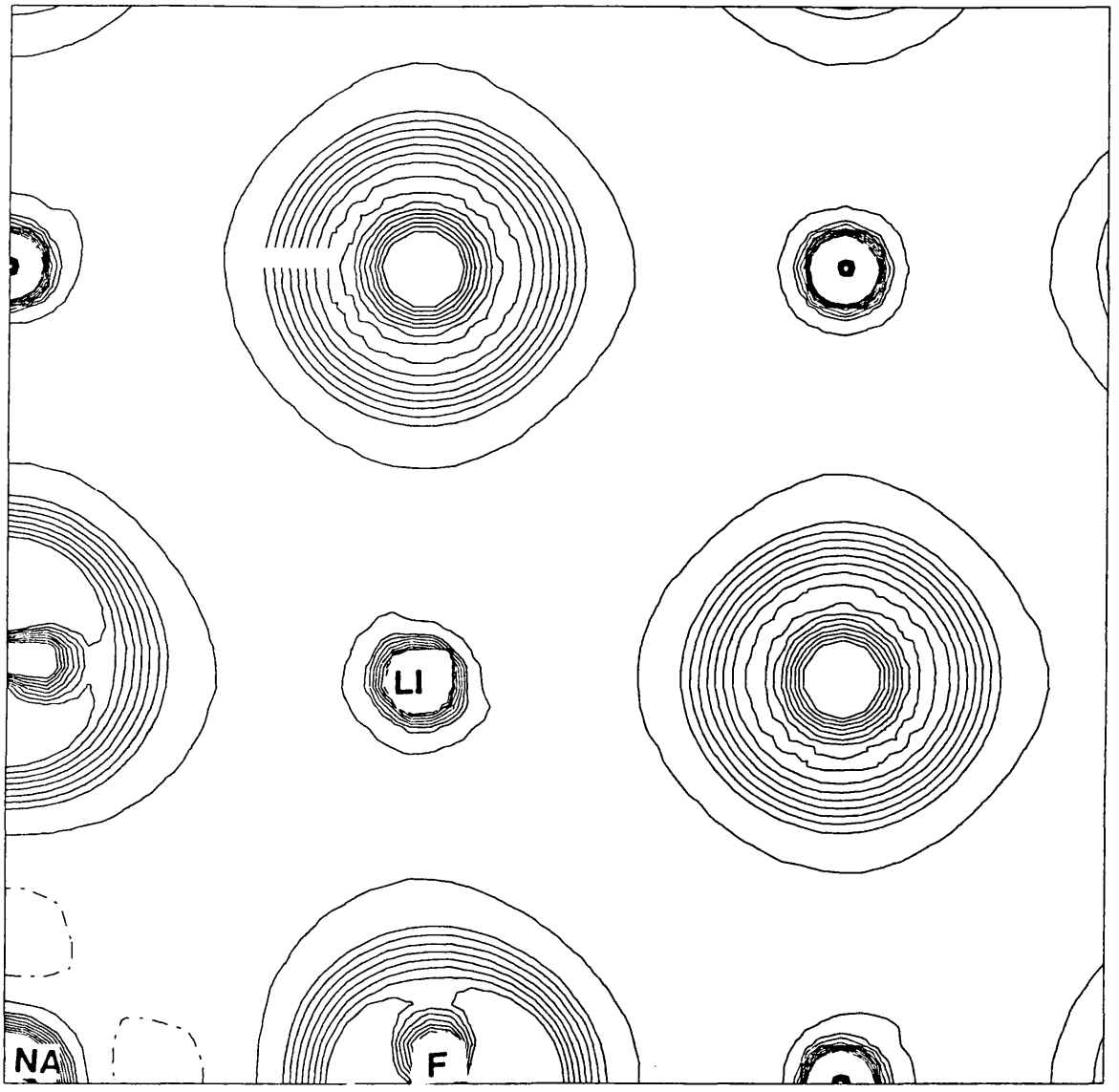

Figure 6.7 Difference electron density maps of the relaxed cluster III (Na+6F+12Li+8F+6Li). The map is drawn in the (100) plane. All the conventions are as in Fig.6.5

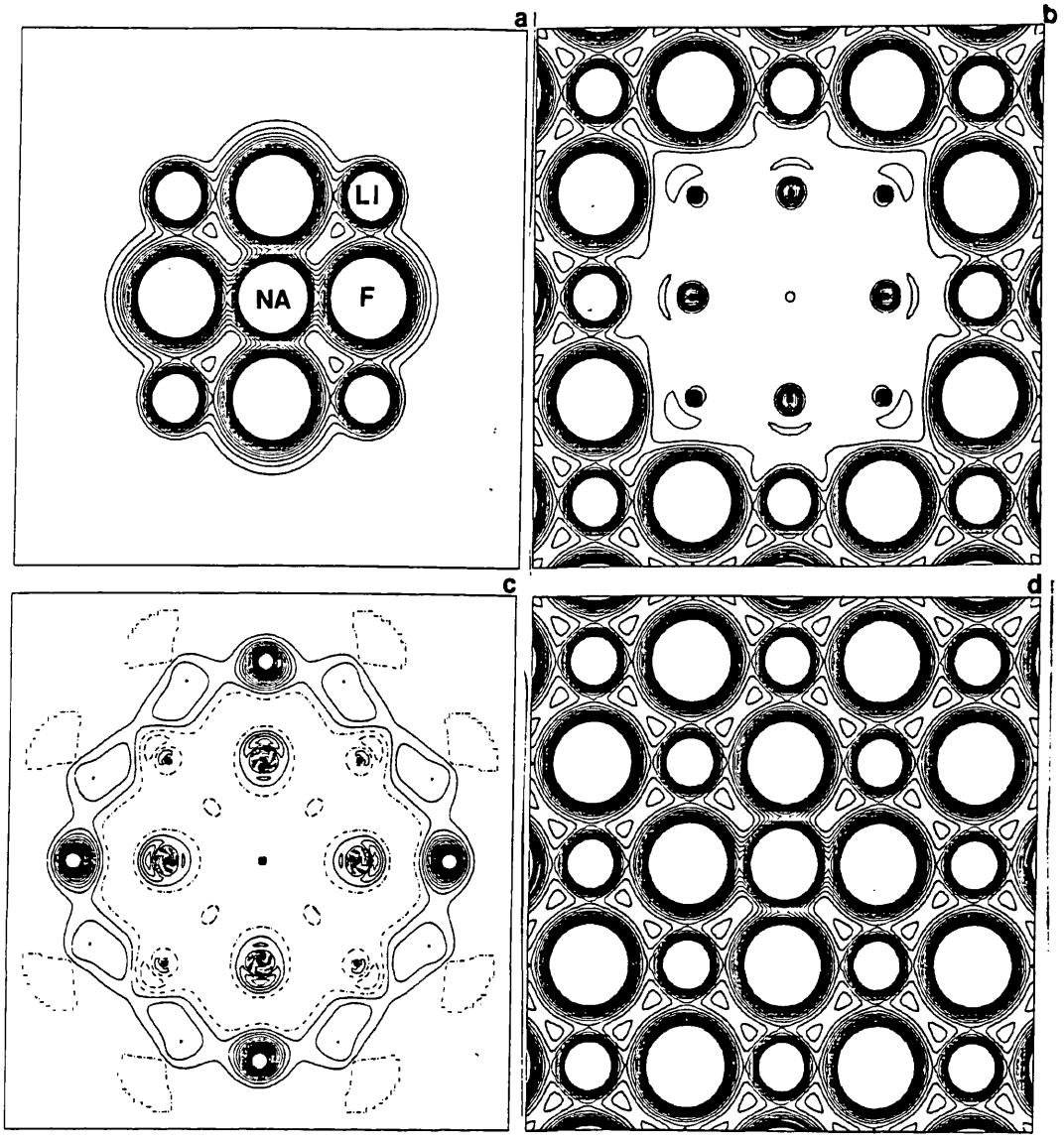

Figure 6.8 Total electron charge density maps of the relaxed cluster II (Na+6F+12Li), corresponding to the contributions to the density matrix as calculated in equations 4.4.36, 4.4.37. pCLUST, pCONST, pCOUPL are shown in (a), (b), (c) respectively. (d) shows the total density map as calculated from the total density matrix P. All the conventions are as in Fig.6.5.

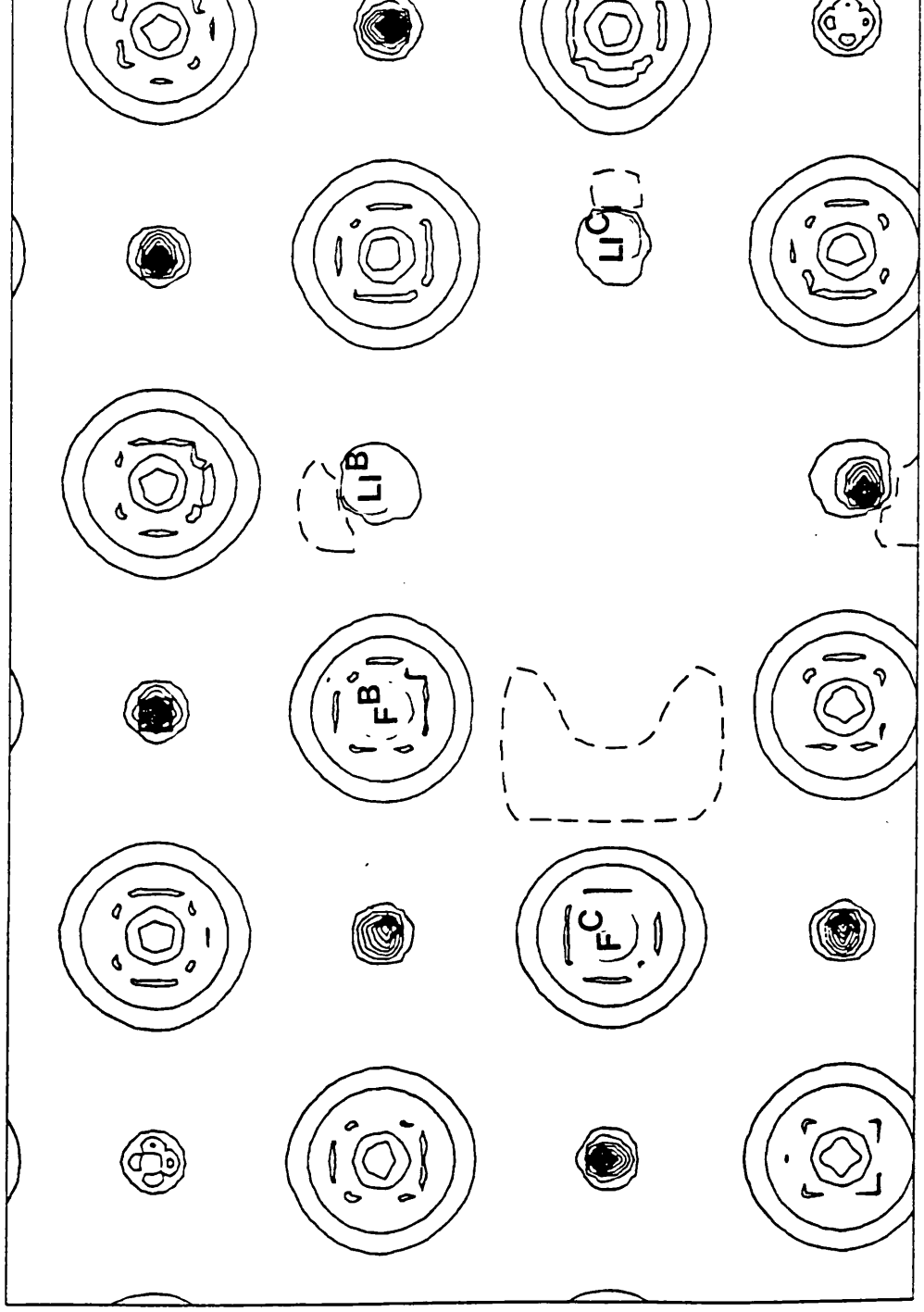

Figure 6.9 Difference electron density maps of the relaxed cluster IV (BSP + 5 Li). The map is drawn in the (100) plane. The interval between the isodensity lines is .004 e/bohr^3. Positive, negative and zero isodensity lines are represented by continuous, dashed and dot-dashed lines.

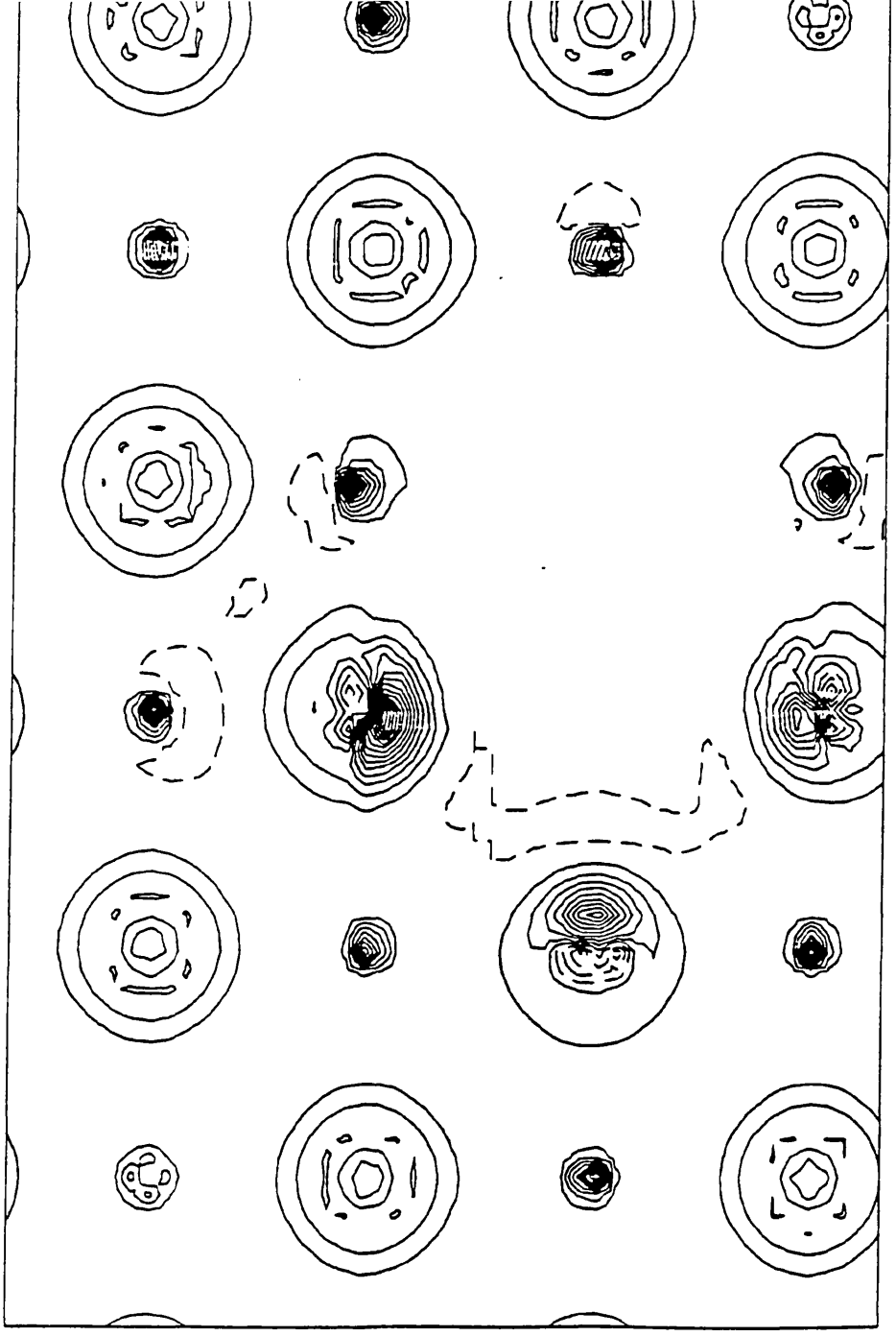

Figure 6.10 Difference electron density maps of the relaxed cluster V (BSP + 5 Li + 5 F). Atoms are positioned as in Fig. 6.9 and the same conventions are used.

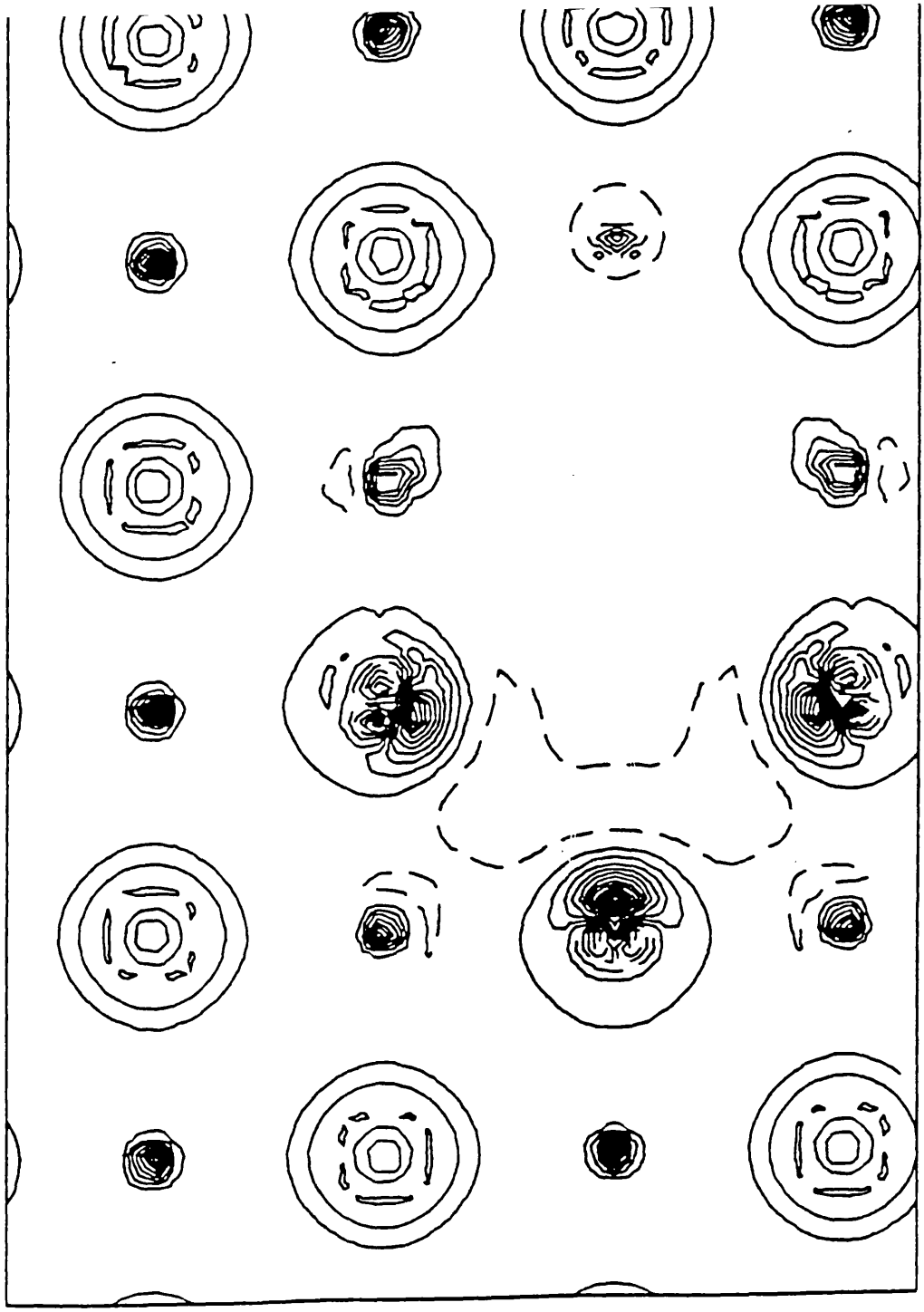

Figure 6.11. Difference electron density maps of the *unrelaxed* cluster V (BSP + 5 Li + 5 F). Atoms are positioned as in Fig. 6.9 and the same conventions are used.

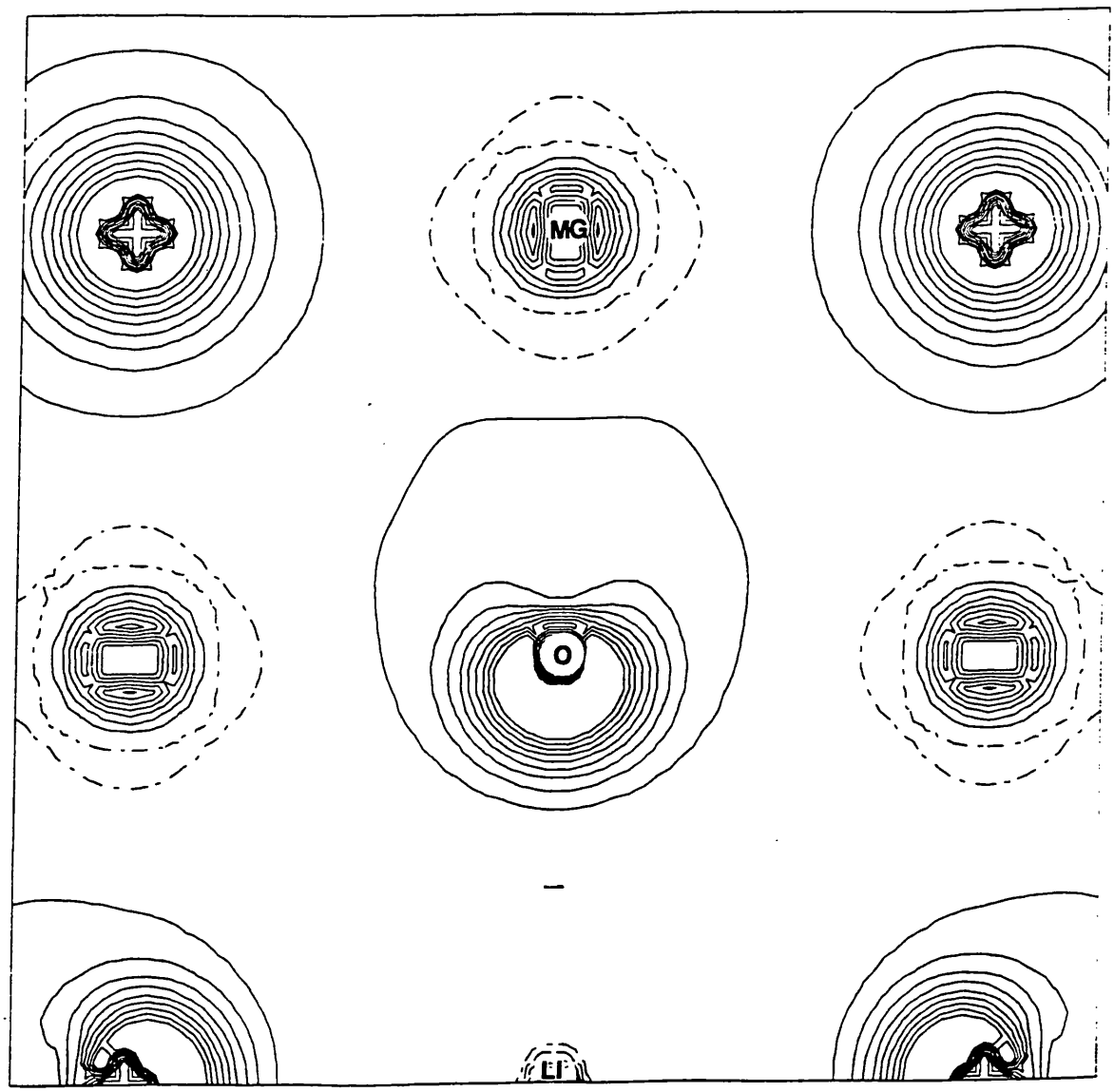

Figure 6.12 Difference electron density maps corresponding to a cluster containing a Li ion surrounded by six O, and embedded in MgO. Conventions are as in Fig. 6.5

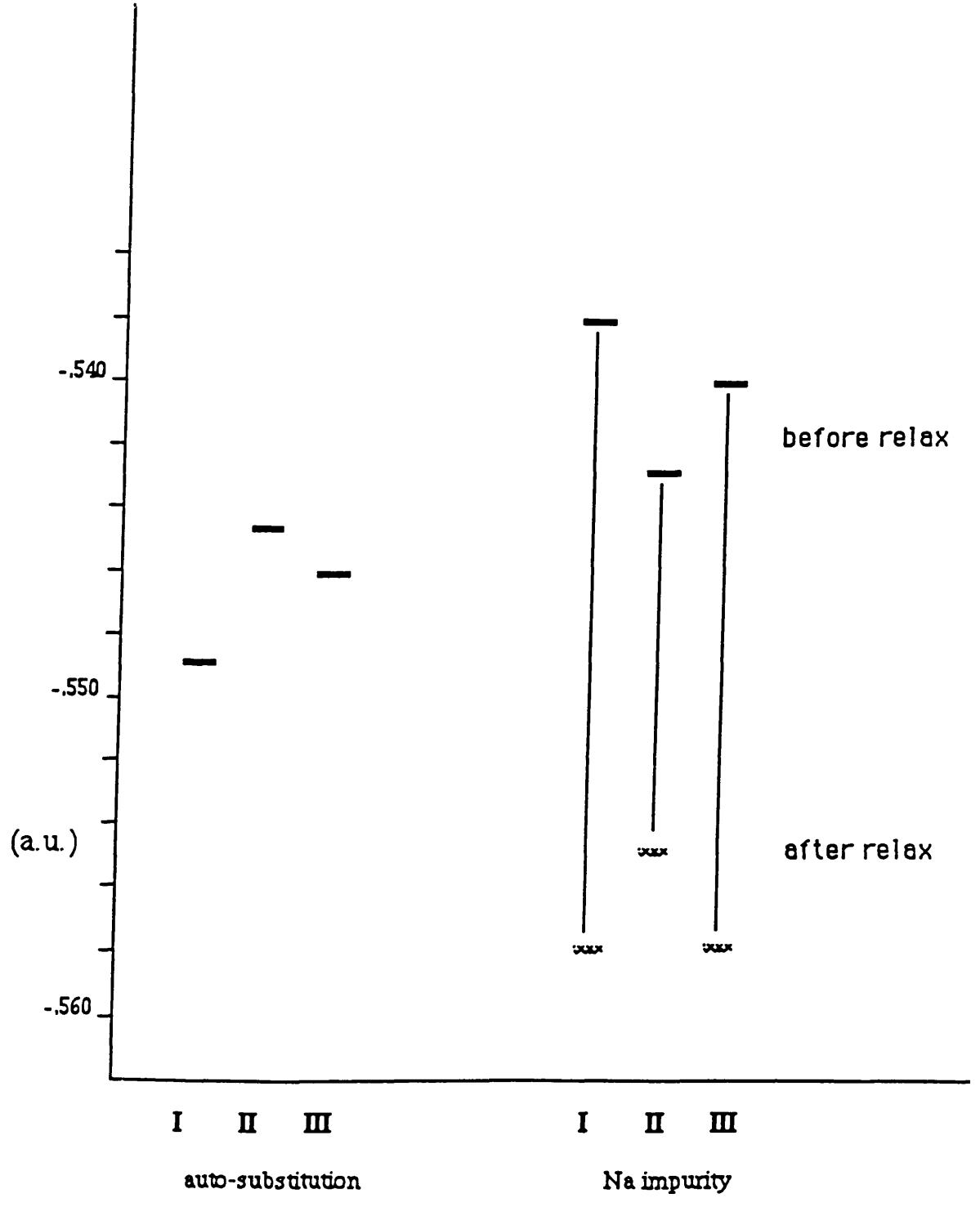

Figure 6.13 Position of the 2p HF levels of F^- as calculated for the ion in the "auto-embedded" cluster CI, CII and CIII and for F^- in the defective clusters (containing the substitutional Na) CI, CII and CIII respectively. The energy scale is in a.u.

REFERENCES

Agullo-Lopez F, Catlow CRA and Townsend PD (1988), Point defects in materials, Academic Press

Cade PE, Stoneham AM and Tasker PW (1984), Phys Rev B, 30, 4621

Catlow CRA and Mackrodt WC (1982), Lecture Notes in Physics, Vol 166, Springer-Verlag, Berlin

Catlow CRA, Diller KM and Norgett MJ (1977), J Phys C, 10, 1395

Dovesi R (1991), personal comm

Fowler PW and Tole P (1988), Surf Sci, 197, 457

Grimes R W, Catlow C R A, Stoneham A M (1989), J Phys Condensed Matter, 1, 7367

Kantorovich L N (1987), Phys Stat Sol (b), 144, 719

Kaufman J V R and Clark C D (1963), Journ Chem Phys, 38, 6 , 1388

Kittel C (1963), Quantum Theory of Solids, Wiley, NY

Lichanot A, Gelize M, Larrieu C, Pisani C (1991), to be published

Lidiard AB (1976) in Henderson B and Hughes AE, (eds), Defects and their structure in non-metallic solids, Plenum, NY

Pandey R and Kunz B A (1988), Phys Rev B, 38, 10150

Saunders VR (1991), personal comm

Shluger A, Grimes RW, Catlow CRA (1991), to be published

Shluger A, Mysovsky S and Nepomnyaschikh A (1988), J Phys Chem Solids, 49,9, 1043

Vail JM (1990), J Phys Chem Solids, Vol 51, no 7, 589

Chapter 7.
Conclusions

The research work presented in this thesis consisted of calculations based on the ab-initio Hartree-Fock approximation. Periodic Hartree-Fock calculations can be considered a 'standard' technique in the sense that the computational algorithms are well established and tested, and that calculations on crystals with a small unit cell yield satisfactory results. Our studies of silica and magnesium silicates, using extended basis sets, show that the range of applications of this technique can indeed be expanded towards more complicated systems. The predictive capability of the technique can be exploited to calculate properties that are difficult to be measured by experiment, for example the density of states and the electronic structure of high-pressure and temperature phases such as the ilmenite-structured $MgSiO_3$. We also obtained a consistent picture of the properties of the Si-O bond in different minerals. Further studies of basis set effects, that are already under way, will provide us with basis sets that can be easily transferred to other structures. Such results will make it possible to perform a systematic investigation of magnesium silicates, of their relative stabilities and electronic structures.

Techniques for the study of point defects, using quantum mechanical methods, are less standardized. The program EMBED developed in this research represents the first attempt to implement at an ab-initio Hartree-Fock level a Perturbed-Cluster embedding technique. From the results presented in the thesis it is possible to conclude that this approach can provide information that is qualitatively more accurate and complete than that from both isolated cluster calculations and atomistic simulation techniques. There are, of course, outstanding problems. The convergence of the SCF is often slow and affected by

numerical noise; the effect of the basis set in the defect region still has to be investigated; charged defects represent a big challenge, especially as regards the inclusion of the long range polarization effects and the localization of the charged state. Intense development is necessary, before the method becomes as standard and reliable as the periodic boundary calculations. On the other hand it is already possible to get an insight into the electronic structure of the defect that is valuable and important, as our results on the polarization effects in the Bound Schottky Pair in LiF show.

Further work using the techniques employed and developed in this thesis should lead to major progress in our ability to calculate detailed electronic properties of complex materials.

APPENDICES

APPENDIX A:

Ab-initio HF molecular codes

In the last 30 years many reliable and general-purpose codes, based on the Hartree-Fock theory, have been made available to the scientific community for the study of molecules.

A practical and detailed guide to the most popular ones is given in 'Handbook of Computational Chemistry', written by T. Clark (1985). Many programs have been distributed to the scientific community via the Quantum Chemistry Program Exchange (QCPE) bullettin, others have been commercialized. We present here a list of some of the codes that have been more widely used. More details can be found in the relevant QCPE bullettin or in the references given below.

Program	Source	Comments
MINDO/3	QCPE 308,309	semi-empirical
MNDO	QCPE 353, 379, 428	semi-empirical
MOPN	QCPE 383	semi-empirical
MOPAC	QCPE 455,464	semi-empirical
GAUSSIAN70	QCPE 236	ab-initio
GAUSSIAN80	QCPE 437,446	ab-initio
MRD-CI	(Buenker et al., 1983)	ab-initio
GAMESS	(Guest et al., 1983)	ab-initio

APPENDIX B:

Calculation of the integrated density of states

In order to perform the integral indicated in equation (4.4.29):

$$N(E) = -1/(i\pi) \int_{\gamma(E)} dz\, G(z) \qquad (B1)$$

we can note that we deal with three types of functions of the variable z, as it is clear from equation (4.4.24) and (4.4.25). They are: $G_{DD}(z)$, $G_{DD}(z)/(z-e)$, $G_{DD}(z)/(z-e)^2$.

The integrated quantities are easily calculated after considering that $G_{DD}(z)$ has analytic cut along the real axis corresponding to band intervals, with a discontinuity that is proportional to the projected density of states (DOS)

$$\rho_{DD}(t) = \frac{1}{i\pi}[\, G_{DD}(t + i0) - G_{DD}(t - i0)\,] \qquad (B2)$$

If $e > E$, we can perform the integration as indicated in (4.4.29), by letting the curve γ approach indefinitely to the real axis, because the factors $1/(z-e)$ or $1/(z-e)^2$ do not introduce singularities along the integration path. For $e < E$, the curve γ' is used instead (as shown in the figure), and advantage is taken of the fact that the contribution from the infinite circle is zero because $G_{\delta\delta'}/(z-e)$ is asymptotically proportional to $1/z^2$. We thus have:

$$N_{DD}(E) = \frac{-1}{i\pi} \int_{\gamma(E)} dz\, G_{DD}(z) = \int_{-\infty}^{E} dt\, \rho_{DD}(t) \qquad (B3)$$

$$M_{DD}(e,E) = \frac{-1}{i\pi}\int_{\gamma(E),\,\gamma'(E)} dz\, G_{DD}(z)/(z-e) =$$

$$= \theta(e-E)\int_{-\infty}^{E} dt\ \rho_{DD}(t)/(t-e) - \theta(E-e)\int_{E}^{+\infty} dt\ \rho_{DD}(t)/(t-e) \qquad \text{(B4)}$$

$$M'_{DD}(e,E) = \frac{-1}{i\pi}\int_{\gamma(E),\,\gamma'(E)} dz\, G_{DD}(z)/(z-e)^2 = \frac{\partial}{\partial e} M_{DD}(e,E) \qquad \text{(B5)}$$

where $\theta(x)$ is the Heaviside step function.

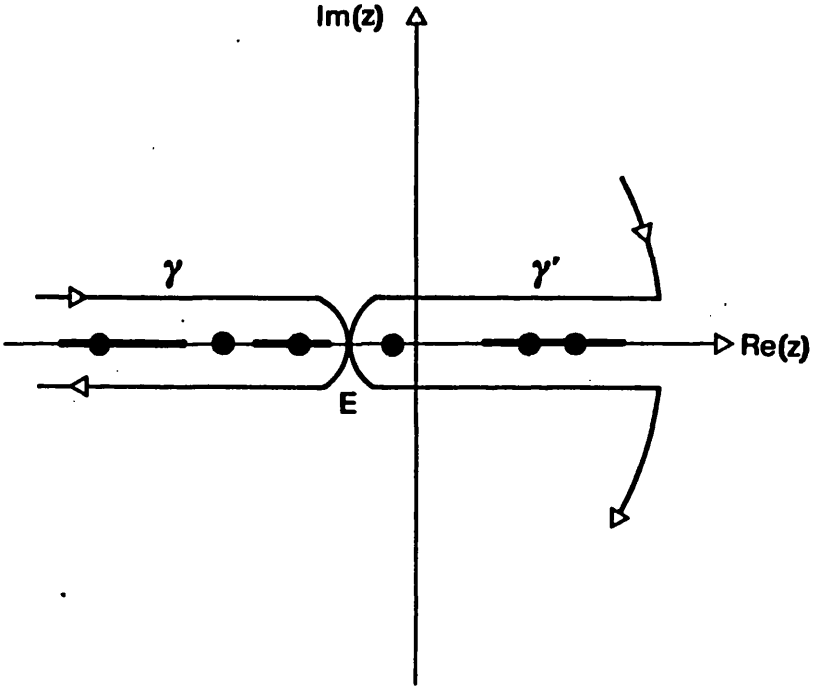

APPENDIX C:

Integration of the density of states

The integrals that appear in B4, B5 and in 4.4.32 and 4.4.33, may be performed analytically using a polynomial expression for the projected DOS. More precisely, $\rho^{f}_{\mu\nu}$ (e) is expressed as a sum of contributions from the various crystal bands, b, each represented by a polynomial of degree l in the band interval (A_b , B_b). The technique used to determine the coefficients of the polynomials, from the knowledge of the eigenvectors and eigenvalues of the perfect crystals in a set of selected k points, is described in the literature (Angonoa et al., 1984; Pisani et al., 1988).

After substituting the polynomial expansion of the DOS associated with each band into equations (4.4.32) and (4.4.33), the integrals are expressed as a sum of band contributions. Fully occupied bands contribute to M(e) values with e> E_F, and vice versa; totally empty bands contribute to M(e) values with e < E_F. The further these bands are from the Fermi energy, and the smaller their width, the less these contributions are affected by details of the DOS, because the denominator (t-e) is large and approximately constant over the band interval. The description of the corresponding DOS may be relatively approximate, i.e., the degree l of the polyniomial may be low. This is particularly true for core bands.

If e is near E_F then the denominator |t-e| may become large, and the M(e) value will depend critically on the details of the DOS in the proximity of the Fermi level. Of course, the problem is much less important in the case of large gap semiconductors or insulators.

APPENDIX D:

Overlap effects on the defect formation energy

The condition $P_D = P_D^f$ plays a crucial role in the embedding technique adopted in this research work. The larger the C cluster is, the better this assumption is justified.

In particular, as discussed in Chapter 4, the proper defect region A should be separated from the outer region D by a sufficiently large boundary zone B. This ideal condition is not easily satisfied in practice, because of the computational requirements. It often happens, as for example in Fig. 6.1, that there are no atoms in B, so that the neighbouring atoms of the defect relax directly towards atoms in D. In this Appendix we will discuss how changes in the S_{CD} block of the overlap matrix affect the P_{DD} block of the density matrix. For this purpose we shall consider the case of self-substitution. The cluster contains an inner part (A'), and a boundary region (B). The 'unrelaxed' and 'relaxed' geometries can be visualized as follows:

I) A' ---- B ---- D

II) A' ------ B -- D

The corresponding overlap matrices, written taking in account their block structure,

$$S = \begin{bmatrix} S_{AA} & S_{AB} & S_{AD} \\ S_{BA} & S_{BB} & S_{BD} \\ S_{DA} & S_{DB} & S_{DD} \end{bmatrix}$$

are:

$$S^I = \begin{bmatrix} S^f & S^f & 0 \\ S^f & S^f & S^f \\ 0 & S^f & S^f \end{bmatrix} \qquad \text{(D1)}$$

$$S^{II} = \begin{bmatrix} S^f & Y & 0 \\ \tilde{Y} & Y' & Y'' \\ 0 & \tilde{Y}'' & S^f \end{bmatrix} = S^I + \begin{bmatrix} 0 & \delta & 0 \\ \tilde{\delta} & \delta' & \delta'' \\ 0 & \tilde{\delta}'' & 0 \end{bmatrix} \qquad \text{(D2)}$$

If relaxation is not large, we assume that the Δ matrix and its δ sub-blocks are 'infinitesimal', in the sense that we shall neglect terms higher than first order in Δ.

We also assume that:

a) the orthonormalized eigenvectors of the system (V') are not changed, and changes in the P matrix are entirely related to modifications in the overlap matrix. We can write:

$$P^f = (S^I)^{-1/2}\, V'^{+}\, \theta\, V'\, (S^I)^{-1/2} \qquad \text{(D3)}$$

$$P \approx (S^{II})^{-1/2}\, V'^{+}\, \theta\, V'\, (S^{II})^{-1/2} = K^{+} P^f K \qquad [K = (S^I)^{1/2}\, (S^{II})^{-1/2}] \qquad \text{(D4)}$$

b) S^I and S^{II} commute. Then:

$$K \approx I - 1/2\, S^I \Delta \qquad (D5)$$

and

$$P \approx P^f - 1/2\, [\, S^I \Delta P^f + P^f \Delta S^I \,] \qquad (D6)$$

Two simplifying approximations are used for the calculations presented in Chapter 6: first we suppose that the corrective term $[\, S^I \Delta P^f + P^f \Delta S^I \,]$ remains unchanged when the 'perfect central region' (A') is substituted with the defect atom(s) (A). This allows us to calculate the correction once and for all in the case of the auto-embedding calculation. Secondly, we assume that the corrective term is linear in Δx (Δx being the relaxation parameter), if Δx is small.

APPENDIX E:

The Ewald sum

It is often necessary to calculate all the Coulombic interactions generated by a periodic lattice of point charges. A direct sum is not a convenient choice, since the series is very slowly converging. More rapid convergence is achieved by applying to each of the component Bravais lattice, the method proposed by Ewald (1921).

First we substitute the actual lattice, that contains M point ions in the unit cell, with M superimposed neutral lattices; each one contains only one of the ions (λ) of the unit cell, (located at s_λ) and is treated independently from the others. The neutrality of each lattice is achieved by adding a compensating uniform background of charge to the distribution due to the point charges. This uniform charge has a density $Z_\lambda\ V^{-1}$ (Z_λ is the nuclear charge associated with the particular ion and V is the unit cell volume). Each charge distribution ($\rho_\lambda(\mathbf{r})$, with $\mathbf{r}$ being the vector of the coordinates of the point where the charge density is calculated) associated to the lattice corresponding to the ion λ, is expressed as a sum of two terms:

$$\rho_\lambda(\mathbf{r}) = \rho_{i\lambda}(\mathbf{r}) + \rho_{j\lambda}(\mathbf{r}), \qquad \text{(E1)}$$

where:

$$\rho_{i\lambda}(\mathbf{r}) = \Sigma_{\mathbf{h}}\, Z_\lambda \{ N_\alpha \exp [-\alpha (\mathbf{r} - s_\lambda - \mathbf{h})^2] - 1/V\} \qquad \text{(E2)}$$

$$\rho_{j\lambda}(\mathbf{r}) = \Sigma_{\mathbf{h}}\, Z_\lambda \{\delta (\mathbf{r} - s_\lambda - \mathbf{h}) - N_\alpha \exp [-\alpha(\mathbf{r} - s_\lambda - \mathbf{h})^2]\} \qquad \text{(E3)}$$

$\rho_{i\lambda}$ consists of a lattice of normalised Gaussian functions minus the uniform charge distribution ; $\rho_{j\lambda}$ is a lattice of point charges minus a set of neutralising Gaussian functions. The sum of these two components gives the neutralised lattice of point charges.

We can then calculate the potentials $V_{i\lambda}(\mathbf{r})$ and $V_{j\lambda}(\mathbf{r})$ generated by the two components of the charge distribution, $\rho_{i\lambda}$ and $\rho_{j\lambda}$. The total potential is given by the sum:

$$V_\lambda(\mathbf{r}) = V_{i\lambda}(\mathbf{r}) + V_{j\lambda}(\mathbf{r}) \qquad \text{(E4)}$$

where:

$$V_\lambda(\mathbf{r}_1) = \int d\mathbf{r}_2 \; \frac{\rho_\lambda(\mathbf{r}_2)}{|\mathbf{r}_1 - \mathbf{r}_2|} \qquad \text{(E5)}$$

In the case of $V_{i\lambda}(\mathbf{r})$, we have a uniform charge distribution, "perturbed", by a Gaussian charge distribution of opposite sign.

Rapidly converging reciprocal space series can be obtained through a Fourier expansion of $\rho_{i\lambda}$ and of $(|\mathbf{r}_1 - \mathbf{r}_2|)^{-1}$; in 3D space the series takes the following form (Tosi, 1964):

$$V_{i\lambda}(\mathbf{r}) = \frac{4\pi}{V} \sum_{\mathbf{K}}{}' \; K^{-2} \exp(-K^2/4\alpha) \exp[i\mathbf{K}\cdot(\mathbf{r}-\mathbf{s}_\lambda)] \qquad \text{(E6)}$$

The larger the gaussian is (and therefore the lower the exponent α), the quicker the convergence will be.

In the case of $V_{j\lambda}(\mathbf{r})$, we note that in $\rho_{j\lambda}$ the unitary point charge centered at $(\mathbf{s}_\lambda - \mathbf{h})$, is screened by a unitary Gaussian charge distribution centred at the same point and with opposite sign. In the limit of infinite exponent α the two distributions cancel; otherwise, the larger the α, the quicker the $\mathbf{h}$ summation converges. By integrating $\rho_{j\lambda}$ in direct space the following formula is obtained:

$$V_{j\lambda}(\mathbf{r}) = Z_\lambda \left[\sum_{\mathbf{h}} (|\mathbf{r} - \mathbf{s}_\lambda - \mathbf{h}|)^{-1} \operatorname{erfc}(\alpha(|\mathbf{r} - \mathbf{s}_\lambda - \mathbf{h}|) - \frac{\pi}{V\alpha} \right] \quad \text{(E7)}$$

$$\text{where } \operatorname{erfc}(x) = 2\pi^{-1/2} \int_x^\infty dz \exp(-z^2) \quad \text{(E8)}$$

The best value for α is chosen in order to minimize the computational time required to evaluate (E6) and (E7) (Catlow and Norgett, 1977).

REFERENCES

Angonoa G, Dovesi R, Pisani C and Roetti C (1984) , Phys Status Şolidi B, 122, 211

Clark T (1985), 'A Handbook of Computational Chemistry', J. Wiley and Sons, NY

Buenker RJ and Peyerimhoff SD (1983), in New Horizon of Quantum Chemistry, ed. P Lowdin and B Pullmann, D Reidel, Dordrecht

Guest MF, Kendrick J and Poper SA (1983), Program GAMESS documentation, SERC Daresbury Laboratory

Catlow CRA and Norgett MJ (1976), AERE Harwell Report M2936

Ewald PP (1921), Ann Phys (Leipzig), 64, 253

Pisani C, Dovesi R, Roetti C (1988), Lecture Notes in Chemistry 48, Springer Verlag: Heidelberg

Tosi MP (1964), Solid State Phys, 16,1

*EMBED*90 - An ab-initio all-electron LCAO Hartree-Fock Program for the Study of Local Defects in Crystals.

CONTENTS.

The *EMBED* program allows the calculation of the HF density matrix and derived properties of point defects in crystalline structures. It is based on the Perturbed Cluster (PC) approximation described in details in reference 1. Some technical aspects are discussed in reference 2.
An essential prerequisite for the program to work, is having available the HF solution for the host crystal, as obtained by means of the *CRYSTAL* program [3]. The information required is Geometry, Symmetry, Basis Set, Fock matrix, and Projected Densities of States (PDOS) of the host.
Except for the last quantity, which is calculated expressly for the *EMBED* program (see section III.1), all information is contained in unit FT9 of *CRYSTAL*.
The "technology" used for the calculation of integrals, the evaluation of long range Coulomb contributions, etc. are similar to those employed in *CRYSTAL*; in fact, many subroutines are common to the two codes.

References

1. C. Pisani, R. Dovesi, R. Nada, and L. Kantorovich , J. Phys/ Chem., ... (1990).
2. C. Pisani, R. Dovesi, R. Nada, and S. Tamiro, Surface Sci. 216, 489 (1989).
3. C. Pisani, R. Dovesi and C. Roetti, Hartree-Fock *ab-initio* treatment of crystalline systems, Lecture Notes in Chemistry, Vol. 48, Springer Verlag, Heidelberg, 1988; R. Dovesi, C. Pisani, C. Roetti, M. Causa' and V. R. Saunders, *CRYSTAL* 88, QCPE Program No. 577, Indiana University, Bloomington, Indiana (1989).
4. C. Pisani, R. Dovesi, and P. Ugliengo, Phys. Stat. Sol. (b) 116, 249 (1983); ibidem, 116, 547 (1983).
5. R. Dovesi, C. Pisani, C. Roetti and V. R. Saunders, Phys. Rev. B 28, 5781 (1983).

II.1 GENERAL INFORMATION ON *EMBED*

The program allows the study of point defects in crystals corresponding to adding, subtracting, or shifting atoms in a localized zone of the crystal (to be identified henceforth as Zone A). For the rest, all atoms are left in their unperturbed position.
As is the case with *CRYSTAL*, atoms are described with a basis set of "Atomic Orbitals" (AO) which are linear combinations of GTOs. Only s and p functions are allowed. AOs are identified in the following with Greek letters (α, β, γ,...).
Only closed shell systems can be investigated.
The approximation on which the PC equations are based, is that important changes in the Density Matrix P and in the PDOS $\rho(\epsilon)$ occur only in a restricted zone of the crystal (Zone C) including and surrounding Zone A; changes in out-of-diagonal elements $P_{\gamma\delta}$ and $\rho_{\gamma\delta}(\epsilon)$ with γ belonging to the C zone, and δ outside it, are allowed for and taken into account, too.

II.2 COMPUTATIONAL INFORMATION ON *EMBED*

EMBED is written in FORTRAN, compatible with the FORTRAN77 standard.

All variables are in SINGLE PRECISION; for compilation on IBM type machines the AUTODOUBLE option of the VS FORTRAN compiler must be used, in order to generate DOUBLE PRECISION variables.

It is organized into two steps (PASS00 and PASS01) which transmit information to each other via disk files: PASS00 just recovers information from *CRYSTAL* results; PASS01 solves the PC equations.
A PROPEMB program is in preparation, for the calculation of properties from the SCF density matrix. For the moment being (Jan. 90) it is confined to the calculation of Electron Charge Density (ECHD) Maps.

TIMER ROUTINE. A timer routine **SECOND** is called in the MAIN program of both PASS00 and PASS01; the only argument of SECOND is a real number, which is supposed to be set to the CPU time in seconds; an ASSEMBLER IBM version of this routine is provided. This routine is supplied by the system on CDC CYBER-205, CRAY and CONVEX systems. Its normal functioning is not essential to the program and it can be replaced by the coding:

```
      SUBROUTINE SECOND(X)
      X=0.
      RETURN
      END
```

The dimensions of all important matrices and arrows are defined as parameters. The "PARAMETER" cards are the same in all subroutines. A "Change" command throughout the FORTRAN source allows such dimensions to be changed.

Many STOP conditions have been introduced related to the 'simple' and 'product dimensions' of the program; a short comment is produced by each STOP condition about the possible origin of the problem.

Matrix multiplications are performed by the MXMB and MXMBN routine.
An ASSEMBLER version can reduce the CPU time by a non-negligible factor.

Card input is taken from FT05, printed output is sent to FT06.
A number of scratch FORTRAN UNITS (FT) are used by *EMBED* to store intermediate quantities: 12 and 13 in PASS00 (which are passed to PASS01); 1,3,4,10,12,13,19,28,29 in PASS01.

Units referring to Cataloged Data Sets for transmitting information either to or from other tasks are:

in PASS00:
- FT09: contains Geometry, Basis set, Symmetry, and Wave function information from *CRYSTAL*;

in PASS01:
- FT26: contains PDOS information from Part 3 of *CRYSTAL* (see section III.1);
- FT32: stores information on P matrix for use as a starting guess in subsequent jobs [optional: used only if INF(173)=1, see section IV.8];
- FT31: contains information on P matrix from preceding jobs for use as a starting guess [optional: used only if INF(174)=1, see section IV.8];
- FT20: contains information on long range correction to the P matrix [optional: used only if LPRINT(60)≠0, see section IV.9].

in PROPEMB units FT09, FT31 are used; unit FT25 is required if data concerning the maps are to be saved for subsequent plotting.

Space allocation:

FT04 contains the bielectronic integrals, and is by far the largest file; for 'big' systems the space allocation is between 20 and 40 MEGAWORDS; a precise estimate of the space allocation for the bielectronic file can be obtained by using the LPR(50)=3 option (see APPENDIX A): the program stops after the selection of the integrals to be evaluated.

FT01 contains the monoelectronic integrals and the bipolar expansion terms; in general it is 10 to 30% of FT04

The other FT units are much smaller; allocations of the order of 0.2 MEGAWORDS were enough for all the investigated cases.

III.1 FROM *CRYSTAL* TO *EMBED*

Preliminary to any embedding calculation is the solution of the HF problem for the host crystal by means of *CRYSTAL*. A single such run can be used for any defect calculation involving that host crystal.
The *CRYSTAL* version to be used for such calculations is *QMIX89*. The COMMON's in *EMBED* that refer to *CRYSTAL* quantities are an exact copy of the corresponding ones in that version of *CRYSTAL*, and are filled in PASS00, after reading the corresponding information from unit FT09.
The instruction manual of *CRYSTAL88* can be used for preparing the input of the calculation (but remember that d functions are not allowed in *EMBED*!).
After running *CRYSTAL* (do not forget to catalog unit FT09), it is necessary to prepare the PDOSs, or, better, the coefficients of their polynomial expansion for each band. The corresponding data will be read by PASS01 on unit FT26.
This task is performed by PARTIII of *CRYSTAL*, using the option EMBE:

CARD	FORMAT	VARIABLE	MEANING AND/OR SUGGESTED VALUES
1	A4	`EMBE`	keyword
2	3I	IS	Shrinking factor for reciprocal space net
		NPOL	number of Legendre polynomials used to expand DOS (if NPOL>25 it is set to 25).
		NUMPRT	number of printing options
----IF.IS.EQ.0----------			
2a	3I	IS1,IS2,IS3	Shrinking factors along B1,B2,B3 (reciprocal lattice vectors); to be used when the unit cell is strongly anisotropic. See comments in section IV.5 of *CRYSTAL* Instruction Manual.
----------IF .NUMPRT.NE.0----------			
2b	2*NUMPRT I	J LPR(J)	printing option; see APPENDIX E of *CRYSTAL* manual for a list (involved J's: 40,59,105,111,112)
3	A4	'END'	

Comments on 'EMBE' calculations:
For the calculation of the PDOS, the Fourier-Legendre technique described in Chapter II.6 of reference 3 is used. The only parameters of importance are IS (which determines the number NKF of sampling k points and the number of symmetrized PWs for the Fourier expansion of k dependent quantities), and NPOL (number of Legendre polynomials used for the expansion of the DOS).
Suggested values for IS: from 4 to 12 for 3-d systems, from 6 to 18 for 2-d systems, and from 10 to 20 for 1-d systems.
Suggested values for NPOL: 10 to 15. The program automatically scales down NPOL for bands which are narrow and/or far from E_{Fermi}.
Example of input cards for DOS calculation:

```
card
 1       EMBE
 2       18 14  3
2b       105 1 112 1 40 8
 3       END
```

No input cards are needed for PASS00. The input for PASS01 is as follows (Note: unless differently stated, Free Format is used throughout ; comments are found in chapter IV.x, as indicated):

CARD	FORMAT	VARIABLE	MEANING AND/OR SUGGESTED VALUES	
1	20A4	TITLE	any string of 80 characters.	
2		NUMPRT	number of printing options (first set)	
--- if NUMPRT.NE.0 ---				
2a	2*NUMPRT I	J,LPR(J)	see APPENDIX A; note that some of the LPR options can produce many thousands of OUTPUT lines. LPR(60)≠0 controls use of long range corrections to P	(IV.8)
	FIRST SET OF "LPRINT" CARD			
3	14I	INF(110)	if ≠0, controls ordering of stars	(IV.1)
		INF(111)	overlap thresh. for Coul.integrals	(IV.2)
		INF(112)	penetration thresh. for Coul. integrals	(")
		INF(113)	overlap thresh. for "mono" integrals	(")
		INF(114)	overlap thresh. for exch. integrals	(")
	FIRST	INF(115)	pseudo-overlap threshold for exchange	(")
	SET	INF(116)	security threshold	(")
	OF	INF(117)	radius quantum zone (a.u.)	(")
	"INF"	INF(118)	pole order	(")
	CARD	INF(119)	derivative order in Madelung zone	(")
		INF(120)	multipole order in Madelung zone	(")
		INF(121)	mixing schedule for Fock matrix	(IV.3)
		INF(122)	safety zone around E_F (a.u./10000)	(")
		INF(123)	E_F (a.u./10000)	IV.4)
4	3F,3I	XOR,YOR,ZOR	Origin of the cluster (a.u.)	(IV.1)
		NSTAA	Number of Stars of Atoms in Zone A	(")
		NSTA1	Number of Stars of Atoms in Zone A'	(")
		NSTCC	Number of Stars of Atoms in Zone C	(")
------- If NSTAA ≠ 0, for each 'first atom' of stars in A -------				
4.1 to 4.NSTARA	4F	ATOMN	Atomic number	(IV.1)
		XA,YA,ZA	Coordinates (a.u.) in crystal frame	(")
5		NUMPRT	number of printing options (second set)	
--- if NUMPRT.NE.0 ---				
5a	2*NUMPRT I	J,LPR(J)	see APPENDIX A; in particular: LPR(48) defines the "percentage of charge renormalization".	
	SECOND SET OF "LPRINT" CARD			(IV.8)
6	10I	INF(170)	number of SCF cycles	(IV.3)
		INF(171)	conv. check [-Log(sqrdev eigval)]	(")
		INF(173)	if ≠0, final P is stored on FT32	(IV.6)
		INF(174)	if ≠0, start.P is read from FT31	(")
	SECOND	INF(175)	if ≠0, "shift" option is used	(IV.3)
	SET	INF(176)	tol.for grouping eigval (a.u./1000)	(IV.5)
	OF	INF(177)	interv. for shift intrpl (")	(IV.3)
	"INF"	INF(178)	lower limit active zone (a.u./1000)	(IV.5)
	CARD	INF(179)	upper limit active zone (")	(")
		INF(180)	nr. cycles bfr. using active zone opt.	(")

↓↓↓↓↓↓↓↓↓↓↓↓↓↓↓↓↓↓↓↓↓↓↓↓ input follows ↓↓↓↓↓↓↓↓↓↓↓↓↓↓↓↓↓↓↓↓↓↓↓↓

```
$ IF NSHL ≠ 0, for each type of atom in cluster C
$
$$$$$$$$$$$$$$$$$$$$$$$$$$$$$$$$$$$$$$$$$$$$$$$$$$$$$$$$$$$$$$$$$$$$$$$$
$ BASIS SET CARDS (same as in CRYSTAL)                          (IV.7)
$ A basis set (BS) must be defined for each different type of atom (t)
$ in Zone C, if there is at least one atom in Zone A.
$ The basis set for each atom has NSHL shells whose AOs are described
$ by NGAUSS contracted Gaussian Type Functions (GTF)
$$$$$$$$$$$$$$$$$$$$$$$$$$$$$$$$$$$$$$$$$$$$$$$$$$$$$$$$$$$$$$$$$$$$$$$$

7.t.1     2I        NAT          atomic number (if NAT<99).
                    NSHL         number of shells in the basis set for atoms
                                 with "atomic number" NAT. If NAT=99 and
                                 NSHL=0, end of basis set INPUT.
---------- for each shell (s) --- (from 1 to NSHL)
7.t.s.1   3I,2F     ITYBAS       basis set type:
                                  0 Pople's standard STO-nG (data provided
                                    by the program) Atomic Numbers 1-36)
                                  1 general BS, defined in card 7.t.s.2 and
                                    following ones
                    LAT          shell type:
                                  0 S  (1 s AO)
                                  1 SP (1 s + 3 p AOs)
                                  2 P  (      3 p AOs)
                                 NGAUSS nr of contracted GTF in the shell
                                 when ITYBAS=0  1≤NGAUSS≤6
                                 when ITYBAS=1, 1≤NGAUSS≤10(or 6 for LAT=3)
                    CHE          formal electronic charge attributed to the
                                 shell (to be used for the atomic
                                 calculation; only 1 open shell per atom is
                                 allowed);
                    SCALE        scale factor; if ITYBAS=0 and SCALE=0., the
                                 standard Pople's scale factor is used.
-------IF ITYBAS.EQ.1 for each one of the NGAUSS functions---------
7.t.s.2 2F(3F)      EXP          exponent of the uncontracted normalized GTF
to                  COEF1        contraction coefficients of the normalized
7.t.s.NGAUSS+1                   Gaussian (if LAT=1, s function coefficient)
                   (COEF2)       contraction coefficients for p functions
                                 (only for LAT=1).
-----------------------------------------------------------------------
To end this INPUT section, a last CARD must be supplied:
   99 0
$$$$$$$$$$$$$$$$$$$$$$$$$$$$$$$$$$$$$$$$$$$$$$$$$$$$$$$$$$$$$$$$$$$$$$$$

-----------------------------------------------------------------------
 8     I           I          if I=999, then EOJ else restart     (IV.6)
----------------------  if I ≠ 999  ------------------------------------
 9     4I          INF(170)
                   INF(121)
                   INF(123)          RESTART CARDS
                   INF(176)
                                        (IV.6)
10     3I          INF(178)
                   INF(179)
                   INF(180)
-----------------------------------------------------------------------
11     I           I          if I=999, then EOJ else restart     (IV.6)
------------  if I ≠ 999 ... same as above etc.etc. -------------------
```

For calculating the density maps, the program PROPEMB must be used, which recovers information from a previous calculation (unit FT31) in the same way as when using the recovery option. The program performs again all the geometrical analysis. The input must be exactly the same as in the previous calculation, although, obviously, the integrals are no longer calculated, and the SCF information is completely ignored.
At the end, the cards defining the plot to be calculated are provided. They closely resemble those used in ***CRYSTAL*** for the same purpose.

CARD	FORMAT	VARIABLE	MEANING AND/OR SUGGESTED VALUES
1 to 7.last			Same as in preceding step
8	4I	NPY	Number of points on the B-A segment.
		IPLOT	NE.0: ECHD values are stored on FT25 for making a PLOT; see appendix H.
			0 : ECHD values are <u>not</u> stored on disk.
		IMODE	LE.0: the domain to be explored will be identified by the cartesian coordinates of points A, B and C;
			GE.1: the domain to be explored will be identified by atoms IA, IB, IC.
		ISATOM	0 : gives ECHD of defective crystal
			1 : gives superposition of atomic ECHDs
----------IF IMODE.LE.0 ----------			
9	3F	XA,YA,ZA	cartesian coordinates of point A in a.u.
10	3F	XB,YB,ZB	cartesian coordinates of point B in a.u.
11	3F	XC,YC,ZC	cartesian coordinates of point C in a.u.
----------IF IMODE.GE.1 ----------			
9'	4I	IA,LA,MA,NA	the nucleus with label IA, located in the crystalline cell with indices (LA MA NA) corresponds to point A;
10'	4I	IB,LB,MB,NB	the nucleus with label IB, located in the crystalline cell with indices (LB MB NB) corresponds to point B;
11'	4I	IC,LC,MC,NC	the nucleus with label IC, located in the crystalline cell with indices (LC MC NC) corresponds to point C.

(Note that the numbers that identify atoms (IA,IB,IC) , and the indices of the crystal cells are as in ***CRYSTAL*** if the atoms do not belong to the A zone; atoms belonging to the A zone are numbered in a sequence starting from N+1, where N is the number of atoms in the elementary cell of the host crystal, and are assigned to the (0,0,0) cell).

IV. COMMENTS ON INPUT INSTRUCTIONS

IV.1 GEOMETRY, ZONES, STARS

a) We use throughout the geometry of the host crystal, as defined by the *CRYSTAL* reference calculation.
The identification of the defective cluster symmetry, and of the atoms that belong to the different zones, is based uniquely on the choice of a "cluster origin" (card 4). It is assumed that all symmetry operators are left in the defective crystal, which leave the origin in its place. Let us define these residual point operators as $V_1,...V_p$. If one wants to reduce the symmetry, it is sufficient to displace the origin to a position of lower symmetry.

b) Atoms, both of the host crystal and substitutional or interstitial ones, are ordered into stars. Atoms belong to the same star if they are related to each other by one of the symmetry operators $V_1,...V_p$.
Stars are numbered in order of increasing distance from the origin, unless otherwise specified (see point d).

c) We define three types of zones, A, A', C, each comprising a given number of stars NSTAA, NSTA1, NSTCC , respectively (card 4).
Consider first zone A'. It includes those atoms of the host crystal which are eliminated for forming the defective crystal. NSTA1 indicates how many stars of atoms of the perfect host crystal belong to A', starting from the most internal one.
Zone A includes those atoms which are added to the crystal after removing the ones in A'. Again, NSTAA gives the corresponding number of stars, with reference to the defective crystal. Note that some of the atoms in A can be the same that have been eliminated previously, perhaps in a slightly modified position. In the INPUT (card 4.1 to card 4.NSTAA) one must provide the atomic number and the coordinates (a.u., referred to the crystal frame) of one atom per each star.
Zone C includes those atoms that belong to the cluster C, to which the PC equations are applied (see section II.1). Note that the number of stars in C, NSTCC, must be greater or equal to NSTAA.
Examples of use of these variables are provided below.
It can finally be mentioned that in the *EMBED* jargon a D^* zone is also defined, which includes those shells external to zone C, which have at least one neighbour in C (according to the tolerances specified below (see IV.2)).

d) A different ordering of the stars other than that simply based on distance from the origin can be useful, for instance in chemisorption problems or in the treatment of molecular crystals. This can be effected by means of INF(110) (card 3).
In order to do that, begin by sketching on a line the different stars in the standard order of distance from the origin (see below). Above each star (to the right hand side of the origin) put a figure referring to the new ordering you want.

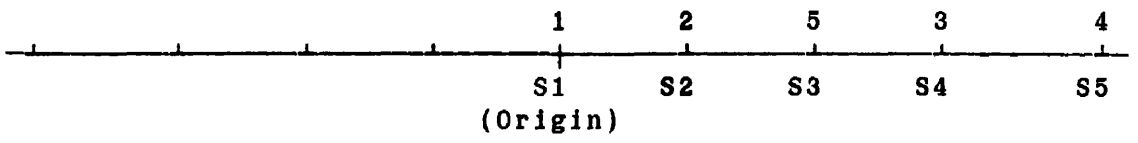

(In the example above, the star that is third in the distance ordering, will become the fifth one). Collect the figures into one number (in the example: 12534) and attribute it to INF(110).

to 0; 21, 213, 2134 are equivalent to each other, etc. Clearly, no more than nine stars can be reordered.

IV.2 TOLERANCES

a) The five parameters INF(111)-INF(115) (card 3) correspond in the order to the ITOL parameters of *CRYSTAL*, as described in reference 5. They control the accuracy of the calculation for the bielectronic COULOMB and EXCHANGE series; the selection is performed according to overlap-like criteria: when the overlap of the involved Atomic Orbitals is smaller than $10^{-ITOL(J)}$ the corresponding integral is disregarded or evaluated in a less precise way. INF(116) is a "safety" tolerance that must be greater than all the preceding ones, but has no influence on the results.
Suggested values:
4 4 4 4 6 7 (soft: see however the ΔP' recovery technique, IV.6)
5 5 5 5 7 9 (good)

b) INF(117-119) (card 3) control the accuracy of the one-electron part of the calculation.
INF(117) specifies the radius (in a.u.) of the "quantum zone", out of which all contributions to the Fock matrix are evaluated according to the Ewald technique. It should be large enough to include all shells in D^* (see point IV.1.c); a value of 20 is often adequate.
INF(118) corresponds to INF(3) of *CRYSTAL*, and corresponds to the max order of the multipolar expansion of the shell charge, in the three-center evaluation of the Coulomb contribution to the Fock matrix (suggested values 2 to 4).
INF(119) gives the maximum order of derivatives of the Madelung potential used in the evaluation of the Fock matrix; suggested value: 2; INF(120) gives the max order of the multipolar expansion of the shell charge, in the evaluation of the Madelung energy; suggested value: 2.

IV.3 CONTROL OF SCF PROCEDURE

a) The SCF procedure is ended when either the number of SCF cycles is above the chosen limit [INF(170): card 6 or card 9], or if the mean square difference of the new eigenvalues of the F_C matrix with respect to the preceding ones is less than 10**[-INF(171)] (card 6 or card 9). As a matter of fact, convergence is always very delicate, and there are in *EMBED* a number of devices that help (in a more or less effective way) convergence to be reached. The best and most natural solution to the problem is to use a good initial guess for the density matrix; this is discussed in section IV.6. We consider here a few other techniques.

b) It is always useful to mix the old to the new F matrix in order to prevent too marked oscillations. The percentage of mixing is defined by INF(121) (card 3 or card 9): this is a four-figure number whose first two figures give the percentage of the old F matrix fed in the new F at the beginning of the SCF cycle. This percentage is linearly modified during the procedure, to end up with the final percentage represented by the last two figures of INF(121). Very high values are generally used, such as 9580 or 9075.

c) One of the reasons for wild oscillations during the SCF procedure is charge transfer outside and inside the cluster. The "net charge" (printed in the output with this name), is the difference between

crystal). F_C eigenvalues jump up and down according to whether there are too many or too few electrons in the cluster. One way to smooth out such oscillations is to (partially) renormalize the P matrix by multiplying its elements by a factor α. The percentage of renormalization is fixed by LPR(48) (card 3): if it is equal to 100 renormalization is complete. This technique is a bit too drastic, especially as far as concerns the calculation of energy (see reference 2), but can be useful when trying to obtain a starting P matrix (IV.x). In these case put LPR(48)=50 to 75; otherwise, LPR(48)=0.

d) A more sophisticated but more delicate and costly technique is the "shift option", which is controlled by INF(175) and INF(177), and by LPR(48) (card 6 and card 3), and is discussed at length in reference 2. Essentially, it consists in shifting rigidly the eigenvalues of F_C by a quantity δ, before applying the PC equations, in such a way as to insure charge normalization in the percentage defined, as before, by LPR(48).
The procedure is activated by defining INF(175)≠0. The evaluation of δ is performed by solving twice at each cycle the PC equations, the first time without any shift, the second time by shifting the eigenvalues by INF(177)/1000 a.u. (for instance,: INF(177)=50). From the two resulting net charges, δ is obtained by linear inter- or extra-polation. Unfortunately, the procedure, though sometimes effective, is very delicate because the dependence of the net charge on the shift is monotonous but very non-linear.

e) Another reason for difficulty in convergence is the fact that during the procedure some cluster eigenvalues pass across the Fermi level E_F. According to the PC equations, the contribution of the corresponding states to the P matrix is evaluated in a completely different way (with reference to the occupied or the virtual crystal manifold). If we are far from convergence, or if the PC approximation is not applicable, the two results may differ appreciably. To make this problem less critical, a safety zone is defined around each eigenvalue [INF(122), card 3]. If the Fermi level falls in the safety zone, the eigenvalue is split into two, one at the top, the other at the bottom of the safety zone, with a weight attached to the two terms according to the lever rule. two contributions are then evaluated to the P matrix, one associated with the top pseudolevel, and making reference to the occupied manifold, the other with the bottom pseudolevel, and referring to the virtual manifold. This procedure is rather effective, and is mandatory when metallic systems are considered [4]. Values in use are INF(122)≈100, corresponding to a safety zone of 0.1 a.u.

IV.4 FERMI ENERGY

For metallic host crystals, the Fermi level is rigidly fixed at the host value. Note that there is no arbitrariness in its position, since the ***EMBED*** calculation is performed using the same conventions and techniques as adopted for the crystal calculation. For non-metals, the standard choice is to set it at the center of the fundamental gap.
This choice is adopted automatically by ***EMBED*** when INF(123) (card 3) is set to zero. It is however possible to redefine E_F by setting it at INF(123)/10000 a.u. (this is the only place where a factor 10000 is adopted for passing from a.u. to INFs; in all other cases use 1000).
The possibilities implicit in the redefinition of E_F are discussed in reference 1.

a) The time required at each SCF cycle for the solution of the PC equations is proportional to NJ, the number of levels grouping degenerate eigenstates. The grouping is necessary not only for reducing computer times, but also because, in the definition of the T^j matrices, differences between eigenvalues appear at the denominator.
A minimum energy separation must therefore be defined for grouping together degenerate or quasi-degenerate levels. This is set in card 6 or card 9 as INF(176) (a.u./1000). Suggested values are 10 to 50.

b) After the first few cycles of the SCF procedure, only states with eigenvalues close to E_F give contributions to P that are changing appreciably. This fact is exploited very effectively by imposing that after a certain cycle [defined as INF(180)] only contributions from states within a certain energy interval [the "active zone", defined by INF(178)-INF(179) in a.u./1000] are redefined, while the others remain fixed. These parameters are provided in card 6 and card 10. The active zone should comprise (at least) the fundamental gap. 3 cycles are usually sufficient for determining the other contributions.

IV.6 RECOVERY OF INFORMATION

a) As stated in section IV.3a, the best way to help convergence is to start from a P matrix not too different from the final one. If no previous information is available, the program automatically uses the host crystal values as an initial guess for all P matrix elements that do not refer to AOs in zone A; in zone A atomic solutions are adopted. This starting P matrix is however severely unbalanced (overlap populations between A and the rest are not taken into account), and convergence may be difficult. If convergence (or, at least, a stable enough solution) has been reached for a given type of defect (for instance, a substitutional impurity of Carbon in Silicon), this can be used as an initial guess for "similar" situations, such as:
- studying relaxation around the impurity,
- treating the same problem with a larger C cluster,
- checking the influence of the position of E_F,
- introducing a change in the exponent of some basis functions:
in all these cases there is a one to one correspondence between old and new AOs. For such purposes, one can use INF(173), INF(174) (card 6).
If INF(173)≠0, at the end of the calculation P is written, together with a set of indices, on unit FT32.
If INF(174)≠0, at the beginning of the calculation P is read from unit FT31 and loaded appropriately as an initial guess.
Note that both options can be switched on at the same time, for instance, during a search for a really good 'seed'.

b) The restart option serves, in a sense, the same purpose, but within one and the same job (cards 8, 9, and 10). This option is activated if any number substitutes '999' in the 8th card. The program then uses the final P matrix from the preceding calculation as an initial guess. However, since integrals are not recalculated, the number of parameters that can be changed is much less than above: they concern the means for helping SCF convergence (IV.3.a,b), the definition of active zone and the tolerance for grouping eigenvalues (IV.5), and, perhaps most important, the redefinition of E_F (IV.4).
Note that the restart option can be repeated as many times as one wants within the same job.

correction" to P).
In order to understand what is meant by that, consider an "autoembedding" case. It corresponds to defining NSTAA, NSTA1, NSTCC in card 4 as 0, 0, n, respectively. That is, nothing is changed in the crystal, and the calculation is performed by considering a C zone comprising n stars of atoms. If the calculation were entirely correct, the resulting P would be exactly the same as for the host crystal. Differences $\Delta P'$ are a measure of approximations in the calculation. It is found that in order to reach a good agreement with the exact results, very tight tolerances must be specified, with very high costs. The errors affect especially terms at the border of the cluster. The idea is that this kind of errors in the coupling correction are largely independent of the type of defect considered, since they are originated by the absence of terms which go very deeply into the surrounding host crystal. Therefore, one can use the value $\Delta P'$ evaluated exactly in an autoembedding calculation for the defect calculation itself.
The procedure is as follows (the temporary unit FT19 and the permanent one FT20 are used):
- Choose a set of tolerances (not too tight ones) and a value of n;
- set (card 2a) LPR(60)=1
- run the autoembedding case 0 0 n for a given origin (card 4)

The corresponding $\Delta P'$ is written on FT20.
In order to use it:
- Consider a defect problem referring to the same origin;
- use the same tolerances;
- choose a triplet NSTAA, NSTA1, NSTCC with NSTCC=n-NSTA1+NSTAA (the border of the C cluster coincides with the preceding one);
- decide from which "shell" on the two sets of atoms in cluster C coincide (for instance, in the case of a carbon impurity in silicon, minimal basis set, the correspondence is between the "old" shells, starting from the fourth one, and the "new" shells, starting from the third one; in the case of a vacancy in silicon, the correspondence starts from the fourth old one with the first new one on). Define i and j the number of shells that must be "suppressed" in the two systems for having the correspondence (in the first example, they are 3 and 2, in the second example they are 3 and 0);
- define (card 2a) LPR(60)=-ijx, that is, a negative three figure number, whose first figure equals i, the second j, and the third is any number (but, if both i and j are 0 and you want to recover $\Delta P'$, x must be different from 0). In the two examples above, LPR(60)=-321 and -301, respectively.

IV.7 BASIS SET

Note that for host crystal atoms, one must use the same basis set as adopted for the periodic calculation that generates units FT09 and FT26; for the choice of those functions, the prescriptions and cautionary statements apply, as described in Chapter V of *CRYSTAL*'s Instruction Manual. For impurity atoms, it seems reasonable that basis set of similar quality are adopted. Not much experience exists, however, concerning this point (see however Nada's study of Li impurities in MgO).

from zero are requested). It is indifferent which one is set where, except for LPR(50) and LPR(60) which should be set in card 2a.
Printing commands that can be activated are specified in Appendix A.
A few LPRs are used as parameters or for special purposes; they are:
- LPR(48) "percentage of normalization" (IV.3.c and d);
- LPR(49) stop after collection of prel. information: see Appendix A
- LPR(50) stop after collection of prel. information: see Appendix A
- LPR(60) "ΔP' creation and recovery" (IV.6.c);

IV.9 EXAMPLES OF INPUT

Example 1.

Cards	Comments
AUTOEMBEDDING (0 0 1) IN HEXAGONAL BN	
1	
60 1	(Will save ΔP' information)
1 5 5 5 5 5 7 8 19 2 2 2 9575 100 0	(No reordering of stars, good tolerances, high mixing, 0.1 a.u. safety zone ar. E_F, no redefinition of E_F)
2.694905 0.00000 0.00000 0 0 1	(The origin coincides with the B atom in *CRYSTAL* coordinates; the C cluster coincides with that boron atom)
0	(No other printing options)
5 7 0 0 0 10 0 -1000 1000 3	(5 iterative cycles are allowed if conv. is not within 10^{-7}; P matrix is neither recovered nor saved; no shift option is used; eigenvalues within 0.01 a.u. are grouped together; after the first three cycles only eigval. within -1 and 1 a.u. are treated self-consly)
999	(end of cards)

```
AL IMPURITY IN HEXAGONAL BN (2 2 3)
0                                       (No printing options)
1 4 4 4 4 5 9 19 2 2 2 9585 300 500     (Not as good tols as in Ex.1;
                                         E_F is set at 0.05 a.u.)
2.694905  0.00000 0.00000    2 2 3      (The origin is as in Ex.1;
                                         2 stars are elimin. (4 atoms);
                                         2 stars are introd.; C cluster
                                         comprises 3 stars, 10 atoms)
13. 2.694905  0.00000 0.00000           (The Al impurity substitutes
                                         the central boron atom)
 7. 1.397452 -2.247253  0. (REL -0.1)   (The star of substituted N atoms
                                         is set 0.1 a.u. inside with
                                         respect to original position)
1
48 50                                   (50% renormaliz.: IV.3.c)
10 7 1 1 0 100 0 -1000 1000 3           ("old" P matrix is read from
                                         FT31; "new" P matrix will be
                                         saved on FT32 for subseq. use:
                                         see Example 1 of section IV.9;
                                         eigval within 0.1 a.u.are
                                         grouped;active zone as in Ex.1)
13 3
0 0 3 2. 0.
0 1 3 8. 0.                             (St. 3G basis set for Al)
0 1 3 3. 0.
5 2
0 0 3 2. 0.                             ( "    "              B)
0 1 3 3. 0.
7 2
0 0 3 2. 0.                             ( "    "              N)
0 1 3 5. 0.
99 0
1                                       (Restart option is activated)
9 9080 0 10                             (E_F is set to crystal value;
                                         eigval. within 0.01 are groupd)
-1000 1000 3                            (Active zone as above)
999
--------------------
Example 3.
Cards                                       Comments

SUBSITUTIONAL C IN SI  (2 2 2)          (Host crystal's a=5.45 A)
1
60 -321                                 ("Long range recovery": IV.6.c)
1.287368 1.287368 1.287368 2 2 2        (Origin at Si ¼ ¼ ¼)
6. 1.287368 1.287368 1.287368           (Impurity at origin)
14. 3.862104 3.862104 -1.287368         (Neigh. of C are unrelaxed)
1 4 4 4 4 6 8 19 2 2 2 90 80 100 0
0
20 6 1 1 0 30 0 -1000 1000 3            ("old" P matrix is read from
                                         FT31, new one saved on FT32)
14 3
0 0 3 2. 0.
0 1 3 8. 0.                             (St. 3G basis set for Si)
0 1 3 4. 1.58                                  (change of scale fac.)
6 2
0 0 3 2. 0.                             ( "    "              C)
0 1 3 4. 0.
99 0
999
```

```
Cards                                          Comments

INTERSTITIAL C IN SI TETRAHEDRAL SITE (1 0 2)
2
60 -21 41 2                                    ("Long range recovery": IV.6.c;
                                                printing geom. information)
1 4 4 4 4 4 6 8 19 2 2 2 9585 100 0
3.862104 3.862104 3.862104 1 0 2               (Origin at centre of cube;
6. 3.862104 3.862104 3.862104                  (C added "   "       "   )
1
48 75                                          (shift option, IV.3.d, is used:
20 6 0 0 1 30 100 -1000 1000 3                  intrp.intrv. 0.1, norm.75%)
14 3
0 0 3 2. 0.
0 1 3 8. 0.                                    (St. 3G basis set for Si)
0 1 3 4. 1.58                                          (change of scale fac.)
6 2
0 0 3 2. 0.                                    ( "    "              C)
0 1 3 4. 0.
99 0
999
--------------------
```

Example 5.

```
Cards                                          Comments

INTERSTITIAL C IN SI HEXAGONAL SITE (1 0 2)
2
60 -21 43 3                                    ("Long range recovery": IV.6.c;
                                                printing neighborhood inform.)
1 4 4 4 4 4 6 8 19 2 2 2 9585 100 0
2.574836 2.574836 5.149472 1 0 2               (Origin at hexagonal site)
6. 2.574836 2.574836 5.149472                  (C added "   "       "   )
0
20 6 0 0 0 30 0 -1000 1000 3
14 3
0 0 3 2. 0.
0 1 3 8. 0.                                    (St. 3G basis set for Si)
0 1 3 4. 1.58                                          (change of scale fac.)
6 2
0 0 3 2. 0.                                    ( "    "              C)
0 1 3 4. 0.
99 0
999
--------------------
```

1. The ECHD is calculated at the nodes of a 2-dimensional net in a parrallelogram-shaped domain defined by points A B and C as in the figure below.

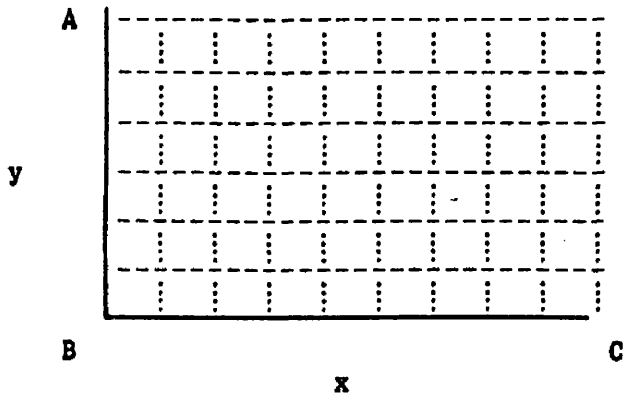

In this example, the number of points on the B-A segment, defined by the input variable NPY, is 7. The A-$\hat{B}$-C angle can differ from 90°.
The number of points along the B-C axis is set automatically by the program in such a way that $\Delta x \approx \Delta y$.
2. The position of the three points A, B and C can be specified both by their cartesian coordinates referred to the "old" origin (IMODE=0), or by the corresponding position of 3 nuclei (IMODE=1). In the latter case, if these nuclei belong to host crystal atoms, they are identified by their label as it appears in the output of *CRYSTAL*, and by the crystallographic indices of the cell in which they are located; if they belong to the A zone, see comment in section III.3. If B and C coincide, the ECHD is calculated along the segment B-A.
3. The B-A direction is taken as the conventional y axis, and B-C represents the x axis.
4. The ECHD values are truncated to 10.0 a.u. and are printed in integer format in units of 10^{-4} a.u. ; on the FT25 unit the truncated densities are stored in a.u. (not multiplied by any factor).
5. The symmetry is used to restrict the calculation of ECHD to the irreducible part of the specified A-B-C domain. To maximize the use of symmetry, the points of the net should include all symmetric positions in the selected plane. For example, make B co-incident with the origin, A and C with the extremes of two lattice vectors, and choose NPY=4n+1 for (100) faces of cubic crystals, or NPY = 6n+1 for (0001) faces of hexagonal crystals.

Example 1. Map in the basal plane concerning the calculation whose input is given in Example 2 of section IV.9. Results stored on unit FT32 there are here read from FT31.

```
AL IMPURITY IN HEXAGONAL BN (2 2 3)
0                                          (No printing options)
1 4 4 4 4 5 9 19 2 2 2 9585 300 500        (Not as good tols as in Ex.1;
                                            other parameters are not used)
2.694905  0.00000 0.00000    2 2 3         (The origin is as in Ex.1;
                                            2 stars are elimin. (4 atoms);
                                            2 stars are introd.; C cluster
                                            comprises 3 stars, 10 atoms)
13. 2.694905  0.00000 0.00000              (The Al impurity substitutes
                                            the central boron atom)
 7. 1.397452 -2.247253  0. (REL -0.1)      (The star of substituted N atoms
                                            is set 0.1 a.u. inside with
                                            respect to original position)
1
48 50                                      (read but not used)
10 7 0 1 0 100 0 -1000 1000 3              (read but not used)
13 3
0 0 3 2. 0.
0 1 3 8. 0.                                (St. 3G basis set for Al)
0 1 3 3. 0.
5 2
0 0 3 2. 0.                                (  "    "              B)
0 1 3 3. 0.
7 2
0 0 3 2. 0.                                (  "    "              N)
0 1 3 5. 0.
99 0
61 1 0 0                                   The map of the defective crystal
5.79    -4.668      0.                     is drawn within a rectangle
-2.69   -4.668      0.                     in the basal plane
-2.69    4.668      0.
```

= APPENDIX A - AVAILABLE PRINTING OPTIONS =

<<<< SUBROUTINE ASTART >>>>

LPR(30)	VARIABLES	COMMENT
>1	S	OVERLAP MATRIX
>2	EIG,R	EIGENVALUES, EIGENVECTORS

<<<< SUBROUTINE ATCALC >>>>

LPR(33)	VARIABLES	COMMENT
>=1	PMUNU	DENSITY MATRIX
=-1	PMUNU	DENSITY MATRIX AT LAST CYCLE
>=2	RISU	COUPLING DENSITY MATRIX
>=3	BCOST	SUM OF CLUSTER DENSITY MATRIX AND CONSTANT DENSITY MATRIX
>=4	EMME	COUPLING MATRIX AND COUPLING MATRIX FIRST DERIVATIVE (FOR EACH EIGVALUE)
LPR(46)		
>0	P CONTRIBUTIONS	CONTRIBS TO P ON 1ST ATOM OF C STARS
>1	... ANALYSIS	....SAME PER EACH EIGENVALUE

<<<< SUBROUTINE BIECLU >>>>

LPR(31)	VARIABLES	COMMENT
=-1	BCOST	FOCK MATRIX AT LAST CYCLE
>=1	BCOST	FOCK MATRIX

<<<< SUBROUTINE CLAVIC >>>>

LPR(43)	VARIABLES	COMMENT
>=1	NACD	NUMBER OF ATOMS IN C+D* ZONE
	NSHCD	NUMBER OF SHELLS IN C+D* ZONE
	JRAB	LIST OF SHELLS IN C+D* ZONE
>=2	NAVIC	NAVIC(MU,LIS) GIVES THE NUMBER OF NEIGHBOURS OF MU WITHIN TOLERANCE TO=TOLL(LIS), WHICH BELONGS TO A ZONE
	IAVIC	IAVIC(MU,NUM) GIVES THE NUM-TH NEIGHBOUR OF MU WITHIN TO
	INVIC	INVIC(MU,LIS), FOR EVERY MU HAVING NEIGHBOURS IN A ZONE, GIVES THEM IN BINARY NOTATION
	NCRYVI	CRYSTAL NEIGHBOURHOOD : NCRYVI(MU,LIS) GIVES THE NUMBER OF NEIGHBOURS OF MU (IN NUMERATION OF PERFECT CRYSTAL) WITHIN TO=TOLL(LIS)
	ICRYVS,ICRYVG	CRYSTAL NEIGHBOURHOOD : ICRYVS(MU,NUM), ICRYVG(MU,NUM) GIVE THE SHELL TYPE AND THE G-VECTOR OF NUM-TH NEIGHBOUR
>=3	IPOLM,IPALM	ADDRESS FOR IRREDUCIBLE AND REDUCIBLE FOCK AND DENSITY MATRICES

LPR(39)	VARIABLES	COMMENT
>0	L,AL,BL,NPT,EE,E, NTUT	BAND, BAND LIMITS, NR OF POLYNOMIALS, FERMI LEVEL, EIGENVALUE, DIMENSION OF EMME MATRIX

<<<< SUBROUTINE ENEMAD >>>>

LPR(34)	VARIABLES	COMMENT
=2 OR >8	I,K,VIVI	POTENTIAL (AND DERIVATIVES) IN THE POSITION OCCUPIED BY I-TH NUCLEUS AND CREATED BY K-TH ATOM OF PERFECT (FIRST PRINT) AND DEFECTIVE CRYSTAL

<<<< SUBROUTINE LOWDCL >>>>

LPR(32)	VARIABLES	COMMENT
>0	EIG	EIGENVALUES
=-2	R	EIGENVECTORS AT CYCLE 0 AND AT LAST CYCLE
>2	R	EIGENVECTORS
>=4	F	FOCK MATRIX (C,C)

<<<< SUBROUTINE MADCLU >>>>

LPR(1)	VARIABLES	COMMENT
>0	X3	POSITION IN WHICH POTENTIAL IS COMPUTED
	EAIJ	CONTRIBUTION TO POTENTIAL FROM ATOMS
	DERINT	FIRST DERIVATIVES
	DERONT	SECOND DERIVATIVES

<<<< SUBROUTINE MADEL2 >>>>

LPR(1)	VARIABLES	COMMENT
>0	VOL,FAT,...	INFORMATION ON EWALD PARAMETERS

<<<< SUBROUTINE MONCLU >>>>

LPR(44)	VARIABLES	COMMENT
>0	NSHTOT	NUMBER OF SHELLS IN QUANTUM ZONE
>1	IVET	LIST OF PENETRATING SHELLS IN EACH DISTRIBUTION (L1,L2), WHERE L1 IS IN C ZONE AND L2 IS A NEIGHBOUR OF L1
>2	OTZ	KINETIC INTEGRALS
	ATZ	NUCLEAR-ELECTRON ACTRATION INTEGRALS (N.B.: IN EACH ATZ(I), CORRESPONDING TO A PREFIXED DISTRIBUTION (L1,L2), IS CONTAINED THE SUM WITH RESPECT TO ALL PENETRATING NUCLEI IN (L1,L2)
>3	CJ	FIELD INTEGRALS

```
 0        QVRS                    MULTIPOLE MOMENT OF PRIMITIVE SHELLS
                                  IN HOST CRYSTAL UP TO ORDER L=LPR(20)
>1                                SUM OF NET AND NUCLEAR CHARGES
>5                                MULTIPOLES FOR ALL COUPLES OF AOs
-------------------------------------------------------------------
<<<< SUBROUTINE MULPO1 >>>>

LPR(20)   VARIABLES               COMMENT

>3        QVRS                    MULTIPOLE MOMENT OF UNPERTURBED PART
                                  OF SHELLS IN C* ZONE,
                                  UP TO ORDER L=LPR(20)-2
-------------------------------------------------------------------
<<<< SUBROUTINE PCOST >>>>

LPR(38)   VARIABLES               COMMENT

>0        PCOST                   CONSTANT CONTRIB. TO DENSITY MATRIX

-------------------------------------------------------------------
<<<< SUBROUTINE PIL >>>>

LPR(39)   VARIABLES               COMMENT

>0        EPIUS,EMENS,FAC1,FAC2   BAND LIMITS (IN X UNITS), FACTORS TO
                                  INTERPOLATE EMME VALUE
                                  (N.B.: THIS PRINTING IS ACTIVATED
                                  ONLY IF EIGENVALUE FALLS INSIDE
                                  CRITICAL INTERVAL)

-------------------------------------------------------------------
<<<< SUBROUTINE PSTART >>>>

LPR(30)   VARIABLES               COMMENT

>0         PMUNU                  STARTING DENSITY MATRIX
-------------------------------------------------------------------
<<<< SUBROUTINE QGACLU >>>>

LPR(20)   VARIABLES               COMMENT

>2        QVRS                    MULTIPOLE MOMENT OF SHELLS IN C+D*
                                  ZONE IN THE CLUSTER, UP TO ORDER L
                                  =LPR(20)-2
>4                                INDIVIDUAL CONTRIB. TO MULTIPOLES

LPR(48)
=N           N                    PERCENT OF NORMALIZATION OF CHARGE
-------------------------------------------------------------------
<<<< SUBROUTINE SCFCLU >>>>

LPR(31)   VARIABLES               COMMENT
=-1       BCOST                   FOCK MATRIX AT CYCLE 0

LPR(33)   VARIABLES               COMMENT
=-1       BCOST                   DENSITY MATRIX AFTER FIRST CALL TO
                                  ATCALC
-------------------------------------------------------------------
```

LPR(42)	VARIABLES	COMMENT
>=1	BCOST	CONSTANT CONTRIBUTION TO THE FOCK MATRIX (MADELUNG, KINETIC, NUCLEI-ELECTRONS BIELECTRONIC ATTRACTION, BIELECTRONIC REPULSION)
>=2	L1,L2,L3,L4	SHELL INDICES OF BIELECTR. INTEGRALS
>=3	RP	CORRESPONDING VALUE OF INTEGRAL

<<<< SUBROUTINE SYMEMB >>>>

LPR(41)	VARIABLES	COMMENT
>=1	IATG	FROM THE PRIMITIVE ATOM AND FROM THE G-VECTOR CORRESPONDING TO A HOST CRYSTAL ATOM, IT GIVES THE ATOM IN THE NUMERATION OF CLUSTER
	INAW	FROM CLUSTER ATOM GIVES PRIMITIVE AT.
	IISY	FROM THE ATOM OF THE CLUSTER IT GIVES THE GENERATING SYMMETRY OPERATOR
	INVOR	FOR EACH STAR AND SYMMETRY OPERATOR IV IT GIVES THE ATOM B=IV**(-1)*A
	IFATH	FROM THE ATOM OF THE CLUSTER IT GIVES THE STAR TO WHICH IT BELONGS
>=2	MVFN	NUMBER OF SYMMETRY OPERATOR IN THE DEFECTIVE SOLID (LABELS REFER TO THE OPERATORS IN THE PERFECT CRYSTAL)
	IMVN	LIST OF SYMMETRY OPERATORS IN THE DEFECTIVE SOLID
	IFFW	INVERSE INFORMATION: FOR EACH SYMM. OPERATOR OF THE PERFECT CRYSTAL, IT GIVES THE CORRESPONDING LABEL IN THE SUBSET OF THE CLUSTER SYMMETRY GROUP
	ISYY	ISYY(V1,V2) GIVES SYMMETRY OPERATOR V3=V1*V2
>=3	MG123	VECTOR SUM OF THREE G-VECTORS IN THE THE PERFECT CRYSTAL
>=4	INZ,IINA,IIG,R(I)	THEY ARE THE ANALOGOUS OF INZW, INAW, IIGW BUT ARE REFERRED TO THE PERFECT CRYSTAL. R IS THE SQUARE OF THE DISTANCE BETWEEN THE ORIGIN OF THE CRYSTAL AND THE I-TH STAR

<<<< SUBROUTINE SYME2 >>>>

LPR(41)	VARIABLES	COMMENT
>=5	NACLUS	FROM THE SHELL IN THE NUMERATION OF CLUSTER, IT GIVES THE ATOM IN THE NUMERATION OF CLUSTER
	NICLUS	FROM THE SHELL IN THE NUMERATION OF CLUSTER, IT GIVES THE ATOM IN THE NUMERATION OF PERFECT CRYSTAL
	LATLAP	FROM THE SHELL IN THE NUMERATION OF CLUSTER, IT GIVES THE SHELL IN THE NUMERATION OF PERFECT CRYSTAL
	NINIS	FROM THE ATOM IN THE NUMERATION OF CLUSTER, IT GIVES THE FIRST SHELL IN THE NUMERATION OF CLUSTER

LPR(31)	VARIABLES	COMMENT
>=2	BCOST	FOCK MATRIX (CONSTANT+MONOELECTRONIC CONTRIBUTIONS)

<<<< SUBROUTINE VICINI >>>>

LPR(41)	VARIABLES	COMMENT
>=6	ILL	NEIGHBOURS OF THE SHELL PASSED AS AN ARGUMENT TO VICINI WITHIN THE GIVEN TOLERANCE

==========

<<<< CONTROL CONDITIONS >>>>

LPR(49)	COMMENT
=1	SHELCL is not called
=2	MONCLU is not called

<<<< STOP CONDITIONS >>>>

LPR(50)	COMMENT
=1	stop after SYMEMB
=2	stop after MONCLU
=3	stop after SHELCL without comp. of integrals
=4	stop after SHELCL

<<<< SPECIAL FEATURES OF COMPUTATION >>>>

LPR(60) ——> (see section IV.8)

LPR(101), LPR(102) (standard values 5, 8)
These two parameters are used for specifying the computational conditions for the calculation of the irreducible integral that enters the evaluation of the M and M' matrices (Ref. 1, eq. B3, B4).
LPR(101) specifies which option must be used, either the "analytic" calculation, or the power series expansion of $1/(x-e)$; high values of LPR(101) correspond to the former option being preferred to the latter except in the case of very narrow bands, far from E_F. If the power series option is active, LPR(102) specifies the number of significant figures of the result.

INDEX OF "LPR" OPTIONS : 1 (Madclu), 11 (Mulpol), 20 (Qgaclu,Mulpol, Mulpo1), 30 (Astart, Pstart), 31 (Bieclu, Scfclu,Totclu), 32 (Lowdcl), 33 (Atcalc, Scfclu), 34 (Enemad, Monclu), 38 (Pcost), 39 (Emmeca), 41 (Symemb, Syme2, Vicini), 42 (Shelcl), 43 (Clavic), 44 (Monclu), 48 (Qgaclu), 49 (Control cond.), 50 (Stop cond.)

COMMON CDALL

Information about the set C - C+D*

JRAB(NJRAB)	JRAB(JR) GIVES THE JR-TH SHELL L1 OF THE SET C+D* N.B.: shells are not arranged by distance
IRABS(NIRABS)	IRABS(L) GIVES THE POSITION IR OCCUPIED BY SHELL L BELONGING TO C ZONE
JRABS(NJRABS)	JRABS(L1) GIVES THE POSITION JR IN THE VECTOR JRAB occupied by shell L1 belonging to C+D* zone
IPALM(NIRAB,NJRAB)	IPALM(IR,JR) IS THE STARTING POSITION OF THE sub-matrix (C - C+D*) corresponding to the shells L,L1

****

COMMON CLUST

IMVN(48)	IMVN(I) IS THE I-TH SYMMETRY OPERATOR OF THE defective crystal
INZW(NSTACD)	INZW(IST) GIVES THE FIRST ATOM CORRESPONDING to the star IST
INAW(NATOCD)	INAW(IAT), FROM THE ATOM IAT OF THE CLUSTER, GIVES the primitive atom
IIGW(NATOCD)	IIGW(IAT), FROM THE ATOM IAT OF THE CLUSTER, GIVES THE G-VECTOR
IISY(NATOCD)	IISY(IAT) FROM THE ATOM IAT OF THE CLUSTER, GIVES THE SYMMETRY OPERATOR
IATG(NAGIAP)	FROM PRIMITIVE ATOM IAP AND FROM G-VECTOR IG IATG((IAP-1)*NAF+IG) gives the atom IAT of the cluster, where NAF is the number of atoms in elementary cell IATG((IAP-1)*NAF+IG)=0 if atom belongs to A1 zone
NINIS(NATOCD)	NINIS(IAT) FROM THE ATOM IAT OF THE CLUSTER, GIVES the first shell of IAT in the numeration of cluster
NACLUS(NJRABS)	NACLUS(ISH) FROM SHELL ISH OF THE CLUSTER, GIVES the atom IAT of the cluster
NICLUS(NJRABS)	NICLUS(ISH) FROM SHELL ISH OF THE CLUSTER, GIVES THE PRIMITIVE ATOM IAP
LATLAP(NJRABS)	LATLAP(ISH) FROM SHELL ISH OF THE CLUSTER, GIVES the primitive shell
NSTIG(NNSTIG)	PROVIDES ADDRESSES FOR EMME MATRICES
NTIP(NCHNA)	NTIP(IAT) GIVES TYPE OF ATOM IN ZONE A
IFATH(NATOCD)	IFATH(IAT), FROM THE ATOM IAT, GIVES THE STAR IST to which it belongs
INVOR(NINVOR)	INVOR(I) FOR EACH STAR I AND SYMMETRY OPERATOR IV gives the atom B=IV**(-1)*A
IFFW(48):	Symmetry operators in the defective solid (labels are referred to operators in the perfect crystal
ISYY(48,48):	ISYY(V1,V2) gives the symmetry operator VI*V2

A Zone neighbourhoods

IAVIC(NIAV1,NIAV2)	IAVIC(MU,NUM) GIVES THE NUM-TH NEIGHBOUR OF THE shell MU within tolerance TO (see after)
NAVIC(NIAV1,6)	NAVIC(MU,LIS) GIVES THE NUMBER OF NEIGHBOURS OF MU within tolerance TO=TOLL(LIS)
INVVIC(NJRABS,6)	INVVIC(MU,LIS) FOR EVERY MU HAVING SOME NEIGHBOUR IN A ZONE, GIVES SUCH ONES IN BINARY NOTATION

Crystal neighbourhoods

ICRYVS(NSHCRY,NIAV2)	ICRYVS(MU,NUM) GIVES NUM-TH NEIGHBOUR OF THE shell MU into the cell
ICRYVG(NSHCRY,NIAV2)	ICRYVG(MU,NUM) GIVES THE NUM-TH G-VECTOR OF THE shell MU into the cell
NCRYVI(NSHCRY,6)	NCRYVI(MU,LIS) GIVES THE NUMBER OF NEIBRS OF MU (in the numeration of perfect crystal) within tolerance TO=TOLL(LIS)

****

COMMON MOLEC

XOR(3)	COORDINATES OF THE ORIGIN OF THE CLUSTER
CHNA(NCHNA)	CHN(I) CHARGE OF THE DEFECTIVE ATOMS IN THE STAR I of A zone
XXA(3,NCHNA)	XXA(3,I) ARE THE COORDINATE OF THE DEFECTIVE ATOMS in the star I of A zone

****

COMMON PFCOST

PMUNU(NPRID)	DENSITY MATRIX (C,C+D*)
BCOST(NPIRR)	FOCK MATRIX (C IRR.,C+D*) (MONCLU,...) or density matrix (C irr.,C+D*) (atcalc)
QVRS(NJRAB*25)	MULTIPOLE MOMENTS. QVRS IS A BLOCK VECTOR. EACH block corresponds to a component of the multipole and has a length equal to the number of shells in C+D* zone. In the first block, shell charges are arranged in same order present in JRAB vector. N.B.: in MULPOL, QVRS are referred to the perfect CRYSTAL. THEN EACH BLOCK HAS A LENGTH OF LAF,NUMBER of shells in the perfect crystal.

****

COMMON PPROVV

ICORB(NJRAB)	ICORB(L+1)-ICORB(L) GIVES THE NUMBER OF AO corresponding to the L-th shell of vector JRAB (see COMMON CDALL)
ILICA(NJRAB)	ILICA(M+1)-ILICA(M) IS THE NUMBER OF NEIGHBOURS IN D zone of the M-th shell of vector JRAB
LICA(NLICA)	IN LICA, FOR EACH SHELL OF JRAB, ARE LISTED THE corresponding neighbours in D zone

```
COMMON /CONTUD

Information about the set C irreducible - (C+D*)'

JSAB(NJRAB)          JSAB(JS) GIVES THE JS-TH SHELL L1 OF THE SET FORMED
                     by the neighbours of shells in C irriducible zone
                     (set (C+D*)')
                     N.B.: shells are not arranged by distance
ISABS(NIRABS)        ISABS(L) GIVES THE POSITION IS IN THE VECTOR ISAB
                     occupied by shell L belonging to C irriducible zone
JSABS(NJRABS)        JSABS(L1) GIVES THE POSITION JS IN THE VECTOR JSAB
                     occupied by shell L1 belonging to the (C+D*)' zone
IPOLM(NSTARC,NJRAB)   IPOLM(IS,JS) IS THE STARTING POSITION OF THE
                     sub-matrix (C irr.- (C+D*)') corresponding to the
                     shells L,L1

*************************************************************************

COMMON SHIFT

EIGOLD(NAOC)         MEMORIZES EIGVALS FOR SHIFT OPTION
FOLD(NAOC,NAOC)      MEMORIZES FOCK MATRIX
EIG(NAOC)            MEMORIZES NEW EIGENVALUES

*************************************************************************
```

APPENDIX C. MEANING OF INF AND PAR VARIABLES

********** INFORMATION ON CLUSTER **********

INF(101) = NOF NUMBER OF ATOMS IN A ZONE+ NAF
INF(102) = NSTAA number of stars in A zone
INF(103) = NSTCC number of stars in C zone
INF(104) = NSTF number of stars classified
INF(105) = NATF number of atoms classified
INF(106) = MVFN number of symmetry operators in the cluster group
INF(107) = INTPER = 0 computes all bielectronic integrals
if = 1 computes only the integrals involving
A zone
INF(108) = NREC N. OF BLOCKS OF BIELECTRONIC INTEGRALS (NUMBER OF
I/O operations on unit IO04)
INF(109) = LAFCLU laf calculated for the crystal
INF(124) = NSTA1 NUMBER OF STARS IN ZONE A'
INF(125) = NEIGE NUMBER OF GROUPED EIGENVALUES
INF(126) = LIMB DIMENSION OF IRREDUCIBLE P MATRIX
INF(127) = IRIMB " " REDUCIBLE " "
INF(129) = NLIN NUMBER OF ATOMS IN ZONE A'
INF(130) = NATC NUMBER OF ATOMS IN ZONE C
INF(131) = NATA NUMBER OF ATOMS IN ZONE A
INF(150) = INDEX number of sub matrix of field integrals written on
unit IO01
INF(151) = NSHLC NUMBER OF SHELLS IN ZONE C
INF(152) = ITOX order number of hardest tolerance
INF(153) = NSHLA NUMBER OF SHELLS IN ZONE A
INF(154) = NSHCD total number of shells in C+D* zone
INF(155) = NACD number of atoms in C+D* zone
INF(160) = ICONT total number of AO in the cluster
INF(165) = IBLOS number of I/O blocks of multipole integrals
used in QGACLU
INF(172) = NCYC CYCLE NUMBER

********** INFORMATION READ BY THE SUBROUTINE INPUTE ********

INF(110) = IJK IF NOT ZERO, REORDERS STARS OF ATOMS
INF(111) = T1 bielectronic coulomb overlap
INF(112) = T2 bielectronic coulomb penetrating
INF(113) = T3 monoelectronic
INF(114) = T4 exchange overlap
INF(115) = T5 exchange pseudooverlap
INF(116) = T6 highest security tolerance
INF(117) = T7 radius quantum zone
INF(118) = T8 pole order
INF(119) = T9 derivative order in madelung zone
INF(120) = T10 external multipole order in Madelung zone
INF(121) = T11 percent of mixing for fock matrix in scf
INF(122) = T12 DELTA/10000. (see EMMECA)
INF(123) = T13 Fermi level/10000. (if = 0, Fermi level is not
REDEFINED)

```
 INF(170) =        max number of SCF cycles
 INF(171) =        tolerance for convergency in scf
 INF(173) =        if equal 1 density matrix is written on external
                   unit (io32) for recovery
 INF(174) =        if equal 1 density matrix is read from external
                   unit (io31) for recovery
 INF(175) =        if equal 1 then use the "shift option", wich is a
                   constant shift of the eigenvalues set in the SCFCLU
                   (this option disables the renormalization option)
 INF(176) =        TOL FOR GROUPING EIGENVALUES
 INF(177) =        INTERVAL FOR SHIFT INTERPOLATION
 INF(178) =        LOWER LIMIT FOR "ACTIVE ZONE"
 INF(179) =        UPPER   "          "     "
 INF(180) =        N.CYCLES BEFORE USING ACTIVE ZONE OPTION


********** INFORMATION FROM CRYSTAL ******************************

 INF(2)   = MVF    number of symmetry operations in perfect crystal
 INF(7)   = NDF    number of bands in the system
 INF(10)  = NTUT   fock and density irriducible matrix dimension
 INF(24)  = NAF    number of atoms in elementary cell of host crystal
 INF(20)  = LAF    number of shells in elementary cell of host crystal


********** PAR(i) VARIABLES DEFINED DURING THE PROGRAM ************

 PAR(20) = NNUC    nuclear charge in A+B zone (subroutine SYMEMB)
 PAR(22) = QCLU1   sum of net charge in C=A'+B zone with electronic
                   charge in D* zone and with NNUC (subroutine MULPOL)
 PAR(30) = ENU     (SUBROUTINE ENECAL)
 PAR(33) = ENER    (SUBROUTINE ENEMAD)
 PAR(34) = ENE1    (SUBROUTINE ENESCF)
 PAR(35) = ENE2    (SUBROUTINE TOTCLU)
 PAR(36) = ENAC    (SUBROUTINE ENECAL)
 PAR(37) = ENAT    (SUBROUTINE ENECAL)
 PAR(50) = CELEC   total number of electrons in the cluster
```